Balanced Heat Transport and Optimal Cooling

by

Binglin Song

A dissertation submitted in partial fulfillment
of the requirements for the degree of
Doctor of Philosophy
(Mathematics)
in the University of Michigan
2023

Doctoral Committee:

Professor Ian Tobasco, University of Illinois Chicago, Co-Chair
Professor Selim Esedoglu, Co-Chair
Professor Krishna Garikipati
Professor Divakar Viswanath

Binglin Song

bingsong@umich.edu

ORCID iD: 0009-0008-7920-6576

Acknowledgments

I would like to express my heartfelt gratitude to my advisor, Professor Ian Tobasco, for his constant support and kindness. He became my advisor during the hardest time I've ever faced and his patience and advice carried me out of those days. I want to thank him not only for his guidance academically, but also for his encouragement and thoughtfulness as a mentor and friend. His enthusiasm in mathematics and positivity in life have always been and will continue inspiring me to explore both in the world of mathematics and out. I want to thank him for teaching me how to stay cool both in a heated disk and in life.

I also want to thank my co-advisor, Professor Selim Esedoglu, for his thoughtfulness and generosity. Each time I talk to him, I would get great advices on my career and life. I would want to thank my late advisor, Professor Charles Doering, who guided my into the world of fluids and flows. He showed me how to enjoy mathematics with passion and curiosity. I will always miss his smile everytime we talk math and football. I want to thank Professor Krishna Garikipati and Professor Divakar Viswanath for being in my committee and their interest in my thesis.

I am grateful for having so many great faculties in the math department. I want to thank Professor Silas Alben, Zaher Hani, Mattias Jonsson and Sijue Wu for their inspiring courses and advices. I want to thank Teresa Stokes who took great care of my life as a grad student and showed me all the interesting aspects of a grad student outside mathematics.

Finally I want to thank my family and friends for their support. I want to thank my mom and dad for listening to my worries and supporting me for all these years. I want to thank my friends for the joyful time we spent together these years. Without them, my grad life would be a lot less colorful.

TABLE OF CONTENTS

LIST OF FIGURES

FIGURE

ABSTRACT

In this dissertation, we study the problem of designing an optimal incompressible fluid flow to achieve the most efficient heat transfer between a pair of balanced heat source and sink. We obtain *a priori* bounds on the heat transfer in terms of various measures of bulk flow intensity, such as the mean kinetic energy. A key question in our analysis is how the choice of source–sink function should enter into the optimization. We begin in Chapter III by presenting our results on the two-dimensional version of this problem from [SFT23], where we obtained a general bound on heat transfer in terms of a Hardy norm of the source–sink function, and introduced a 'pinching' flow design to saturate the scaling law of this bound for a pair of point-like sources and sinks. We discuss the implications of our bounds for physical, buoyancy-driven internally heated convection, which is a cousin of the more famous Rayleigh–Bénard problem. Chapter IV extends our bounds on heat transfer in various directions, to higher dimensions as well as to a dumbbell-shaped domain with a pair of point source and sink separated by a thin neck. Chapter V improves our analysis of the point source–sink problem by finding the optimal prefactor in our bound on heat transfer, for a subclass of radially symmetric heat profiles. Interestingly, we find that the bulk properties of the fluid flow do not enter into the leading order optimization of heat transfer in this setup. Instead, the heat transfer is set first and foremost by the particular choice of pinching flow profile nearby the sources and sinks. We end with a short conclusion section that provides some suggestions for future work.

CHAPTER I

Introduction

1.1 Overview

Waking up in a cold winter morning, there is nothing better than a hot cup of coffee. However, a lot of times, the scorching temperature stops you from taking even a sip of it. How to cool a cup of coffee effectively is a simple enough question but the mechanism and theories behind this problem actually capture the nature of so many aspects of our lives. From liquid metal batteries [SZ16], to mantle convections underneath the ground [MB20, STO01], heat transfer has been a topic discussed in math, physics, geography and many other areas. Determining the upper limits of heat transfer efficiency and designing mechanical structures to approach that limit have been important topics for decades.

These heat transfer problems can be characterized by the heat source types. The well-known Rayleigh–Bénard convection(RBC) considers heating from the top or bottom boundaries of a fluid layer. With the first systematic experiments conducted by French experimentalist Henri Bénard dating back to 1900 [Bé00] and Lord Rayleigh's analytical explanations in 1916 [Ray16], researchers had been focusing on RBC and produced various results regarding heat transfer efficiency both numerically and analytically. Heat transfer for RBC is traditionally measured using the dimensionless Nusselt number (Nu) which is the ratio of total heat flux to conductive heat flux. Of broad and current interest is quantifying Nu in terms of the Rayleigh number (R) and Prandtl number (Pr) where R is related to the temperature difference across the fluid layer and Pr is related to ratio of heat transfer between convection and conduction. We'll take a deeper look at these

parameters later in Section 2.1 when introducing our governing equations. One main open question in this area is the asymptotic scaling of Nu with respect to R as $R \to \infty$. The two contending theories are the 'classical' regime ($Nu \sim R^{1/3}$) proposed by Malkus and Priestley in 1954 at the same time [Mal54, Pri54] and the 'ultimate' regime ($Nu \sim R^{1/2}$) proposed by Spiegel in 1963 [Spi63]. Various experiments have been carried out with most data pointing towards the $Nu \sim R^{1/3}$ regime [CCC$^+$01, NSD00, UMS11]. Numerical simulations also exhibit the 'classical' regime results for $R \in [10^{10}, 10^{15}]$ [HFN$^+$12, IKJK20]. However, as R gets larger, the computational cost gets increasingly more expensive. So it becomes really difficult to do numerical simulations for R going beyond the 10^{15} scale especially in higher dimensions. As the time of writing this dissertation, we have no numerical evidence showing 'ultimate' regime.

The type of heat driven flow we consider in this dissertation is a variant of RBC: we study internally heated convection(IHC) where the flow is driven by heating inside the bulk instead of on the boundary. This type of heating arises in many areas. The liquid batteries and mantle convection in the earth mentioned above all involve internal heating. Contrary to the RBC case, recent experiments and numerical simulations show that the 'ultimate' regime is obtainable [LAG18, BLAG19]. In fact, there are simulations showing heat transfer beyond the 'ultimate' regime [MLBG19]. As a result, the topic of IHC has attracted recent theoretical interests. In this dissertation, we study the heat transfer of IHC analytically and derive *a priori* bounds for the heat transfer efficiency with examples demonstrating the flow designs that help us achieve these bounds.

To measure the heat transfer in IHC, a wide variety of quantities like the Nussult number [KGOM22] and mean temperature [GS12, Gol15] have been used. Here, we choose to measure the efficiency of heat transfer via the mean-squared temperature gradient. This makes sense as a diagnostic tool since by Fourier's law, the diffusive heat flux is proportional to the negative gradient of the temperature. Therefore, a highly efficient heat transfer will tend to minimize (a norm of) the temperature gradient. Many studies have been carried out assuming an unbalanced heat profile which means the net heat added to the system is non-zero. Some examples are uniform heat source [LDB04, GS12, Gol15, WD11, WD12, Gol16], arbitrary heat profiles with positive

spatial-temporal average [Tob22] and heat releasing particles [DY22]. In this dissertation, we will focus on IHC with balanced heat profiles (net heat added to the system is zero) and insulating boundary conditions. Our goal will be to deduce *a priori* bounds for heat transfer that work for a large set of heat profiles.

To construct *a priori* bounds, a widely used method is the 'background method' introduced by Doering and Constantin in 1990s [DC94, CD95, DC96]. Later, the method was applied to mixing efficiency problems [TDG04, DT06, TP08, Thi12] where, like in this dissertation, the goal was to understand how quickly a temperature-like quantity could be stirred up to a nearly constant state. Adapting the optimal control approach introduced in [DT19, Tob22], which integrates the idea of 'background method' and 'optimal designs', will lead us to identify the scaling law of the optimal heat transfer depending on the strength of the advection. For the main part of our analysis, we drop the momentum equation and replace it with a kinetic energy constraint since this allows us to construct nearly optimal flows. We'll exhibit examples, prove that the bounds are sharp and finally study a particular case, namely the point source–sink profile to identify the optimal prefactor in the scaling law. Altogether, our result will shed light on what it takes to design fluid flows that optimally transfers heat between source and sink.

1.2 Layout of the dissertation

We start with background material in Chapter II including the governing equations in Section 2.1, Poincaré type and div-curl lemmas we'll use throughout our analysis in Section 2.3. Then in Section 2.4 we address the well-posedness of our governing equation and establish L^∞ estimates on our temperature field given some reasonable restrictions on our heat profile functions.

Chapter III starts our analysis of IHC which contains our results from the published paper [SFT23] where we established our *a priori* bounds for the advection–diffusion equation and Boussinesq equations and found these bounds to be sharp in two-dimensional examples. In Chapter IV we construct more examples extending these results to higher dimensions and a thin neck domain. A main theme is a 'pinching' flow design which we show is optimal for point source–sink heat

functions in 2-d.

Comparing these flows in different domains and dimensions, we notice that the dominant heat transfer is determined by the portion of the flow where pinching happens rather than the bulk flow between the source and sink of the heat profile thus, we have some freedom in choosing how and where the pinching happens to achieve the same scaling. Chapter V turns to analyze the best possible prefactor in pinching-based heat transfer. We transform our problem to a prescribed Jacobian type problem which has been studied in the literature in various settings [Mos65, DM90, CDK12, CD12, GKL21b, GKL21a, GKL23]. Adapting the proof from [GKL21a], we update our *a priori* bound from [SFT23] by obtaining its optimal prefactor for radially symmetric source–sink functions.

We close the dissertation with a short conclusion section describing the dominant heat transfer scaling and prefactor results. Furthermore, we propose some related open questions regarding internally heated flow and some scenarios where the 'pinching' flow designed could be useful.

CHAPTER II

Governing Equations, Poincaré Type Lemmas and Well-Posedness

In the following sections, we start by introducing the main equations governing our studies. Then in Section 2.2 we introduce some common notations used throughout the dissertation. In Section 2.3, we prove a Poincaré type lemma and a div-curl lemma which we will use in later chapters. Finally, in Section 2.4 we show the governing advection-diffusion equation for our optimization is well-posed even if the velocity field is only assumed to have bounded kinetic energy and to be divergence-free. This requires some delicate but more or less standard Nash-type estimates on the L^∞ norm of the temperature.

2.1 Advection–Diffusion Equations

Heat in a moving fluid can be transported in two main ways: advection and diffusion where advection is the transport of heat by the bulk motion of fluid and diffusion (or more precise, molecular diffusion) is the thermal motion of fluid particles in the microscopic scale. In other words, advection denotes the bulk transfer of heat by a fluid flow and diffusion denotes the microscopically random flux of heat from high temperature to low temperature regions. Mathematically, the heat change comes in three forms: advection driven by fluid flow ($\boldsymbol{u} \cdot \nabla T$), diffusion in the fluid (ΔT), and bulk heat sources and sinks (f). Combining these three factors, we have the following dimensional advection-diffusion equation which governs most of the analysis in this dissertation:

$$\partial_{t^*} T^* + \boldsymbol{u}^* \cdot \nabla^* T^* = \kappa \Delta^* T^* + H f$$

where stars (*) denote dimensional quantities and operators. Here, f sets the already non-dimensional heat source–sink function with heating rate H. The coefficient of thermal diffusivity is given as κ. Throughout the dissertation, we work on bounded Lipschitz domains $\Omega \subset \mathbb{R}^d$ with $d \geq 2$ satisfying insulating boundary conditions:

$$\hat{\boldsymbol{n}} \cdot \nabla T^* = 0 \quad \text{at} \quad \partial\Omega.$$

Another common assumption we have is the divergence-free condition and no-penetration boundary condition on the velocity field $\boldsymbol{u}$:

$$\begin{aligned} \nabla^* \cdot \boldsymbol{u}^* &= 0 \quad \text{in} \quad \Omega, \\ \boldsymbol{u}^* \cdot \hat{\boldsymbol{n}} &= 0 \quad \text{at} \quad \partial\Omega. \end{aligned}$$

Sometimes, we also require $\boldsymbol{u}$ to obey the momentum equation specified by the dimensional Boussinesq equations:

$$\partial_{t^*} \boldsymbol{u}^* + \boldsymbol{u}^* \cdot \nabla^* \boldsymbol{u}^* + \rho^{-1} \nabla^* p^* = \nu \Delta^* \boldsymbol{u}^* + \alpha g T^* \boldsymbol{g}$$

Here, $\boldsymbol{g} = \nabla^* \varphi^*$ gives the non-dimensional acceleration of buoyancy with the gravitational coefficient as g and the coefficient of thermal expansion as α. ρ denotes the density and ν gives the kinematic viscosity. We use a conservative acceleration field, and note the consistent lack of a minus sign in the potential.

The above system involves a lot of parameters and units. For such systems, nondimensionalization is a common technique used to simplify and re-parametrize the problem. Here, we first fix a representative lengthscale L; for example, we may take $L = |\Omega|^{\frac{1}{d}}$ where $|\Omega|$ is the volume of the domain Ω. We then introduce the nondimensional variables

$$\boldsymbol{x} = L^{-1} \boldsymbol{x}^*, \qquad t = \tau^{-1} t^*, \qquad \boldsymbol{u} = \frac{\tau}{L} \boldsymbol{u}^*, \qquad p = P^{-1} p^*, \qquad T = \theta^{-1} T^*, \tag{II.1}$$

where τ, P and θ are time, pressure and temperature scales to be determined (fixing τ and L as time and length scales immediately sets L/τ as the velocity scale). Substituting these choices into the above equations gives, after some manipulations,

$$\partial_t \boldsymbol{u} + \boldsymbol{u} \cdot \nabla \boldsymbol{u} + \frac{P\tau^2}{\rho L^2} \nabla p = \frac{\nu\tau}{L^2} \Delta \boldsymbol{u} + \frac{\alpha g \theta \tau^2}{L} T \boldsymbol{g}, \tag{II.2a}$$

$$\nabla \cdot \boldsymbol{u} = 0, \tag{II.2b}$$

$$\partial_t T + \boldsymbol{u} \cdot \nabla T = \frac{\tau\kappa}{L^2} \Delta T + \frac{\tau H}{\theta} f. \tag{II.2c}$$

Now choose $\tau = L^2/\kappa$ to be the diffusive timescale, $P = \rho L^2/\tau^2$ as the pressure scale, and $\theta = \tau H$ as the temperature scale. Consequently, the equations become

$$\partial_t \boldsymbol{u} + \boldsymbol{u} \cdot \nabla \boldsymbol{u} + \nabla p = \frac{\nu}{\kappa} \Delta \boldsymbol{u} + \left(\frac{\alpha g H L^5}{\kappa^2 \nu} \right) \left(\frac{\nu}{\kappa} \right) T \boldsymbol{g}, \tag{II.3a}$$

$$\nabla \cdot \boldsymbol{u} = 0, \tag{II.3b}$$

$$\partial_t T + \boldsymbol{u} \cdot \nabla T = \Delta T + f. \tag{II.3c}$$

Upon defining

$$Pr := \frac{\nu}{\kappa}, \quad R := \frac{\alpha g H L^5}{\kappa^2 \nu}, \tag{II.4}$$

we arrive at the standard nondimensional Boussinesq equations which we'll use throughout the dissertation:

$$\partial_t \boldsymbol{u} + \boldsymbol{u} \cdot \nabla \boldsymbol{u} + \nabla p = Pr \Delta \boldsymbol{u} + PrRT \boldsymbol{g}, \tag{II.5a}$$

$$\nabla \cdot \boldsymbol{u} = 0, \tag{II.5b}$$

$$\partial_t T + \boldsymbol{u} \cdot \nabla T = \Delta T + f \tag{II.5c}$$

in Ω with boundary conditions:

$$\boldsymbol{u} \cdot \hat{\boldsymbol{n}} = 0, \tag{II.6a}$$

$$\hat{\boldsymbol{n}} \cdot \nabla T = 0 \tag{II.6b}$$

at $\partial\Omega$.

2.2 Useful Notation

Here we summarize some common notational conventions that we'll use throughout the dissertation. We use $X \vee Y$ and $X \wedge Y$ for the maximum and minimum of two quantities. We write $X \lesssim Y$ if there is a constant C with $X \leq CY$, and $X \sim Y$ if $X \lesssim Y \lesssim X$. If the constant C depends on a parameter a, we indicate this by writing $X \lesssim_a Y$. The notation $X \ll Y$ means that $X/Y \to 0$ in a limit. Likewise, $o(X)$ is a quantity tending to zero upon division by X.

The d-dimensional volume of a set A is $|A|$. The average of φ over A is then

$$\fint_A \varphi \mathrm{d}\boldsymbol{x} = \frac{1}{|A|} \int_A \varphi \mathrm{d}\boldsymbol{x}.$$

The notations $\langle\varphi\rangle_\tau$ and $\langle\varphi\rangle$ give spatial-temporal averages over Ω and up to time τ, or across infinite time, respectively:

$$\langle\varphi\rangle_\tau = \fint_0^\tau \fint_\Omega \varphi(\boldsymbol{x}, t) \mathrm{d}\boldsymbol{x} \mathrm{d}t \quad \text{and} \quad \langle\varphi\rangle = \limsup_{\tau\to\infty} \langle\varphi\rangle_\tau .$$

We only use the limit superior long-time average.

As usual, $L^p(\Omega)$ is the space of functions whose p-th power is integrable on Ω. We write $H^1(\Omega)$ for the Sobolev space of functions in $L^2(\Omega)$ whose weak derivatives are in $L^2(\Omega)$. We use $H^{-1}(\Omega)$ for the space of continuous linear functionals on $H^1(\Omega)$ that are mean-free, meaning that they take

constant functions to zero, and define the dual norm

$$\|g\|_{H^{-1}(\Omega)} := \max_{\varphi(\boldsymbol{x})} \frac{\int_\Omega g\varphi \mathrm{d}\boldsymbol{x}}{\left(\int_\Omega |\nabla\varphi|^2 \mathrm{d}\boldsymbol{x}\right)^{\frac{1}{2}}} = \left(\int_\Omega \left|\nabla\Delta^{-1}g\right|^2 \mathrm{d}\boldsymbol{x}\right)^{\frac{1}{2}}. \tag{II.7}$$

This and other such maximizations are performed over non-constant $\varphi \in H^1(\Omega)$. Not every $g \in H^{-1}(\Omega)$ is a function, in which case the 'integral' $\int_\Omega g \cdot \mathrm{d}\boldsymbol{x}$ stands for the action of g as a functional. Hardy and BMO spaces will be used; see Section 3.3.1 for definitions and a brief review.

Finally, since this dissertation deals only with insulating temperature boundary conditions, we write Δ^{-1} for the inverse Laplacian operator with Neumann boundary conditions. In formulas, $h = \Delta^{-1}g$ if $⨍_\Omega h \mathrm{d}\boldsymbol{x} = 0$ and

$$\begin{cases} \Delta h = g & \text{in } \Omega \\ \hat{\boldsymbol{n}} \cdot \nabla h = 0 & \text{at } \partial\Omega \end{cases}.$$

2.3 Some Useful Lemmas

In this section, we present some useful inequalities we will use in the following sections.

Lemma 2.3.1. *Let $\Omega \subset \mathbb{R}^d$ be a bounded, Lipschitz domain. We have the following Poincaré-type inequality:*

$$\|\mathbf{u}\|_{L^2(\Omega)} \leq C(\Omega, d)\|\nabla\mathbf{u}\|_{L^2(\Omega)}$$

for all $\mathbf{u}$ satisfying the no-penetration boundary conditions $\mathbf{u}\cdot\hat{\mathbf{n}} = 0$ at $\partial\Omega$.

Proof. We prove this lemma by contradiction. Suppose there exists a sequence $\{\mathbf{u}_n\}_{n=1}^\infty$ such that

$$\|\mathbf{u}_n\|_{L^2(\Omega)} = 1 \quad \text{and} \quad \|\nabla\mathbf{u}_n\|_{L^2(\Omega)} \to 0$$

where the first statement holds for all n, and the second limiting statement holds as $n \to \infty$.

Applying the usual Poincaré inequality involving subtracting the mean, we get that

$$\|\mathbf{u}_n - \fint_\Omega \mathbf{u}_n\|_{L^2(\Omega)} \lesssim_{\Omega,d} \|\nabla \mathbf{u}_n\|_{L^2(\Omega)} \to 0.$$

Recall the normal trace map $\mathbf{u} \mapsto \mathbf{u} \cdot \hat{\mathbf{n}}$ maps $L^2(\Omega) \cap \{\boldsymbol{u} | \nabla \cdot \boldsymbol{u} = 0\} \to H^{-1/2}(\partial\Omega)$ continuously [GR86]. Therefore,

$$\| \fint_\Omega \mathbf{u}_n \cdot \hat{\mathbf{n}}\|_{H^{-1/2}(\partial\Omega)} \to 0$$

by the no-penetration boundary conditions on $\mathbf{u}_n$.

We claim this last line implies that

$$\fint_\Omega \mathbf{u}_n \to \mathbf{0}.$$

Since we are discussing the convergence of vectors in $\mathbb{R}^d$ to zero, and since all norms on finite dimensional space are equivalent, we must simply show that

$$\mathbf{c} \mapsto \|\mathbf{c} \cdot \hat{\mathbf{n}}\|_{H^{-1/2}(\partial\Omega)}$$

defines a norm on $\mathbb{R}^d$. The only non-obvious point to check is that if $\mathbf{c} \cdot \hat{\mathbf{n}} = 0$ as an element of $H^{-1/2}(\partial\Omega)$, then $\mathbf{c} = \mathbf{0}$. The former statement means that

$$\int_{\partial\Omega} \mathbf{c} \cdot \hat{\mathbf{n}}(x) \varphi(x) \, d\mathcal{H}^{d-1}(x) = 0$$

whenever $\varphi \in H^1(\Omega)$, since the dual $H^{1/2}(\partial\Omega)$ of $H^{-1/2}(\partial\Omega)$ is nothing other than the trace of $H^1(\Omega)$. In particular, we can work with $\varphi \in C^\infty(\overline{\Omega})$ in which case it becomes clear that all we are saying is that

$$\mathbf{c} \cdot \hat{\mathbf{n}} = 0 \quad \mathcal{H}^{d-1}\text{-a.e. on } \partial\Omega.$$

To conclude, we note that the outwards pointing unit normal $\hat{\mathbf{n}}$ to any bounded Lipschitz domain cannot be a.e. constant. Hence, $\mathbf{c}$ is perpendicular to a basis and it follows that $\mathbf{c} = \mathbf{0}$.

At this point, we have shown that

$$\mathbf{u}_n \to \mathbf{0} \quad \text{in } L^2(\Omega).$$

This is a contradiction, since we started by taking $\{\mathbf{u}_n\}$ to have L^2-norm equal to one for all n. This completes the proof of the desired Poincaré-type inequality.

□

Another inequality we use repeatedly is the div-curl inequality of Coifman, Lions, Meyers and Semmes [CLMS90] adapted to our no-penetration boundary conditions.

Lemma 2.3.2. *If $\boldsymbol{u}(\boldsymbol{x})$ and $\boldsymbol{v}(\boldsymbol{x})$ belong to $L^2(\Omega)$ with $\boldsymbol{u}$ being divergence-free, $\boldsymbol{u} \cdot \hat{\boldsymbol{n}} = 0$ at $\partial\Omega$, and $\boldsymbol{v}$ being curl-free, we have the following inequality:*

$$\|\boldsymbol{u} \cdot \boldsymbol{v}\|_{\mathcal{H}^1(\Omega)} \lesssim_{\Omega,d} \|\boldsymbol{u}\|_{L^2(\Omega)} \|\boldsymbol{v}\|_{L^2(\Omega)} \tag{II.8}$$

Proof. The original div-curl lemma of Coifman, Lions, Meyers and Semmes gives us

$$\|\boldsymbol{u} \cdot \boldsymbol{v}\|_{\mathcal{H}^1(\mathbb{R}^d)} \lesssim_d \|\boldsymbol{u}\|_{L^2(\mathbb{R}^d)} \|\boldsymbol{v}\|_{L^2(\mathbb{R}^d)}. \tag{II.9}$$

for $\boldsymbol{u}(\boldsymbol{x})$ and $\boldsymbol{v}(\boldsymbol{x})$ belonging to $L^2(\mathbb{R}^d; \mathbb{R}^d)$ satisfying divergence-free and curl-free conditions respectively. Note that as $\boldsymbol{u}$ satisfies no-penetration boundary conditions, we can extend $\boldsymbol{u}$ with $\mathbf{0}$ to $\mathbb{R}^d$ preserving divergence free condition. And for $\boldsymbol{v}$, note that as $\boldsymbol{v} = \nabla\varphi$ for some potential φ on Ω, we can apply Sobolev extension theorem to φ which gives us an extension $\tilde{\varphi}$ on $\mathbb{R}^d$ such that

$$\|\nabla\tilde{\varphi}\|_{L^2(\mathbb{R}^d)} \leq C(\Omega) \|\nabla\varphi\|_{L^2(\Omega)}.$$

Combining the above arguments, we have the inequality in the lemma.

□

2.4 Well-Posedness of the Problem

Looking back at the governing equations II.5 introduced in Section 2.1, before analyzing the relationship between $\boldsymbol{u}$ and T, one must first ask whether solutions are well-defined. To be more precise, we need to address the following three questions:

(i) How are the solutions defined (in the sense of weak solutions) ?

(ii) Does the weak solution exist?

(iii) Is the weak solution unique?

We study these questions for the advection-diffusion equation

$$\partial_t T + \boldsymbol{u} \cdot \nabla T = \Delta T + f \tag{II.10}$$

which is the core equation in our analysis. Other than the insulating and no-penetration boundary conditions II.6 introduced in Section 2.1, we will further assume the following mean-free conditions throughout the dissertation:

$$⨍_\Omega T(\boldsymbol{x}, t)\mathrm{d}\boldsymbol{x} = ⨍_\Omega f(\boldsymbol{x}, t)\mathrm{d}\boldsymbol{x} = 0$$

for all time $t > 0$.

Remark 2.4.1. If the velocity field $\boldsymbol{u}(\cdot, t) \in L^\infty(\Omega)$ for a.e. $t > 0$ with uniformly bounded spatial norm, the standard arguments for hyperbolic equations would ensure the existence and uniqueness of weak solutions [Eva10]. Our technical challenge is to adapt to the case where $\left\langle |\boldsymbol{u}|^2 \right\rangle < \infty$ and divergence-free. We'll be able to show weak solutions exist and are unique once we demand $T \in L^\infty(\Omega)$ for a.e. $t > 0$ so $\boldsymbol{u} \cdot \nabla T = \nabla \cdot (\boldsymbol{u}T)$ can be defined in the sense of distributions. The crucial steps in these arguments follow the "Neumann boundaries" analog of what is presented in the notes [KRR12].

Remark 2.4.2. As the problem we are dealing with is balanced heat transport with insulating boundary conditions, it may seem too much to assume T is mean-free. Actually, if we assume the

solutions exists and take the time derivative of spatial integral of T, plugging in equation II.10, we have

$$\begin{aligned}\partial_t\left(\int_\Omega T\mathrm{d}\boldsymbol{x}\right) &= \int_\Omega \partial_t T\mathrm{d}\boldsymbol{x} = \int_\Omega \Delta T\mathrm{d}\boldsymbol{x} + \int_\Omega f\mathrm{d}\boldsymbol{x} - \int_{\partial\Omega} \boldsymbol{u}\cdot\nabla T\mathrm{d}\boldsymbol{x} \\ &= \int_{\partial\Omega} \hat{\boldsymbol{n}}\cdot\nabla T\mathrm{d}s + \int_\Omega f\mathrm{d}\boldsymbol{x} - \int_{\partial\Omega} T\boldsymbol{u}\cdot\hat{\boldsymbol{n}}\mathrm{d}s = 0\end{aligned}$$

using divergence theorem. The last step follows from the insulation, no-penetration boundary conditions and f being mean-free. It follows that the spatial mean of T is constant for all time $t > 0$. So we may just assume T to be mean-free.

Remark 2.4.3. In the later chapters, we may add extra requirements on f or $\boldsymbol{u}$ when necessary, especially in Chapter V when doing prefactor analysis. However, the divergence-free conditions and boundary conditions in II.5 and II.6 will always remain active.

In the following subsections, we will define weak solutions in the usual ways and prove that under prescribed constraints on the heat profile f, we are able to ensure L^2 and L^∞ bounds of our temperature field T which guarantees the well-posedness of our problem via a common Galerkin approximation approach as used in [Eva10].

2.4.1 Weak Solutions and L^2 Estimates

In this subsection, we will start by introducing weak solutions and prove an L^2 estimate on T which is crucial in our variational principle analysis later in Chaper III.

As our velocity field is divergence free and we work under the assumption that $\left\langle|\boldsymbol{u}|^2\right\rangle < \infty$, we try to start with minimal regularity requirements on $\boldsymbol{u}$ and add necessary assumptions on the source function f to make sure we get wanted estimates.

Let $(\cdot,\cdot)$ denote the duality pairing between H^{-1} and H^1 that are mean-free introduced in Section 2.2. Adapting the definition from [Eva10], we say that

$$T \in L^2_{\text{loc}}([0,\infty); H^1(\Omega)) \quad \text{with} \quad \partial_t T \in L^2_{\text{loc}}([0,\infty); H^{-1}(\Omega)) \tag{II.11}$$

is a *weak solution* of the above PDE II.10 if

$$(\partial_t T, \varphi) + \int_\Omega (\nabla T - \mathbf{u}T) \cdot \nabla \varphi = (f, \varphi) \tag{II.12}$$

a.e. in time, for all $\varphi \in H^1(\Omega)$. The space $L^2_{\text{loc}}([0,\infty); H^1(\Omega))$ is defined to be the space of all strongly measurable functions $g : [0, T) \to H^1(\Omega)$ satisfying

$$\int_K \|g\|^2_{H^1(\Omega)} \mathrm{d}t < \infty$$

for any compact $K \subset [0,\infty)$. The definition of $L^2_{\text{loc}}([0,\infty); H^{-1}(\Omega))$ is similar with the H^1 norm inside the integrand replaced by the H^{-1} norm. When we encounter such spaces later on, we may use short hands $L^2_{t,loc}X_{\boldsymbol{x}}$ to denote functions that lies in spatial Banach space X for each time $t \in [0, T)$ satisfying the above integrable condition with the X norm in the integrand.

Note that the defining equation of weak solution in II.12 comes from multiplying II.10 by φ and integration by parts formally using divergence free and no-penetration boundary conditions. This technique is used commonly to define weak solutions which allows us to have weaker regularity restriction on the solution sets. It follows from usual arguments such as Section 5.9.2, Theorem 3 in [Eva10] that II.11 implies $T : [0,\infty) \to L^2(\Omega)$ is continuous, and hence we can impose initial data simply by requiring

$$\lim_{t\to 0} T(\cdot, t) = T_0 \in L^2(\Omega).$$

In the usual arguments from [Eva10], the coefficients $\boldsymbol{u}$ is assumed to be L^∞ bounded so that the integrations make sense. Since we wish to take $\boldsymbol{u} \in L^2_{t,\text{loc}}L^2_{\mathbf{x}}$, to make sure $\int_\Omega \mathbf{u}T \cdot \nabla T$ makes sense and

$$\int_\Omega \mathbf{u}T \cdot \nabla T = 0$$

we need

$$T(\cdot, t) \in L^\infty(\Omega) \quad \text{a.e. } t > 0.$$

This L^∞ bound would ensure the product $\mathbf{u}T \in L^2$ for $t > 0$ and thus the above integral makes sense. Eventually the L^∞-boundedness of solutions at positive times will be justified with an *a priori* estimate in the next Section 2.4.2. But first, we establish some standard estimates involving the L^2-norm of T.

Proposition 2.4.4. *Let T be the weak solution defined above satisfying II.11. Let $f \in L^2_{loc}([0,\infty); H^{-1}(\Omega))$ be such that*

$$\frac{1}{t}\int_0^t e^{-2\lambda_1(1-\frac{\epsilon}{2})(t-s)}||f(\cdot,s)||^2_{H^{-1}(\Omega)}\,ds \to 0 \quad \text{as } t \to \infty \tag{II.13}$$

for some $\epsilon > 0$ with λ_1 being the first non-trivial Neumann eigenvalue of the (negative) Laplacian on Ω (i.e., it is the largest constant such that $\lambda_1\|\theta\|^2_{L^2(\Omega)} \le \|\nabla\theta\|^2_{L^2(\Omega)}$ for all mean-zero $\theta \in H^1(\Omega)$). Then we have the following estimates on T:

$$\frac{d}{dt}||T||^2_{L^2(\Omega)} + 2(1-\frac{\epsilon}{2})||\nabla T||^2_{L^2(\Omega)} \le \frac{1}{\epsilon}||f||^2_{H^{-1}(\Omega)} \tag{II.14}$$

$$||T(\cdot,t)||^2_{L^2(\Omega)} \ll t \quad \text{as } t \to \infty. \tag{II.15}$$

Remark 2.4.5. Note that the condition II.13 holds for steady $f = f(\mathbf{x})$.

Proof. Using the H^{-1}-norm II.7, testing the equation II.12 by T at a.e. time shows that

$$\begin{aligned}\frac{d}{dt}\frac{1}{2}||T||^2_{L^2(\Omega)} + ||\nabla T||^2_{L^2(\Omega)} &= (f,T)\\ &\le ||f||_{H^{-1}(\Omega)}||\nabla T||_{L^2(\Omega)}\\ &\le \frac{1}{2\epsilon}||f||^2_{H^{-1}(\Omega)} + \frac{\epsilon}{2}||\nabla T||^2_{L^2(\Omega)}\end{aligned}$$

for any $\epsilon > 0$ and, upon rearrangement, we get the first bound on T:

$$\frac{d}{dt}||T||^2_{L^2(\Omega)} + 2(1-\frac{\epsilon}{2})||\nabla T||^2_{L^2(\Omega)} \le \frac{1}{\epsilon}||f||^2_{H^{-1}(\Omega)}$$

For the next bound, Poincaré's inequality states for our mean-zero temperature fields,

$$\lambda_1 ||T||^2_{L^2(\Omega)} \leq ||\nabla T||^2_{L^2(\Omega)}.$$

then we get

$$\frac{d}{dt}||T||^2_{L^2(\Omega)} + 2\lambda_1(1 - \frac{\epsilon}{2})||T||^2_{L^2(\Omega)} \leq \frac{1}{\epsilon}||f||^2_{H^{-1}(\Omega)}.$$

and integrating in the time domain from 0 to t gives

$$||T(\cdot,t)||^2_{L^2(\Omega)} \leq ||T(\cdot,0)||^2_{L^2(\Omega)} e^{-2\lambda_1(1-\frac{\epsilon}{2})t} + \frac{1}{\epsilon}\int_0^t e^{-2\lambda_1(1-\frac{\epsilon}{2})(t-s)}||f(\cdot,s)||^2_{H^{-1}(\Omega)}\, ds. \quad \text{(II.16)}$$

Then it follows from our assumption on f that

$$||T(\cdot,t)||^2_{L^2(\Omega)} \ll t \quad \text{as } t \to \infty.$$

□

Remark 2.4.6. Note that from the bound II.14, we see that

$$f \in L^2_{t,\text{loc}} H^{-1}_{\mathbf{x}} \implies T \in L^2_{t,\text{loc}} H^1_{\mathbf{x}}$$

and we will therefore assume that

$$f \in L^2_{\text{loc}}([0,\infty); H^{-1}(\Omega))$$

as this is consistent with the desired estimates on T.

Remark 2.4.7. The second bound II.15, though not an L^p bound, is a crucial bound we need in the later sections to make sure $\langle |\nabla T|^2 \rangle = \langle fT \rangle$ using integration by parts.

2.4.2 L^∞ Estimates

We now adapt Nash's argument as presented in Kiselev, Roquejoffre and Ryzhik's notes [KRR12] to produce a sufficient condition on f for controlling the L^∞-norm of a weak solution T.

Proposition 2.4.8. *Suppose the initial temperature $T_0 = T(\cdot, 0) \in L^2(\Omega)$ as we assumed in the previous sections, and the sink-source function f satisfies*

$$\int_0^t \frac{1}{(t-s)^{\frac{d}{2p}}} ||f(\cdot, s)||_{L^p(\Omega)}\, ds < \infty \quad \forall\, t > 0.$$

for some $p \in [d/2, \infty]$, then we have $T \in L^\infty(\Omega)$ for a.e. $t > 0$ and

$$||T(\cdot, t)||_{L^\infty(\Omega)} \lesssim_{\Omega, d} \frac{1}{t^{\frac{d}{2p}}} ||T_0||_{L^p(\Omega)} + \int_0^t \frac{1}{(t-s)^{\frac{d}{2p}}} ||f(\cdot, s)||_{L^p(\Omega)}\, ds. \tag{II.17}$$

Proof. Recall by Duhamel's principle,

$$T(\cdot, t) = S_{0,t} T_0 + \int_0^t S_{s,t} f(\cdot, t)\, ds$$

where $S_{s,t}$ denotes the forward-time solution operator from time s to time t, and $S_{s,t} g(\boldsymbol{x}, \tau)$ is defined by solving

$$\begin{cases} \partial_\tau w + \mathbf{u} \cdot \nabla w = \Delta w & \text{in } \Omega \times (s, t] \\ \hat{\mathbf{n}} \cdot \nabla w = 0 & \text{at } \partial\Omega \end{cases} \tag{II.18}$$

with $w(\cdot, s) = g(\cdot, s)$. Note that as our initial data are mean-free, we have the solution w is also mean-free. Therefore, taking spatial L^∞ norm on both sides,

$$||T(\cdot, t)||_{L^\infty(\Omega)} \leq ||S_{0,t} T_0||_{L^\infty(\Omega)} + \int_0^t ||S_{s,t} f(\cdot, t)||_{L^\infty(\Omega)}\, ds. \tag{II.19}$$

So if we can find an estimate of the forward time operator $S_{s,t}$ using initial data, we could get an L^∞ bound in terms of T_0 and f. Under our insulation boundary condition, using the parabolic

maximum principle result from [PW84], we have the following bound:

$$||S_{0,t}w||_{L^\infty(\Omega)} \leq ||w||_{L^\infty(\Omega)}.$$

If we can further show an $L^1 \to L^\infty$ bound of the operator $S_{s,t}$, we can use interpolation theorem to show $S_{s,t}$ being bounded from L^p to L^∞ for any $p \in (1, \infty)$.

Observe that

$$\|S_{0,t}\|_{L^1\to L^\infty} = \|S_{0,\frac{t}{2}}S_{0,\frac{t}{2}}\|_{L^1\to L^\infty} \leq \|S_{0,\frac{t}{2}}\|_{L^1\to L^2}\|S_{0,\frac{t}{2}}\|_{L^2\to L^\infty}. \tag{II.20}$$

Here, to simplify the proof, we use properties of adjoint operators.

Let $A : X_1 \to X_2$ be a linear map between Banach spaces X_1, X_2, and let

$$\langle \varphi, f \rangle_{X_i}$$

denote the action of functional $\varphi \in X_i^*$ on $f \in X_i$ for $i = 1, 2$ where X_i^* is the dual of X_i. We call $A^* : X_2^* \to X_1^*$ the adjoint of A induced by A in the sense that for any $\varphi \in X_2^*$ and $f \in X_1$, we have

$$\langle A^*\varphi, f \rangle_{X_1} = \langle \varphi, Af \rangle_{X_2}.$$

In our case, as the Banach spaces are L^p spaces, the action of functional on vectors can be identified with the spatial integral of their product. Note that from the definition of adjoint operators, it's follows that $(A^*)^*|_{X_i} = A$ and $\|(A^*)^*\|_{X_i} = \|A\|_{X_i}$.

Here we claim that the adjoint operator $S^*_{0,\frac{t}{2}}$ will have the same bound from L^1 to L^2 as $S_{0,\frac{t}{2}}$(to be proved later in Lemma 2.4.10), which implies

$$||S_{0,\frac{t}{2}}||_{L^2\to L^\infty} = ||(S^*_{0,\frac{t}{2}})^*||_{L^2\to L^\infty} = ||S^*_{0,\frac{t}{2}}||_{L^1\to L^2} = ||S_{0,\frac{t}{2}}||_{L^1\to L^2}. \tag{II.21}$$

The above result will reduce our problem to focus on the bound from L^1 to L^2. Now similar to the

L^2 estimate case, let's start with the defining equation for $S_{s,t}$ II.18. Multiplying both sides by w and integration by parts as usual, we get

$$\frac{d}{dt}\frac{1}{2}||w||^2_{L^2(\Omega)} \leq -||\nabla w||^2_{L^2(\Omega)}.$$

To introduce the L^1 norm into the inequality, we can use the Gagliardo–Nirenberg inequality which shows for all mean zero w that

$$||w||_{L^2(\Omega)} \lesssim_\Omega ||w||^\theta_{L^1(\Omega)}||\nabla w||^{1-\theta}_{L^2(\Omega)} \quad \text{with} \quad \theta = \frac{2}{2+d}.$$

Upon rearrangement,

$$||\nabla w||_{L^2(\Omega)} \gtrsim_\Omega \frac{||w||^{1+2/d}_{L^2(\Omega)}}{||w||^{2/d}_{L^1(\Omega)}}$$

and combining this with the differential inequality we conclude that

$$\frac{d}{dt}||w||^2_{L^2(\Omega)} \leq -C(\Omega)\frac{||w||^{2+4/d}_{L^2(\Omega)}}{||w||^{4/d}_{L^1(\Omega)}}.$$

Now let w_+, w_- be the positive and negative parts of w respectively which solves II.18 with their corresponding initial data. We would have

$$\frac{d}{dt}\int_\Omega w_\pm = 0$$

using divergence-free and Neumann boundary conditions. So we have the L^1 norm of w itself is conserved, i.e.,

$$||w(\cdot,t)||_{L^1(\Omega)} = ||w(\cdot,0)||_{L^1(\Omega)} \quad \text{a.e. } t > 0.$$

Hence,

$$\frac{d}{dt}||w||^2_{L^2(\Omega)} \leq -C(\Omega)\frac{||w||^{2+4/d}_{L^2(\Omega)}}{||w(\cdot,0)||^{4/d}_{L^1(\Omega)}}.$$

Now if we call

$$X(t) = ||w(\cdot, t)||^2_{L^2(\Omega)}$$

we have shown the differential inequality

$$X' \leq -cX^{1+2/d} \quad \text{with} \quad c = \frac{C(\Omega)}{||T(\cdot, 0)||^{4/d}_{L^1(\Omega)}}.$$

Integrating this up from 0 to t yields that

$$\frac{1}{X^{2/d}(t)} \geq \frac{2}{d}ct + \frac{1}{X^{2/d}(0)}.$$

Note that

$$\frac{1}{X^{2/d}(0)} = \frac{1}{||w(\cdot, 0)||^{4/d}_{L^2(\Omega)}} \lesssim_{\Omega,d} \frac{1}{||w(\cdot, 0)||^{4/d}_{L^1(\Omega)}} = \frac{c}{C(\Omega)}.$$

Hence,

$$X(t) \lesssim_d \frac{1}{c^{d/2}t^{d/2}}.$$

Unpacking the definitions shows that

$$||w(\cdot, t)||^2_{L^2(\Omega)} \lesssim_{\Omega,d} \frac{1}{t^{d/2}}||w(\cdot, 0)||^2_{L^1(\Omega)}$$

which says

$$||S_{0,t}w||_{L^2(\Omega)} \lesssim_{\Omega,d} \frac{1}{t^{\frac{d}{4}}}||w(\cdot, 0)||_{L^1(\Omega)}.$$

Plugging into II.20 and using II.21, we get

$$||S_{0,t}w||_{L^\infty(\Omega)} \lesssim_{\Omega,d} \frac{1}{t^{\frac{d}{2}}}||w(\cdot, 0)||_{L^1(\Omega)}.$$

Then interpolation (Riesz-Thorin) theorem tells us that

$$||S_{0,t}w||_{L^\infty(\Omega)} \lesssim_{\Omega,d} \frac{1}{t^{\frac{d}{2p}}}||w||_{L^p(\Omega)}$$

for all $p \in (1, \infty)$.

Using the above estimate in II.19, we have

$$||T(\cdot,t)||_{L^\infty(\Omega)} \lesssim_{\Omega,d} \frac{1}{t^{\frac{d}{2p}}}||T_0||_{L^p(\Omega)} + \int_0^t \frac{1}{(t-s)^{\frac{d}{2p}}}||f(\cdot,s)||_{L^p(\Omega)}\, ds.$$

Of course, the first term remains bounded since we will anyways take $T_0 \in L^2(\Omega) \subset L^1(\Omega)$. The second term remains bounded by our our assumption on f.

□

Looking at the integrand in the above inequality, it seems that the assumption rests crucially on what happens for $s \approx t$. So we may improve our L^∞ estimate to emphasize the significance of taking $s \approx t$.

Corollary 2.4.9. *Instead of the assumption on f in the above result, we may impose the following weaker assumption on f:*

$$\int_0^t \frac{e^{-(1-\epsilon)\lambda_1(t-s)}}{(t-s)^{\frac{d}{2p}}}||f(\cdot,s)||_{L^p(\Omega)}\, ds < \infty \quad \forall\, t > 0$$

for some $\epsilon \in (0,1)$ and $p \in [d/2, \infty)$ which again gives us an L^∞ estimate:

$$||T(\cdot,t)||_{L^\infty(\Omega)} \lesssim_{\Omega,d} \frac{e^{-(1-\epsilon)\lambda_1 t}}{\epsilon^{\frac{d}{2p}} t^{\frac{d}{2p}}}||T_0||_{L^p(\Omega)} + \int_0^t \frac{e^{-(1-\epsilon)\lambda_1(t-s)}}{\epsilon^{\frac{d}{2p}}(t-s)^{\frac{d}{2p}}}||f(\cdot,s)||_{L^p(\Omega)}\, ds.$$

Proof. Using the exponential decay in L^2 of solutions established in the previous subsection II.16 on the homogeneous system II.18, taking $\epsilon \to 0$, we get

$$||S_{0,t}w||_{L^2(\Omega)} = ||w(\cdot,t)||_{L^2(\Omega)} \leq ||w(\cdot,0)||_{L^2(\Omega)} e^{-\lambda_1 t}.$$

Here, we use this by writing, for any $\epsilon \in (0,1)$

$$S_{0,t} = S_{t-t\epsilon/2,t} S_{t\epsilon/2,t-t\epsilon/2} S_{0,t\epsilon/2}$$

and applying the bounds

$$||S_{t-t\epsilon/2,t}||_{L^2 \to L^\infty} \vee ||S_{0,t\epsilon/2}||_{L^1 \to L^2} \lesssim_{\Omega,d} \frac{1}{t^{\frac{d}{4}} \epsilon^{\frac{d}{4}}} \quad \text{and} \quad ||S_{\frac{t}{3},\frac{2t}{3}}||_{L^2 \to L^2} \leq e^{-(1-\epsilon)\lambda_1 t}$$

the third of which is our exponential decay estimate in L^2. Thus,

$$||S_{0,t}||_{L^1 \to L^\infty} \lesssim_{\Omega,d} \frac{e^{-(1-\epsilon)\lambda_1 t}}{\epsilon^{\frac{d}{2}} t^{\frac{d}{2}}}$$

emphasizing the importance of $t \approx 0$. Now the conclusion is that

$$||T(\cdot,t)||_{L^\infty(\Omega)} \lesssim_{\Omega,d} \frac{e^{-(1-\epsilon)\lambda_1 t}}{\epsilon^{\frac{d}{2p}} t^{\frac{d}{2p}}} ||T_0||_{L^p(\Omega)} + \int_0^t \frac{e^{-(1-\epsilon)\lambda_1 (t-s)}}{\epsilon^{\frac{d}{2p}} (t-s)^{\frac{d}{2p}}} ||f(\cdot,s)||_{L^p(\Omega)}\, ds.$$

This allows us to assume the existence of some $a \in (0,1)$ and $p \in [d/2, \infty]$ such that

$$\int_0^t \frac{e^{-a\lambda_1 (t-s)}}{(t-s)^{\frac{d}{2p}}} ||f(\cdot,s)||_{L^p(\Omega)}\, ds < \infty \quad \forall\, t > 0$$

in order to guarantee the desired L^∞ bound. □

Finally, we discuss the adjoint operator $S^*_{0,t}$ and prove the bound we claimed in II.21.

Lemma 2.4.10. *Let $S_{0,t}$ be the operator defined in II.18, we have the adjoint operator $S^*_{0,t}$ satisfies the same bound as $S_{0,t}$ from $L^1(\Omega)$ to $L^2(\Omega)$.*

Proof. Let φ be solutions of II.18 with initial conditions $\varphi(\cdot,0) = f(\cdot)$. And let ψ be the solution

to the following equation:

$$\begin{cases} \partial_\tau \psi(\cdot,\tau) - \mathbf{u}(\cdot, t-\tau)\cdot\nabla w(\cdot,\tau) = \Delta w(\cdot,\tau) & \text{in } \Omega\times(0,t] \\ \hat{\mathbf{n}}\cdot\nabla w = 0 & \text{at } \partial\Omega \end{cases} \tag{II.22}$$

with initial condition $\psi(\cdot,0) = g(\cdot,0)$. Note that as $\boldsymbol{u}$ is divergence-free, we have $-\mathbf{u}(\cdot,t-\tau)$ is still divergence-free. Treating $-\mathbf{u}(\cdot,t-\tau)$ as another divergence-free velocity field, all the results we have proved for II.18 still applies to the above equation. So as long as we can show that the above equation defines adjoint operator $S^*(0,t)$, our claim is proved. To show II.22 gives us the adjoint operator $S^*(0,t)$, it suffices to show that

$$\int_\Omega g(\boldsymbol{x})\varphi(\boldsymbol{x},t)\mathrm{d}\boldsymbol{x} = \int_\Omega f(\boldsymbol{x})\psi(\boldsymbol{x},t)\mathrm{d}\boldsymbol{x}.$$

Let

$$B(s) = \int_\Omega \psi(\boldsymbol{x},t-s)\varphi(\boldsymbol{x},s)\mathrm{d}\boldsymbol{x}$$

then taking time derivative and plugging in II.18 and II.22, we get

$$\begin{aligned} \frac{dB}{ds} &= \int_\Omega \psi(\boldsymbol{x},t-s)\left(\Delta\varphi(\boldsymbol{x},s) - \boldsymbol{u}(\boldsymbol{x},s)\cdot\nabla\varphi(\boldsymbol{x},s)\right)\mathrm{d}\boldsymbol{x} \\ &\quad - \int_\Omega \left(\Delta\psi(\boldsymbol{x},t-s) + \boldsymbol{u}(\boldsymbol{x},s)\cdot\nabla\psi(\boldsymbol{x},t-s)\right)\varphi(\boldsymbol{x},s)\mathrm{d}\boldsymbol{x} \\ &= \int_\Omega -\nabla\psi(\boldsymbol{x},t-s)\cdot\left(\nabla\varphi(\boldsymbol{x},s) - \boldsymbol{u}(\boldsymbol{x},s)\varphi(\boldsymbol{x},s)\right)\mathrm{d}\boldsymbol{x} \\ &\quad + \int_\Omega \left(\nabla\psi(\boldsymbol{x},t-s) + \boldsymbol{u}(\boldsymbol{x},s)\psi(\boldsymbol{x},t-s)\right)\cdot\nabla\varphi(\boldsymbol{x},s)\mathrm{d}\boldsymbol{x} \\ &= \int_\Omega \nabla\cdot\left(\boldsymbol{u}\varphi\psi\right)\mathrm{d}\boldsymbol{x} = 0 \end{aligned}$$

where the last step follows from divergence theorem and $\boldsymbol{u}$ being divergence-free with no-penetration

conditions. So we have

$$\int_\Omega g(\boldsymbol{x})\varphi(\boldsymbol{x},t)\mathrm{d}\boldsymbol{x} = B(t) = B(0) = \int_\Omega f(\boldsymbol{x})\psi(\boldsymbol{x},t)\mathrm{d}\boldsymbol{x}$$

as wanted and the result follows. □

2.4.3 Existence and Uniqueness of Weak Solutions

Recall

$$(\partial_t T, \varphi) + \int_\Omega (\nabla T - \mathbf{u}T)\cdot\nabla\varphi = (f,\varphi). \tag{II.23}$$

To show existence of weak solutions, we first show a sequence of approximation of solutions exists and then show the sequence has converging subsequence with limit satisfying II.23. This is the classical Galerkin approximation method. Throughout this subsection, we assume the velocity field $\boldsymbol{u} \in L^2_{t,\text{loc}}L^2_{\mathbf{x}}$ and heat profile satisfies

$$\lim_{\tau\to\infty}\frac{1}{\tau}\int_0^\tau e^{-2a_0\lambda_1(\tau-t)}\|f(\cdot,t)\|^2_{H^{-1}(\Omega)}\,\mathrm{d}t = 0$$
$$\text{and}\quad \int_0^\tau \frac{e^{-a_1\lambda_1(\tau-t)}}{(\tau-t)^{\frac{d}{2p}}}\|f(\cdot,t)\|_{L^p(\Omega)}\,dt < \infty \quad \forall\,\tau>0$$

for $a_0, a_1 \in (0,1)$ and $p \in [d/2,\infty]$ so that the L^2 and L^∞ estimates 2.4.4, 2.4.9 can be taken for granted.

Let $\{\phi_n\}_{n=1}^\infty$ be an orthogonal basis of $H^1(\Omega)$ and an orthonormal basis of $L^2(\Omega)$. Fixing an initial temperature $T_0 \in H^1(\Omega)\cap L^\infty(\Omega)$, we have a result regarding approximation of solutions:

Lemma 2.4.11. *For each integer $n \geq 1$, we can find functions $T_n : [0,T] \to H^1(\Omega)$ of form:*

$$T_n(t) = \sum_{k=1}^n c_n^k(t)\phi_k \tag{II.24}$$

satisfying

$$(\partial_t T_n, \phi_k) + \int_\Omega (\nabla T_n - \mathbf{u} T_n) \cdot \nabla \phi_k = (f, \phi_k), \tag{II.25}$$

$$c_n^k(0) = (T_0, \phi_k) \tag{II.26}$$

for $k = 1, \cdots, n$.

Proof. Plugging II.24 into II.25, we get a linear system of initial value ODEs which has unique absolutely continuous solutions for a.e. $0 < t < T$ according to standard existence theory for ODEs. So we have the approximate solutions exist. □

With the above sequence of approximate solutions, we can show existence and uniqueness:

Theorem 2.4.12. *The sequence of solutions constructed in Lemma 2.4.11 has a convergent subsequence whose limit gives us a weak solution of II.23.*

Proof. As the heat profile f satisfies the assumptions of Propositions 2.4.4, 2.4.8, the proof in the propositions can be easily modified to show the sequence of solutions $\{T_n\}_{n=1}^\infty$ are bounded uniformly in $L^2_{\text{loc}}([0,\infty); H^1(\Omega) \cap L^\infty(\Omega))$. To see $\{\partial_t T_n\}_{n=1}^\infty$ are also bounded in $L^2_{\text{loc}}([0,\infty); H^{-1}(\Omega))$, consider any fixed integer n and $\phi \in H^1(\Omega)$. Suppose $\|\nabla \phi\|_{L^2(\Omega)} = 1$. Let ϕ^1 be the projection of ϕ onto the linear subspace spanned by $\{\phi_k\}_{k=1}^n$. Then we have

$$(\partial_t T_n, \phi) = (\partial_t T_n, \phi^1) = (f, \phi^1) - \int_\Omega (\nabla T_n - \mathbf{u} T_n) \cdot \nabla \phi^1.$$

Taking absolute value on both sides gives

$$|(\partial_t T_n, \phi)| \leq C(\|f\|_{H^{-1}(\Omega)} + \|T_n\|_{H^1(\Omega)} + \|T_n\|_{L^\infty(\Omega)})$$

which implies

$$\|\partial_t T_n\|_{H^{-1}(\Omega)} \leq C(\|f\|_{H^{-1}(\Omega)} + \|T_n\|_{H^1(\Omega)} + \|T_n\|_{L^\infty(\Omega)}).$$

As $T_n \in L^2_{\text{loc}}([0,\infty); H^1(\Omega) \cap L^\infty(\Omega))$, taking time integral on any compact time set on both sides shows $\{\partial T_n\}_{n=1}^\infty \in L^2_{\text{loc}}([0,\infty); H^{-1}(\Omega))$. Thus we can find subsequence converging weakly to some $T \in L^2_{\text{loc}}([0,\infty); H^1(\Omega) \cap L^\infty(\Omega))$ with the time derivative of the subsequence converging weakly to $\partial T \in L^2_{\text{loc}}([0,\infty); H^{-1}(\Omega))$. For simplicity, let's still denote the subsequence by $\{T_n\}_{n=1}^\infty$.

Now for any fixed integer $N > 0$, find $\varphi \in C^1([0,\infty); H^1(\Omega))$, such that $\varphi = \sum_{k=1}^N d_k(t)\phi_k$. Then we would have

$$(\partial_t T_m, \varphi) + \int_\Omega (\nabla T_m - \mathbf{u} T_m) \cdot \nabla \varphi = (f, \varphi)$$

for all $m \geq N$. Passing to the limit gives us

$$(\partial_t T, \varphi) + \int_\Omega (\nabla T - \mathbf{u} T) \cdot \nabla \varphi = (f, \varphi).$$

As such φ is dense in $L^2_{\text{loc}}([0,\infty); H^1(\Omega))$, the above equality holds for any $\varphi \in L^2_{\text{loc}}([0,\infty); H^1(\Omega))$.

Now, let $\varphi_0 := \varphi(\boldsymbol{x}, 0)$, where $\varphi \in C^1([0,\infty); H^1(\Omega))$ and $\varphi(\cdot, T) = 0$, we have

$$-(T_m, \partial\varphi) + \int_\Omega (\nabla T_m - \mathbf{u} T) \cdot \nabla \varphi = (f, \varphi) + (T_m(\cdot, 0), \varphi_0)$$
$$-(T, \partial\varphi) + \int_\Omega (\nabla T - \mathbf{u} T) \cdot \nabla \varphi = (f, \varphi) + (T(\cdot, 0), \varphi_0)$$

Passing to the limit in the first equation shows $T(\cdot, 0) = T_0$ as such φ_0 are dense in $H^1(\Omega)$. And a weak solution has been found. □

The uniqueness follows easily from our L^∞ estimates as $T_0 = f = 0$ would imply $T = 0$. So now we've shown the problem we study is well-posed.

CHAPTER III

Balanced Heat Transfer

Having setup the base for our study, we describe our results for balanced heat transfer on internally heated domains from [SFT23]. We'll show a variational principle for a rather general set of heat profiles and demonstrate the sharpness of the dominant heat transfer up to a prefactor using a periodic heat profile and a concentrated profile. In the later example, we introduce the idea of the 'pinching' flow design which also plays an important role when optimizing the prefactors in later chapters.

The present chapter is joint work with G. Fantuzzi and I. Tobasco. [SFT23]

3.1 Introduction

Determining absolute limits on heat transport by a moving fluid is a fundamental scientific challenge. It is motivated not only by questions of planetary physics, e.g., where convection driven by radioactive decay influences plate tectonics and the generation of magnetic fields [MB20, STO01], but also by the search for optimal heat exchangers [Alb17, FADJ21]. Internally heated flows have recently attracted renewed interest after experiments and numerical simulations [LAG18, BLAG19, KGOM22] revealed that their heat transport can significantly exceed the known limits on 'ordinary' boundary-driven (Rayleigh–Bénard) convection. For certain well-balanced source–sink profiles of internal heating and cooling, the flows that set up in response to gravity appear to transport heat at a rate independent of the molecular diffusivity, achieving the 'mixing-length' or 'ultimate' transport scaling. However, it remains a challenge to determine theoretically which properties of the internal heating are crucial to achieving highly efficient transport. Indeed, for an arbitrary balanced

source–sink profile in an arbitrary fluid domain, it is not at all clear from the outset what transport will result.

Thinking of the general question of assessing heat transport across a fluid domain, the first challenge is to select a globally-defined yet meaningful diagnostic measure of transport efficiency. Many known quantities that give equivalent measures for boundary-driven convection are no longer comparable for internally heated flows, and can end up following different scaling laws. We choose to measure heat transport using the mean-squared temperature gradient averaged over space and time. Since by Fourier's law the diffusive heat flux is controlled by the temperature gradient, it is reasonable to expect that a highly efficient transfer protocol finds a way to minimize temperature gradients overall. Other authors have studied the mean temperature [LDB04, GS12, Gol15, WD11, WD12], root-mean-squared temperature [LAG18, BLAG19, MLBG19] or vertical heat flux [AFCW21, AFCW22, KAF$^+$22]. For particular choices of source–sink distributions and boundary conditions such quantities are equivalent to our measure [Gol16], but this is not generally true.

Having selected a measure of transport, one can seek flows optimizing its value, subject to various constraints. A tractable goal for analysis, that we pursue in this paper, is to produce *a priori* bounds on transport holding for general classes of admissible flows. In particular, we shall derive a lower bound on the mean thermal dissipation of an internally heated flow, which takes into account its mean kinetic energy as well as the shape of the imposed source–sink distribution and the flow domain. We also derive a similar bound holding for buoyancy-driven internally heated convection. We work with balanced source–sink distributions that add and subtract the same amount of heat overall. The case of imbalanced heating has been studied extensively in the literature: bounds on measures of heat transport are known for uniform internal heating under a variety of boundary conditions [LDB04, GS12, Gol15, WD11, WD12, Gol16], as well as for essentially arbitrary source–sink distributions in a disc with a constant temperature boundary [Tob22]. Bounds on balanced heat transfer have also been obtained, for periodic flows under an assumption of statistical homogeneity and isotropy [STD07, TDG04, DT06, TP08], and for smooth source–sink

distributions that vary only in the gravity direction across a fluid layer [MLBG19]. Here, we treat a much broader class of velocities, source–sink functions and flow domains. We also give examples illustrating the sharpness of our bounds.

There are various approaches to *a priori* bounds in fluid mechanics, but for buoyancy-driven convection the relevant results can be traced back at least to the work of Malkus, Howard and Busse [Mal54, How63, Bus69, How72, Bus79] as well as to the 'background method' of Doering and Constantin [DC94, CD95, DC96]. We follow a two-step approach that is similar to the 'optimal wall-to-wall' approach of [HCD14, TD, DT19], and also to an approach that has been used with horizontal convection [SKB04, WY09, RBLY19]. First, we drop the momentum equation and optimize heat transfer subject to the advection-diffusion equation alone. The resulting optimal transfer rate depends on the advective intensity, measured in a chosen norm. Then, we restore the momentum equation via a balance law relating the velocity norm to an appropriate Rayleigh number. Algebraic manipulation leads to an *a priori* bound on the heat transport of momentum-conserving flows.

Using our setups in Section 2.1, let $\Omega \subset \mathbb{R}^d$ be a bounded Lipschitz domain in dimension $d \geq 2$, and introduce a temperature field $T(\boldsymbol{x}, t)$ solving the inhomogeneous and non-dimensional advection-diffusion equation with insulating boundary conditions

$$\begin{cases} \partial_t T + \boldsymbol{u} \cdot \nabla T = \Delta T + f & \text{in } \Omega, \\ \hat{\boldsymbol{n}} \cdot \nabla T = 0 & \text{at } \partial\Omega. \end{cases} \tag{III.1}$$

To ensure the source–sink function $f(\boldsymbol{x}, t)$ is balanced, we set

$$\fint_\Omega f(\boldsymbol{x}, t) \mathrm{d}\boldsymbol{x} = 0$$

where $\fint_\Omega \cdot \mathrm{d}\boldsymbol{x}$ denotes averaging over the flow domain (per the notation in Section 2.2). The advecting velocity $\boldsymbol{u}(\boldsymbol{x}, t)$ obeys the divergence-free condition $\nabla \cdot \boldsymbol{u} = 0$ in Ω, along with the no-penetration boundary conditions $\boldsymbol{u} \cdot \hat{\boldsymbol{n}} = 0$ at $\partial\Omega$. Note $\hat{\boldsymbol{n}}$ is the outwards-pointing unit normal

to the domain boundary. These conditions on f and $\boldsymbol{u}$ imply that the mean temperature $\fint_\Omega T \mathrm{d}\boldsymbol{x}$ is constant in time, and we take it to be zero without loss of generality.

Given this setup, we seek bounds on the mean-squared temperature gradient

$$\langle |\nabla T|^2 \rangle := \limsup_{\tau\to\infty} \fint_0^\tau \fint_\Omega |\nabla T(\boldsymbol{x},t)|^2 \,\mathrm{d}\boldsymbol{x}\mathrm{d}t$$

where for definiteness we use the limit superior. In Section 3.2, we derive a pair of 'variational' upper and lower bounds:

$$\left\langle 2f\xi - |\nabla\xi|^2 - |\nabla\Delta^{-1}(\partial_t\xi + \boldsymbol{u}\cdot\nabla\xi)|^2 \right\rangle \le \left\langle |\nabla T|^2 \right\rangle \le \left\langle |\nabla\eta|^2 + |\nabla\Delta^{-1}(\partial_t\eta + \boldsymbol{u}\cdot\nabla\eta - f)|^2 \right\rangle \tag{III.2}$$

where $\xi(\boldsymbol{x},t)$ and $\eta(\boldsymbol{x},t)$ are test functions whose choice can be optimized (see 3.2.1). The operator Δ^{-1} is the Neumann inverse Laplacian, defined in Section 2.2. A version of our lower bound on $\langle |\nabla T|^2 \rangle$ with a steady test function $\xi(\boldsymbol{x})$ appeared in a previous paper on mixing in periodic domains [STD07], along with similar bounds on $\langle T^2 \rangle$ and $\langle |\nabla\Delta^{-1}T|^2 \rangle$ (see also [TDG04, DT06, TP08] and [Thi12] for a review). To complete the picture, we allow for time-dependent test functions defined on general domains, and also provide the complementary upper bound in III.2. Moreover, we prove in 3.2.4 that these bounds are sharp in the steady case $f = f(\boldsymbol{x})$ and $\boldsymbol{u} = \boldsymbol{u}(\boldsymbol{x})$, meaning that an optimal choice of test function evaluates $\langle |\nabla T|^2 \rangle$. This is the analog of results obtained in [TD, DT19, STD20] for boundary-driven flows and in [Tob22] for internally-heated flows with cooled boundaries. Rather than repeat the 'symmetrization argument' from these papers, we present a different and likely more flexible proof in which the test functions are introduced as Lagrange multipliers for enforcing the advection-diffusion equation (much like the argument in [STD07]).

Section 3.3, 3.4 go on to ask what the variational bounds III.2 imply for optimal flows. By optimal, we mean flows that minimize $\langle |\nabla T|^2 \rangle$ subject to a constraint on the flow intensity, such as might be given by fixing the value of the mean kinetic energy $\langle |\boldsymbol{u}|^2 \rangle$. To ease the presentation, we treat steady source–sink functions $f(\boldsymbol{x})$ that are not identically zero from here on; we expect our results can be extended to unsteady sources/sinks, and we remark on this below. Sec 3.3 starts by

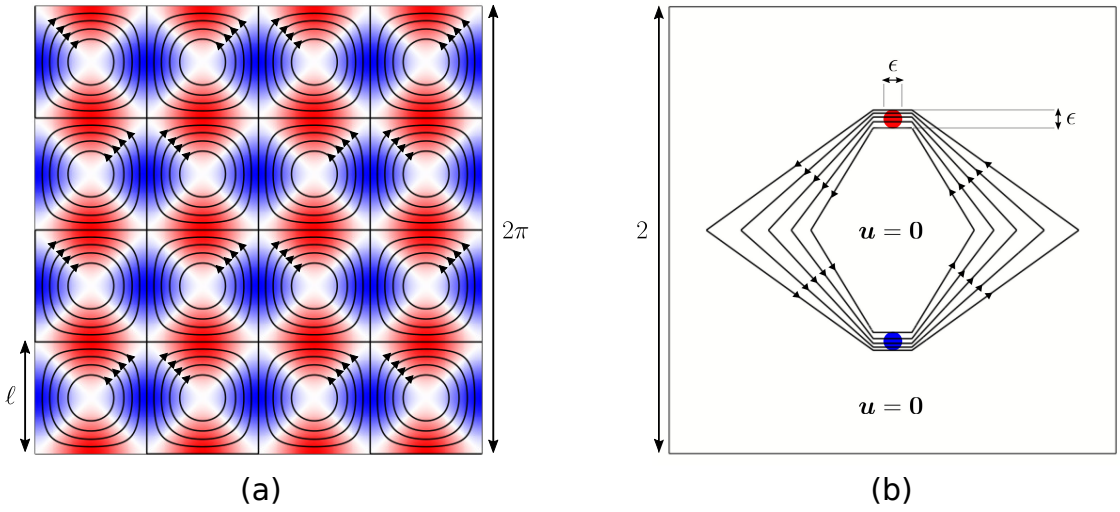

Figure III.1: Examples of nearly optimal flows. Heat sources (red) and sinks (blue) oscillate sinusoidally on a scale $\sim \ell$ in (a) and are concentrated in regions of size $\sim \epsilon$ in (b). Black lines with arrows show streamlines of the cellular flow achieving $\langle|\nabla T|^2\rangle \sim Pe^{-2}$ in (a) and of the 'pinching' flow achieving $\langle|\nabla T|^2\rangle \sim \log^2(\epsilon^{-1})\, Pe^{-2}$ in (b). The squared Péclet number Pe^2 sets the kinetic energy of the flows.

bounding $\langle|\nabla T|^2\rangle$ in terms of the mean kinetic energy: we show that there are positive constants C_1, C_2 and C_3 depending on the domain Ω, the dimension d and the source–sink distribution f such that

$$\langle|\nabla T|^2\rangle \geq \frac{C_1}{C_2 + C_3\langle|\boldsymbol{u}|^2\rangle}. \tag{III.3}$$

This follows from 3.3.1 and the subsequent discussion on how to select ξ. A similar bound was proved in [STD07, DT06, Thi12] for periodic and statistically homogeneous, isotropic flows.

We too think of the ratios C_1/C_2 and C_1/C_3 as (squared) norms that detect the structure of the sources and sinks. In the conductive limit $\langle|\boldsymbol{u}|^2\rangle \to 0$, the first ratio dominates the bound and can be chosen, as usual, to involve a negative Sobolev norm (see III.24). In the advective limit $\langle|\boldsymbol{u}|^2\rangle \to \infty$ the second ratio is more important; we explain how to choose it based on a Hardy space norm (see III.25). While this norm is not completely unlike the L^1-norm, it produces a strictly better bound for problems with point-like sources and sinks. See Section 3.3.1 for its definition, and Section 3.3.2 for the proof of III.3.

To help clarify our lower bound, and to explain what it takes to find optimal (or at least nearly

optimal) flows, we study a pair of examples in Section 3.3.3 involving sinusoidal heating and cooling or approximate point sources and sinks. Figure III.1 illustrates the setups we have in mind: the heating/cooling in panel (a) varies sinusoidally on a scale $\sim l$; the point-like sources and sinks in panel (b) are concentrated in regions of size $\sim \epsilon$ (the figure shows discs for simplicity). Given these setups, we prove upper and lower bounds on the minimum mean-square temperature gradient that match in terms of their scalings with respect to each example's parameters. Precisely, we show that

$$\min_{\substack{\boldsymbol{u}(\boldsymbol{x},t) \\ \langle|\boldsymbol{u}|^2\rangle \le Pe^2 \\ \partial_t T + \boldsymbol{u}\cdot\nabla T = \Delta T + f}} \langle|\nabla T|^2\rangle \sim \begin{cases} \min\left\{\ell^2, \frac{1}{Pe^2}\right\} & \text{for sinusoidal heating (3.3.3)} \\ \min\left\{\log\frac{1}{\epsilon},\ \left(\log\frac{1}{\epsilon}\right)^2 \frac{1}{Pe^2}\right\} & \text{for concentrated heating (3.3.4)} \end{cases} \tag{III.4}$$

with prefactors that are independent of all parameters. (The notation $X \sim Y$ means that there are numerical constants $C, C' > 0$ such that $CY \le X \le C'Y$). Parsing III.3 in each example produces the lower bound half of III.4. For the matching upper bounds, we construct the flows illustrated in Figure III.1 and select test functions η to estimate their transport via III.2. We use a cellular flow structure for sinusoidal heating and a pinching effect for approximate point sources and sinks. It was the analysis of pinching flows that led us to the Hardy space norm; other, more familiar norms gave strictly sub-optimal bounds.

The search for flows optimizing heat transfer is an active area of research; see [Tob22, MDTY17, IV22] for flows enhancing heat transport with imbalanced heating, and [INRZ10] for flows inhibiting heat transport in non-disc domains. In this section, we base our constructions on an ability to solve the pure and steady advection system

$$\begin{cases} \boldsymbol{u}_0 \cdot \nabla T_0 = f & \text{in } \Omega \\ \nabla \cdot \boldsymbol{u}_0 = 0 & \text{in } \Omega \\ \boldsymbol{u}_0 \cdot \hat{\boldsymbol{n}} = 0 & \text{at } \partial\Omega \end{cases} . \tag{III.5}$$

Though understanding precisely when this system has a solution is a difficult and open problem (see

[Lin17] for a recent account), it is not so difficult to show its relevance for optimizing heat transfer in the advective limit. Section 3.4 studies this limit in detail, and achieves the following conditional result: if III.5 admits a (regular-enough) solution, then

$$\lim_{\mathit{Pe}\to\infty} \min_{\substack{\boldsymbol{u}(\boldsymbol{x}) \\ \|\boldsymbol{u}\|_X \le \mathit{Pe} \\ \boldsymbol{u}\cdot\nabla T = \Delta T + f}} \mathit{Pe}^2 \fint_\Omega |\nabla T|^2 \mathrm{d}\boldsymbol{x} = \min_{\substack{\boldsymbol{u}_0(\boldsymbol{x}), T_0(\boldsymbol{x}) \\ \|\boldsymbol{u}_0\|_X \le 1 \\ \boldsymbol{u}_0\cdot\nabla T_0 = f}} \fint_\Omega |\nabla T_0|^2 \mathrm{d}\boldsymbol{x}.$$

In the right-hand problem, the minimization is over all solutions of III.5. After a rescaling, its optimizers give the limit points of almost-minimizing sequences on the left; see 3.4.2 for the precise statement. Here, we allow for general families of steady velocities belonging to a Banach space X that is continuously embedded into $L^d(\Omega)$, amongst other requirements. The dimensionless parameter $\mathit{Pe} = U^2 L/\kappa$ is the Péclet number, where U is a characteristic velocity scale, L is a characteristic lengthscale and κ is the thermal diffusivity. The result captures the intuition that optimal velocities find a way to minimize thermal dissipation while achieving (essentially) perfect advection, and shows how to compute the optimal prefactor in the scaling law $\min \langle |\nabla T|^2 \rangle \sim C(\Omega, d, f)\, \mathit{Pe}^{-2}$.

Finally, in Section 3.5 we bound the heat transfer of momentum-constrained flows driven by a steady balanced source–sink function $f(\boldsymbol{x})$ and a steady conservative gravitational acceleration $\boldsymbol{g}(\boldsymbol{x})$. In addition to the advection-diffusion equation III.1 for the temperature T, we let the velocity $\boldsymbol{u}$ solve the non-dimensional Boussinesq equation

$$\mathit{Pr}^{-1} \left(\partial_t \boldsymbol{u} + \boldsymbol{u}\cdot\nabla\boldsymbol{u}\right) = \Delta\boldsymbol{u} + \mathit{R}\, T\boldsymbol{g} - \nabla p$$

with $\boldsymbol{g} = \nabla\varphi$. The choice $\varphi = z$ yields the usual Boussinesq equations with gravity in the negative z-direction, and we allow for other choices as well. The non-dimensional parameters *Pr* and *R* are the usual Prandtl number and a 'flux-based' Rayleigh number [Gol16] measuring the strength of the sources and sinks relative to diffusion: $\mathit{Pr} = \nu/\kappa$ and $\mathit{R} = \alpha L^5 Q/(\nu\kappa^2)$. Again, L is a characteristic lengthscale and κ is the thermal diffusivity; also, ν is the kinematic viscosity, α is the

thermal expansion coefficient and Q is a characteristic heating and cooling rate per unit volume (which sets the dimensional amplitude of f). After deriving a set of basic balance laws, we relate the mean enstrophy and energy of the flow to the Rayleigh number, and thereby obtain a trio of Rayleigh-dependent lower bounds (3.5.3). These bounds are in the general form

$$\langle |\nabla T|^2 \rangle \geq \frac{C(\Omega, d, f, \boldsymbol{g})}{R^\alpha}$$

with $\alpha = 0$, $2/3$ or 1 depending on the sign of $\langle f\varphi \rangle$ and for large enough R; we give intuition for this below.

Section 3.6 is a conclusion section that includes a discussion of open questions and future directions of research.

3.2 Variational bounds on heat transfer in an insulated domain

Section 3.2.1 derives upper and lower bounds on the mean square thermal dissipation $\langle |\nabla T|^2 \rangle$ of a general unsteady incompressible flow $\boldsymbol{u}(\boldsymbol{x}, t)$ and a general unsteady and balanced source–sink distribution $f(\boldsymbol{x}, t)$. These bounds involve a pair of test functions, which can be optimized based on the details of $\boldsymbol{u}$ and f. In the steady case where $\boldsymbol{u} = \boldsymbol{u}(\boldsymbol{x})$ and $f = f(\boldsymbol{x})$, the optimization evaluates $\langle |\nabla T|^2 \rangle$ so that the bounds are sharp (see Section 3.2.2). One can also choose the test functions to bound $\langle |\nabla T|^2 \rangle$ in terms of a bulk measure of the flow intensity, such as the mean kinetic energy $\langle |\boldsymbol{u}|^2 \rangle$; we do so starting in Section 3.3.

3.2.1 Variational bounds for unsteady flows and source–sink distributions

Define the admissible set

$$\begin{aligned} \mathcal{A} = \Big\{ & \theta \in L^2_{\text{loc}}\left(0, \infty; H^1(\Omega)\right) : \\ & \partial_t \theta \in L^2_{\text{loc}}\left(0, \infty; H^{-1}(\Omega)\right),\ \theta(\cdot, \tau) \in L^\infty(\Omega) \text{ a.e. } \tau,\ \lim_{\tau \to \infty} \frac{1}{\sqrt{\tau}} \|\theta(\cdot, \tau)\|_{L^2(\Omega)} = 0 \Big\}. \end{aligned} \tag{III.6}$$

Let λ_1 be the first non-trivial Neumann eigenvalue of the (negative) Laplacian on Ω as introduced in Section 2.4.1.

Theorem 3.2.1. *Let $\boldsymbol{u}(\boldsymbol{x},t)$ be divergence-free with $\boldsymbol{u}\cdot\hat{\boldsymbol{n}}=0$ at $\partial\Omega$ and $\langle|\boldsymbol{u}|^2\rangle<\infty$, and let $f(\boldsymbol{x},t)$ satisfy $\fint_\Omega f(\boldsymbol{x},t)\mathrm{d}\boldsymbol{x}=0$ for $t>0$. Assume there exists $a_0,a_1\in(0,1)$ and $p\in[d/2,\infty]$ such that*

$$\begin{aligned}&\lim_{\tau\to\infty}\frac{1}{\tau}\int_0^\tau e^{-2a_0\lambda_1(\tau-t)}\|f(\cdot,t)\|_{H^{-1}(\Omega)}^2\,\mathrm{d}t=0\\ \text{and}\quad&\int_0^\tau\frac{e^{-a_1\lambda_1(\tau-t)}}{(\tau-t)^{\frac{d}{2p}}}\|f(\cdot,t)\|_{L^p(\Omega)}\,dt<\infty\quad\forall\,\tau>0.\end{aligned}\tag{III.7}$$

Given any weak solution $T(\boldsymbol{x},t)$ of

$$\begin{cases}\partial_t T+\boldsymbol{u}\cdot\nabla T=\Delta T+f & \text{in }\Omega\\ \hat{\boldsymbol{n}}\cdot\nabla T=0 & \text{at }\partial\Omega\end{cases}\tag{III.8}$$

with $T(\cdot,0)\in L^2(\Omega)$, the upper and lower bounds

$$\left\langle 2f\xi-|\nabla\xi|^2-|\nabla\Delta^{-1}(\partial_t\xi+\boldsymbol{u}\cdot\nabla\xi)|^2\right\rangle\le\left\langle|\nabla T|^2\right\rangle\le\left\langle|\nabla\eta|^2+|\nabla\Delta^{-1}(\partial_t\eta+\boldsymbol{u}\cdot\nabla\eta-f)|^2\right\rangle\tag{III.9}$$

hold for all $\eta,\xi\in\mathcal{A}$.

Remark 3.2.2. The two assumptions on f in III.7 play different roles. The first one ensures that $\|T(\cdot,\tau)\|_{L^2(\Omega)}\ll\sqrt{\tau}$ as $\tau\to\infty$, so that the integration-by-parts identity $\langle|\nabla T|^2\rangle=\langle fT\rangle$ holds. The second one implies that $T(\cdot,\tau)\in L^\infty(\Omega)$ for a.e. $\tau>0$. This allows us to define the notion of weak solutions in the usual way, by testing the given equation against functions in $H^1(\Omega)$ and integrating by parts (following, e.g., [Eva10]); it also ensures that $\int_\Omega\boldsymbol{u}\cdot\nabla TT\mathrm{d}\boldsymbol{x}=0$. As these remarks are more or less standard fare in parabolic regularity theory [Eva10, Lie96], we shall not present their proofs, but instead point to the notes [KRR12] for an exposition that is readily adapted to our setting. In brief, the desired L^2-bound follows from Gronwall's inequality by testing the equation against T; the L^∞-bound follows from known 'heat kernel' bounds on the forward-time solution map of the homogeneous equation (bounding it from $L^p(\Omega)$ to $L^\infty(\Omega)$ by a multiple of

$e^{-a\lambda_1\Delta t}(\Delta t)^{-d/2p}$ for any $a \in (0,1)$, across a time increment Δt).

Remark 3.2.3. One can do away with the second assumption on f in III.7 by imposing enough integrability on $\boldsymbol{u}$ to the point that $\boldsymbol{u}\cdot\nabla\theta \in H^{-1}(\Omega)$ a.e. in time, for any $\theta \in H^1(\Omega)$. Since by the Sobolev embedding theorem [Eva10] $L^{2d/(d+2)}(\Omega)$ is included in $H^{-1}(\Omega)$ when $d > 2$, it suffices to assume that $\boldsymbol{u} \in L^d(\Omega)$ a.e. in time. The L^∞ assumption on the test functions in $\mathcal{A}$ can then be removed. These statements continue to hold in the borderline case $d = 2$ due to 'div-curl' character of the product $\boldsymbol{u}\cdot\nabla\theta$; see Section 3.3.1 or [Tob22] for more details.

Proof of 3.2.1. We apply the method of Lagrange multipliers, with the advection-diffusion equation III.8 as the constraint and the test functions η and ξ as multipliers. Let $\langle\cdot\rangle_\tau = \fint_0^\tau \fint_\Omega \cdot \,\mathrm{d}\boldsymbol{x}\mathrm{d}t$ be the average of a quantity over $\Omega\times(0,\tau)$. To prove the lower bound in III.9, start with the weak form of the advection-diffusion equation, which states that

$$\langle f\xi - \nabla T\cdot\nabla\xi - \partial_t T\xi - \boldsymbol{u}\cdot\nabla T\xi\rangle_\tau = 0 \tag{III.10}$$

for any $\xi \in \mathcal{A}$ and $\tau > 0$. Thus,

$$\begin{aligned}
\left\langle|\nabla T|^2\right\rangle_\tau &= \left\langle|\nabla T|^2 + 2\left(f\xi - \nabla T\cdot\nabla\xi - \partial_t T\xi - \boldsymbol{u}\cdot\nabla T\xi\right)\right\rangle_\tau \\
&= \left\langle|\nabla T|^2 + 2f\xi - 2\nabla T\cdot\nabla\xi + 2T\left(\partial_t\xi + \boldsymbol{u}\cdot\nabla\xi\right)\right\rangle_\tau - \frac{2}{\tau}\fint_\Omega T\xi\mathrm{d}\boldsymbol{x}\Big|_{t=0}^{t=\tau} \\
&\geq \inf_\theta \left\langle|\nabla\theta|^2 + 2f\xi - 2\nabla\theta\cdot\nabla\xi + 2\theta\left(\partial_t\xi + \boldsymbol{u}\cdot\nabla\xi\right)\right\rangle_\tau - o_\tau(1)
\end{aligned} \tag{III.11}$$

where $o_\tau(1)$ denotes a term that goes to zero as $\tau\to\infty$. To see this last step, note that $\|T(\cdot,\tau)\|_{L^2(\Omega)} \ll \sqrt{\tau}$ as explained in remark 3.2.2. Also, $\|\xi(\cdot,\tau)\|_{L^2(\Omega)} \ll \sqrt{\tau}$ by the definition of the admissible set $\mathcal{A}$ in III.6. Hence,

$$\left|\frac{1}{\tau}\fint_\Omega T\xi\mathrm{d}\boldsymbol{x}\Big|_{t=0}^{t=\tau}\right| \leq \frac{1}{\tau\,|\Omega|}\|T(\cdot,\tau)\|_{L^2(\Omega)}\|\xi(\cdot,\tau)\|_{L^2(\Omega)} + \left|\frac{1}{\tau}\fint_\Omega T(\boldsymbol{x},0)\xi(\boldsymbol{x},0)\mathrm{d}\boldsymbol{x}\right| \to 0 \quad \text{as } \tau\to\infty.$$

To evaluate the infimum in III.11, we make use of its Euler–Lagrange equation

$$\begin{cases} \Delta\theta = \Delta\xi + \partial_t\xi + \boldsymbol{u}\cdot\nabla\xi & \text{on } \Omega \\ \hat{\boldsymbol{n}}\cdot\nabla\theta = 0 & \text{at } \partial\Omega \end{cases}$$

which gives the optimal θ at each fixed time. Testing against θ and integrating by parts shows that

$$\left\langle |\nabla\theta|^2 \right\rangle_\tau = \left\langle \nabla\theta\cdot\nabla\xi - \theta\left(\partial_t\xi + \boldsymbol{u}\cdot\nabla\xi\right)\right\rangle_\tau .$$

Therefore, by III.11,

$$\begin{aligned} \left\langle |\nabla T|^2 \right\rangle_\tau &\geq \left\langle 2f\xi - \left|\nabla\Delta^{-1}\left(\Delta\xi + \partial_t\xi + \boldsymbol{u}\cdot\nabla\xi\right)\right|^2 \right\rangle_\tau - o_\tau(1) \\ &= \left\langle 2f\xi - |\nabla\xi|^2 - \left|\nabla\Delta^{-1}(\partial_t\xi + \boldsymbol{u}\cdot\nabla\xi)\right|^2 \right\rangle_\tau - o_\tau(1). \end{aligned} \tag{III.12}$$

Note the cross term vanishes since

$$2\left\langle \nabla\xi\cdot\nabla\Delta^{-1}\left(\partial_t\xi + \boldsymbol{u}\cdot\nabla\xi\right)\right\rangle_\tau = -2\left\langle \xi\left(\partial_t\xi + \boldsymbol{u}\cdot\nabla\xi\right)\right\rangle_\tau = -\frac{1}{\tau}\int_0^\tau \frac{\mathrm{d}}{\mathrm{d}t}\|\xi\|^2_{L^2(\Omega)}\,\mathrm{d}t = o_\tau(1)$$

by the growth conditions on ξ and the no-penetration conditions for $\boldsymbol{u}$. Taking $\tau\to\infty$ in III.12 yields the lower bound.

The upper bound in III.9 is proved by a similar argument. The key is to find a version of $\langle|\nabla T|^2\rangle$ that lends itself to maximization, rather than minimization. Multiplying the advection-diffusion equation III.8 by T and integrating by parts shows that

$$\langle|\nabla T|^2\rangle_\tau = \langle fT\rangle_\tau + o_\tau(1),$$

as in the first part of remark 3.2.2. This allows us to rewrite

$$\langle|\nabla T|^2\rangle_\tau = \langle 2fT - |\nabla T|^2\rangle_\tau + o_\tau(1)$$

and mimic the previous argument, but with an upper bound. Specifically, using a Lagrange multiplier $\eta \in \mathcal{A}$ in the weak form III.10 of the advection–diffusion equation, we can write that

$$\begin{aligned}
\left\langle 2fT - |\nabla T|^2 \right\rangle_\tau &= \left\langle 2fT - |\nabla T|^2 - 2\left(f\eta - \nabla T \cdot \nabla \eta - \partial_t T \eta - \boldsymbol{u} \cdot \nabla T \eta\right) \right\rangle_\tau \\
&\leq \sup_\theta \left\langle 2f\theta - |\nabla \theta|^2 - 2f\eta + 2\nabla\theta \cdot \nabla\eta - 2\theta\left(\partial_t \eta + \boldsymbol{u} \cdot \nabla \eta\right) \right\rangle_\tau + o_\tau(1) \\
&= \left\langle -2f\eta + \left| \nabla \Delta^{-1} \left(\Delta\eta + \partial_t \eta + \boldsymbol{u} \cdot \nabla \eta - f\right) \right|^2 \right\rangle_\tau + o_\tau(1) \\
&= \left\langle |\nabla \eta|^2 + \left| \nabla \Delta^{-1} (\partial_t \eta + \boldsymbol{u} \cdot \nabla \eta - f) \right|^2 \right\rangle_\tau + o_\tau(1).
\end{aligned}$$

To pass between the first and second lines, integrate by parts to find only $o_\tau(1)$ contributions. Then, optimize over θ like before. Taking $\tau \to \infty$ gives the upper bound. □

3.2.2 Sharpness in the steady case

The variational bounds in 3.2.1 apply to both steady and unsteady $\boldsymbol{u}$ and f. In the steady case, these bounds cannot be improved. We adapt the argument from [TD, DT19].

Corollary 3.2.4. *Let $\boldsymbol{u}(\boldsymbol{x})$, $f(\boldsymbol{x})$ and $T(\boldsymbol{x}, t)$ be as in 3.2.1 (in particular let $f \in L^p(\Omega)$ for some $p > d/2$). Then,*

$$\begin{aligned}
\max_{\xi \in H^1(\Omega) \cap L^\infty(\Omega)} &\fint_\Omega 2f\xi - |\nabla \xi|^2 - |\nabla \Delta^{-1}(\boldsymbol{u} \cdot \nabla \xi)|^2 \, \mathrm{d}\boldsymbol{x} \\
&= \left\langle |\nabla T|^2 \right\rangle = \min_{\eta \in H^1(\Omega) \cap L^\infty(\Omega)} \fint_\Omega |\nabla \eta|^2 + |\nabla \Delta^{-1}(\boldsymbol{u} \cdot \nabla \eta - f)|^2 \, \mathrm{d}\boldsymbol{x}.
\end{aligned} \tag{III.13}$$

Remark 3.2.5. The integrability assumption on f derives from the second part of III.7, which guarantees for steady $T(\boldsymbol{x})$ that $\|T\|_{L^\infty(\Omega)} \lesssim_{\Omega,d,p} \|f\|_{L^p(\Omega)} < \infty$ [KRR12]. The first part of III.7 is redundant by Sobolev embedding [Eva10].

Remark 3.2.6. Following up from remark 3.2.3, if $\boldsymbol{u} \in L^d(\Omega)$ then the result holds for $f \in H^{-1}(\Omega)$ and with test functions $\xi, \eta \in H^1(\Omega)$.

Proof. Optimizing the upper and lower bounds in 3.2.1 over all steady fields $\xi, \eta \in \mathcal{A}$ gives that

$$\begin{aligned}\sup_{\xi \in H^1(\Omega)\cap L^\infty(\Omega)} \fint_\Omega 2f\xi - |\nabla\xi|^2 - |\nabla\Delta^{-1}(\boldsymbol{u}\cdot\nabla\xi)|^2 \,\mathrm{d}\boldsymbol{x} \\ \leq \left\langle |\nabla T|^2 \right\rangle \leq \inf_{\eta \in H^1(\Omega)\cap L^\infty(\Omega)} \fint_\Omega |\nabla\eta|^2 + |\nabla\Delta^{-1}(\boldsymbol{u}\cdot\nabla\eta - f)|^2 \,\mathrm{d}\boldsymbol{x}.\end{aligned} \tag{III.14}$$

There is no loss of generality in taking ξ and η to be mean-free. The resulting variational problems are respectively strictly concave and strictly convex, so that solving them is the same as solving their Euler–Lagrange equations:

$$\begin{aligned}\Delta\xi &= \boldsymbol{u}\cdot\nabla\Delta^{-1}\left(\boldsymbol{u}\cdot\nabla\xi\right) - f, \\ \Delta\eta &= \boldsymbol{u}\cdot\nabla\Delta^{-1}\left(\boldsymbol{u}\cdot\nabla\eta - f\right)\end{aligned}$$

with $\hat{\boldsymbol{n}}\cdot\nabla\xi = \hat{\boldsymbol{n}}\cdot\nabla\eta = 0$ at $\partial\Omega$. Equivalently, we must solve

$$\begin{cases}\boldsymbol{u}\cdot\nabla\eta - f = \Delta\xi \\ \qquad \boldsymbol{u}\cdot\nabla\xi = \Delta\eta\end{cases} \tag{III.15}$$

with the same boundary conditions. The change of variables $T = \xi + \eta$ and $T_{\mathrm{adj}} = \xi - \eta$ recovers the steady heat equation and its adjoint:

$$\begin{aligned}\boldsymbol{u}\cdot\nabla T &= \Delta T + f, \\ -\boldsymbol{u}\cdot\nabla T_{\mathrm{adj}} &= \Delta T_{\mathrm{adj}} + f\end{aligned}$$

with $\hat{\boldsymbol{n}}\cdot\nabla T = \hat{\boldsymbol{n}}\cdot\nabla T_{\mathrm{adj}} = 0$ at $\partial\Omega$. These last equations define T and T_{adj} and ensure their boundedness, due to the second part of our assumption III.7 on f and remark 3.2.2. Hence, $\xi := (T + T_{\mathrm{adj}})/2$ and $\eta := (T - T_{\mathrm{adj}})/2$ are admissible in III.14, and we can proceed to evaluate their bounds.

First, note that

$$\left\langle |\nabla T|^2 \right\rangle = \fint_\Omega |\nabla \xi|^2 + |\nabla \eta|^2 \, \mathrm{d}\boldsymbol{x} \tag{III.16}$$

because testing the second equation in III.15 against ξ yields

$$\fint_\Omega \nabla \eta \cdot \nabla \xi \mathrm{d}\boldsymbol{x} = -\fint_\Omega \boldsymbol{u} \cdot \nabla \xi \xi \mathrm{d}\boldsymbol{x} = 0.$$

Now, substitute $\xi = \Delta^{-1}(\boldsymbol{u} \cdot \nabla \eta - f)$ into the right-hand side of III.16 to obtain

$$\left\langle |\nabla T|^2 \right\rangle = \fint_\Omega |\nabla \eta|^2 + \left|\nabla \Delta^{-1}(\boldsymbol{u} \cdot \nabla \eta - f)\right|^2 \, \mathrm{d}\boldsymbol{x}.$$

This verifies the optimality of η and proves the second half of 3.2.4. To prove the first half, note the identity

$$\fint_\Omega |\nabla \eta|^2 \mathrm{d}\boldsymbol{x} = \fint_\Omega f\xi - |\nabla \xi|^2 \mathrm{d}\boldsymbol{x} \tag{III.17}$$

which derives from testing the first equation in III.15 by ξ and the second by η and combining the results. Indeed,

$$\fint_\Omega f\xi - |\nabla \xi|^2 - |\nabla \eta|^2 \, \mathrm{d}\boldsymbol{x} = \fint_\Omega f\xi - |\nabla \xi|^2 + (\boldsymbol{u} \cdot \nabla \xi)\eta \, \mathrm{d}\boldsymbol{x} = \fint_\Omega f\xi - |\nabla \xi|^2 - (\boldsymbol{u} \cdot \nabla \eta)\xi \, \mathrm{d}\boldsymbol{x} = 0.$$

Combining III.16 and III.17 and using that $\eta = \Delta^{-1}(\boldsymbol{u} \cdot \nabla \xi)$ we conclude that

$$\left\langle |\nabla T|^2 \right\rangle = \fint_\Omega 2\,|\nabla \eta|^2 + |\nabla \xi|^2 - |\nabla \eta|^2 \, \mathrm{d}\boldsymbol{x} = \fint_\Omega 2f\xi - |\nabla \xi|^2 - \left|\nabla \Delta^{-1}\boldsymbol{u} \cdot \nabla \xi\right|^2 \mathrm{d}\boldsymbol{x}$$

as required. □

3.3 Bounds on energy-constrained flows

The previous section achieved upper and lower bounds on $\langle |\nabla T|^2 \rangle$ in terms of a pair of test functions, the choice of which was left up to the reader depending on the application. We now

demonstrate how knowledge of the mean kinetic energy $\langle|\boldsymbol{u}|^2\rangle$ along with the structure of the source–sink distribution f can be used to achieve the lower bound

$$\langle|\nabla T|^2\rangle \geq \frac{C_1}{C_2 + C_3\langle|\boldsymbol{u}|^2\rangle}. \tag{III.18}$$

We base our approach on a well-known inequality of Coifman, Lions, Meyers and Semmes [CLMS90], which we introduce in Section 3.3.1 along with the requisite functional analysis involving Hardy and BMO spaces. This inequality explains how the advection term $\boldsymbol{u}\cdot\nabla T$ inherits additional regularity beyond a typical dot product from the fact that it involves divergence- and curl-free fields. Using it, we achieve III.18 in Section 3.3.2.

Section 3.3.3 goes on to discuss a pair of examples where our methods establish the scaling law of $\min\ \langle|\nabla T|^2\rangle$ with respect to $\langle|\boldsymbol{u}|^2\rangle$ and certain features of f. In each example, we apply 3.3.1 with a suitable test function to deduce a lower bound. We then saturate the scaling behaviors of this bound by constructing nearly optimal velocity fields. Part of the puzzle is to understand when flowing is significantly better than not, and indeed this is reflected by a cross-over in the optimal scaling laws achieved in 3.3.3 and 3.3.4.

3.3.1 A brief introduction to $\mathcal{H}^1$ and BMO

First, we introduce the functional analytic framework we use to prove our kinetic energy-based bounds. We leave out most of the proofs, and point to the references [Miy90, Ste93, Cha94, CDS05] for full details. Given a domain $\Omega \subset \mathbb{R}^d$, the Hardy space $\mathcal{H}^1(\Omega)$ and space of bounded mean oscillation functions $\mathrm{BMO}(\Omega)$ are defined as follows.[1] Starting with $\mathcal{H}^1(\Omega)$, we fix a smooth and compactly supported function $\rho(\boldsymbol{x}) \geq 0$ with $\int_{\mathbb{R}^d}\rho\mathrm{d}\boldsymbol{x} = 1$, and define the associated *maximal function* operator by

$$M_\rho f(\boldsymbol{x}) = \sup_{\delta>0}\left|\int_\Omega \frac{1}{\delta^d}\rho\left(\frac{\boldsymbol{x}-\boldsymbol{z}}{\delta}\right) f(\boldsymbol{z})\,d\boldsymbol{z}\right|, \quad \boldsymbol{x}\in\mathbb{R}^d. \tag{III.19}$$

[1] In the notation of reference [CDS05], we are defining $\mathcal{H}^1_z(\Omega)$ and $\mathrm{BMO}_r(\Omega)$. We omit the subscripts to lighten the notation.

This definition records the 'worst-case averages' of a given function $f(\boldsymbol{x})$ against rescaled copies of the probability density ρ (actually, it is the extension of f by zero from Ω to $\mathbb{R}^d$ that is being averaged). The *Hardy space* $\mathcal{H}^1(\Omega)$ then consists of all $f \in L^1(\Omega)$ such that $M_\rho f \in L^1(\mathbb{R}^d)$, a condition that turns out to be independent of ρ. This is a Banach space under the norm

$$\|f\|_{\mathcal{H}^1(\Omega)} = \int_{\mathbb{R}^d} M_\rho f(\boldsymbol{x}) \mathrm{d}\boldsymbol{x}$$

which embeds continuously into $L^1(\Omega)$ per the inequality $\|\cdot\|_{L^1(\Omega)} \leq \|\cdot\|_{\mathcal{H}^1(\Omega)}$ (a consequence of Lebesgue differentiation). The reverse inequality fails, however, as an example based on approximating a Dirac mass shows. Indeed, let $\boldsymbol{x}_0 \in \Omega$ and consider a sequence of functions $\{f_\epsilon\}$ that have L^1-norm equal to one, and are defined by taking $f_\epsilon = \epsilon^{-d}$ on the ball $B_\epsilon(\boldsymbol{x}_0)$ of radius $\epsilon > 0$ centered at $\boldsymbol{x}_0$ and $f_\epsilon = 0$ otherwise. Taking $\delta(\boldsymbol{x}) \sim |\boldsymbol{x} - \boldsymbol{x}_0| \vee \epsilon$ in III.19 yields the lower bound $M_\rho f_\epsilon(\boldsymbol{x}) \gtrsim \delta^{-d}(\boldsymbol{x})$, the L^1-norm of which diverges logarithmically as $\epsilon \to 0$. This calculation is at the heart of our pinching flow example in Section 3.3.3.2.

Being a Banach space, $\mathcal{H}^1(\Omega)$ has a dual. A famous result of Fefferman identifies $\mathcal{H}^1(\Omega)^*$ with a function space introduced by John and Nirenberg [JN61] in connection with John's work on elasticity. The space of *bounded mean oscillation* functions $\mathrm{BMO}(\Omega)$ consists of all functions $g(\boldsymbol{x})$ for which

$$\|g\|_{\mathrm{BMO}(\Omega)} = \sup_{Q \subset \Omega} \fint_Q \left| g(\boldsymbol{x}) - \fint_Q g \right| \mathrm{d}\boldsymbol{x} < \infty$$

where Q is a d-dimensional cube. Modulo constants, this is a norm under which $\mathrm{BMO}(\Omega)$ is a Banach space. The duality between $\mathcal{H}^1(\Omega)$ and $\mathrm{BMO}(\Omega)$ is realized by the inequality

$$\left| \int_\Omega f g \, \mathrm{d}\boldsymbol{x} \right| \lesssim_{\Omega,d} \|f\|_{\mathcal{H}^1(\Omega)} \|g\|_{\mathrm{BMO}(\Omega)} \tag{III.20}$$

which holds at first for $f \in \mathcal{H}^1(\Omega)$ and $g \in \mathrm{BMO}(\Omega) \cap L^\infty(\Omega)$, and then for all $g \in \mathrm{BMO}(\Omega)$ by continuous extension. It follows directly from the definitions that $\|\cdot\|_{\mathrm{BMO}(\Omega)} \leq 2\|\cdot\|_{L^\infty(\Omega)}$ so that $L^\infty(\Omega)$ embeds continuously into $\mathrm{BMO}(\Omega)$. Again, the reverse direction fails: the function

$\log(|\boldsymbol{x} - \boldsymbol{x}_0|)$ belongs to $\mathrm{BMO}(\Omega)$ (see [Ste93, Ch. IV]) but is not in $L^\infty(\Omega)$ if $\boldsymbol{x}_0 \in \Omega$. This too shows up in our discussion of pinching flows.

Finally, we recall the div-curl inequality of Coifman, Lions, Meyers and Semmes with a bounded Lipschitz domain Ω proved in 2.3.2,

$$\|\boldsymbol{u} \cdot \boldsymbol{v}\|_{\mathcal{H}^1(\Omega)} \lesssim_{\Omega,d} \|\boldsymbol{u}\|_{L^2(\Omega)} \|\boldsymbol{v}\|_{L^2(\Omega)} \tag{III.21}$$

if $\boldsymbol{u}$ is divergence-free with $\boldsymbol{u} \cdot \hat{\boldsymbol{n}} = 0$ at $\partial\Omega$, and if $\boldsymbol{v}$ is curl-free. We shall make repeated use of the above inequality.

3.3.2 Bounding the heat transfer of energy-constrained flows

Combining the main result of Section 3.2.1 with the functional analysis recalled above, we bound $\langle |\nabla T|^2 \rangle$ from below in terms of the mean kinetic energy $\langle |\boldsymbol{u}|^2 \rangle$. With an eye towards the examples of Section 3.3.3, we state this result for steady $f(\boldsymbol{x})$ while allowing $\boldsymbol{u}(\boldsymbol{x}, t)$ and $T(\boldsymbol{x}, t)$ to be unsteady (however, see the remark below).

Corollary 3.3.1. *Let $\boldsymbol{u}(\boldsymbol{x}, t)$, $f(\boldsymbol{x})$ and $T(\boldsymbol{x}, t)$ be as in 3.2.1 (or as in remark 3.2.3). There is a constant $C > 0$ depending only on Ω and d such that*

$$\left\langle |\nabla T|^2 \right\rangle \geq \frac{\left(\fint_\Omega \xi f \mathrm{d}\boldsymbol{x} \right)^2}{\fint_\Omega |\nabla \xi|^2 \mathrm{d}\boldsymbol{x} + C \|\xi\|^2_{\mathrm{BMO}(\Omega)} \langle |\boldsymbol{u}|^2 \rangle} \tag{III.22}$$

for every non-constant $\xi \in H^1(\Omega) \cap L^\infty(\Omega)$ (or $H^1(\Omega)$, respectively).

Remark 3.3.2. The same bound holds for unsteady $f(\boldsymbol{x}, t)$ with $\langle \xi f \rangle$ in place of $\fint_\Omega \xi f$, though if the time-average of f vanishes identically then this is not a useful bound. To improve the result, one should use unsteady test functions $\xi(\boldsymbol{x}, t)$ following 3.2.1. This leads to a bound with an additional term $C\langle |\nabla \Delta^{-1} \partial_t \xi|^2 \rangle$ in the denominator, the implications of which we leave to future work.

Proof. Applying 3.2.1 with a steady test function $\xi(\boldsymbol{x})$ gives the lower bound

$$\langle |\nabla T|^2 \rangle \geq 2 \fint_\Omega f\xi \,\mathrm{d}\boldsymbol{x} - \fint_\Omega |\nabla \xi|^2 \,\mathrm{d}\boldsymbol{x} - \langle |\nabla \Delta^{-1} \boldsymbol{u} \cdot \nabla \xi|^2 \rangle.$$

Substituting $\lambda\xi$ for ξ and optimizing $\lambda \in \mathbb{R}$, there follows

$$\langle |\nabla T|^2 \rangle \geq \frac{\left(\fint_\Omega f\xi \,\mathrm{d}\boldsymbol{x}\right)^2}{\fint_\Omega |\nabla \xi|^2 \,\mathrm{d}\boldsymbol{x} + \langle |\nabla \Delta^{-1} \boldsymbol{u} \cdot \nabla \xi)|^2 \rangle}. \tag{III.23}$$

Note the denominator is non-zero by our hypothesis on ξ. We proceed to estimate $\langle |\nabla \Delta^{-1} \boldsymbol{u} \cdot \nabla \xi)|^2 \rangle$. At almost every time,

$$\int_\Omega |\nabla \Delta^{-1} \boldsymbol{u} \cdot \nabla \xi|^2 \mathrm{d}\boldsymbol{x} = \max_{\varphi(\boldsymbol{x})} \left(\frac{\int_\Omega \boldsymbol{u} \cdot \nabla \xi \, \varphi \,\mathrm{d}\boldsymbol{x}}{\|\nabla \varphi\|_{L^2(\Omega)}} \right)^2 = \max_{\varphi(\boldsymbol{x})} \left(\frac{\int_\Omega \boldsymbol{u} \cdot \nabla \varphi \, \xi \,\mathrm{d}\boldsymbol{x}}{\|\nabla \varphi\|_{L^2(\Omega)}} \right)^2.$$

By the duality of $\mathcal{H}^1$ and BMO in III.20 and the div-curl inequality III.21,

$$\left| \int_\Omega \boldsymbol{u} \cdot \nabla \varphi \, \xi \,\mathrm{d}\boldsymbol{x} \right| \lesssim_{\Omega,d} \|\boldsymbol{u} \cdot \nabla \varphi\|_{\mathcal{H}^1(\Omega)} \|\xi\|_{\mathrm{BMO}(\Omega)} \lesssim_{\Omega,d} \|\boldsymbol{u}\|_{L^2(\Omega)} \|\nabla \varphi\|_{L^2(\Omega)} \|\xi\|_{\mathrm{BMO}(\Omega)}.$$

Combining these statements and averaging in time, there follows

$$\langle |\nabla \Delta^{-1} \boldsymbol{u} \cdot \nabla \xi)|^2 \rangle \lesssim_{\Omega,d} \langle |\boldsymbol{u}|^2 \rangle \cdot \|\xi\|^2_{\mathrm{BMO}(\Omega)}.$$

Substituting into III.23 yields the bound

$$\langle |\nabla T|^2 \rangle \geq \frac{\left(\fint_\Omega \xi f \mathrm{d}\boldsymbol{x}\right)^2}{\fint_\Omega |\nabla \xi|^2 \mathrm{d}\boldsymbol{x} + C(\Omega, d) \|\xi\|^2_{\mathrm{BMO}(\Omega)} \langle |\boldsymbol{u}|^2 \rangle}. \qquad \square$$

How should the test function $\xi(\boldsymbol{x})$ be chosen in this last result? The answer depends, of course, on the domain Ω, the dimension d and the structure of the source–sink function f. It also depends on the magnitude of $\langle |\boldsymbol{u}|^2 \rangle$. On the one hand, for sufficiently small kinetic energies one expects to be able to 'cross out' the second term in the denominator of III.22, and select ξ through the

maximization

$$\max_{\xi(\boldsymbol{x})} \frac{\left(\int_\Omega \xi f \mathrm{d}\boldsymbol{x}\right)^2}{\int_\Omega |\nabla \xi|^2 \mathrm{d}\boldsymbol{x}} = \|f\|^2_{H^{-1}(\Omega)}. \tag{III.24}$$

This leads to the choice $\xi = \Delta^{-1} f$. On the other hand, for large $\langle |\boldsymbol{u}|^2 \rangle$ one is lead to the maximization

$$\max_{\xi(\boldsymbol{x})} \frac{\left(\int_\Omega \xi f \mathrm{d}\boldsymbol{x}\right)^2}{\|\xi\|^2_{\mathrm{BMO}(\Omega)}} \sim_{\Omega,d} \|f\|^2_{\mathcal{H}^1(\Omega)} \tag{III.25}$$

by the duality between $\mathcal{H}^1(\Omega)$ and $\mathrm{BMO}(\Omega)$. Here the best choice of ξ is less apparent, though one achieving this equivalence is always guaranteed to exist. (We guess that time-dependent f could be handled similarly by a suitable smoothing in time of the choices in III.24 and III.25, taking into account the additional term $\langle |\nabla \Delta^{-1} \partial_t \xi|^2 \rangle$ from remark 3.3.2.) Of course, once one makes a choice for ξ, it can be plugged back into III.22 to achieve a lower bound with known constants at all values of $\langle |\boldsymbol{u}|^2 \rangle$. We demonstrate this in examples below.

3.3.3 Two examples

We now apply our variational bounds to a pair of examples involving oscillatory or concentrated heating and cooling. In each example, we deduce the scaling law of $\min \langle |\nabla T|^2 \rangle$ with respect to its parameters, along with velocity fields achieving the optimal scalings. See Section 3.3.3.1 for oscillatory heating and our accompanying cellular flows, and Section 3.3.3.2 for concentrated heating and our pinching flows.

3.3.3.1 Sinusoidal heating and cellular flows

Our first example optimizes heat transfer between a periodic pattern of sources and sinks. Let $\Omega = (0, 2\pi)^2$ and take

$$f(\boldsymbol{x}) = \frac{1}{2} \cos\left(\frac{2y}{\ell}\right) - \frac{1}{2} \cos\left(\frac{2x}{\ell}\right). \tag{III.26}$$

The parameter $\ell^{-1} \in \mathbb{N}$ sets the period of the pattern.

Proposition 3.3.3. *Under the above setup,*

$$\min_{\substack{\boldsymbol{u}(\boldsymbol{x},t)\\ \langle|\boldsymbol{u}|^2\rangle\le Pe^2\\ \partial_t T+\boldsymbol{u}\cdot\nabla T=\Delta T+f}} \langle|\nabla T|^2\rangle \sim \min\left\{\ell^2, \frac{1}{Pe^2}\right\}$$

for all $\ell^{-1}\in\mathbb{N}$ and $Pe\ge 0$. The alternatives are achieved by no flow (ℓ^2) or by the cellular flow (Pe^{-2}) depicted in Figure III.1a of the introduction.

Proof of the lower bound. We begin with the general lower bound

$$\left\langle|\nabla T|^2\right\rangle \ge \frac{\left(⨍_\Omega \xi f \mathrm{d}\boldsymbol{x}\right)^2}{⨍_\Omega |\nabla\xi|^2\mathrm{d}\boldsymbol{x} + C(\Omega)\|\xi\|^2_{\mathrm{BMO}(\Omega)}\, Pe^2} \tag{III.27}$$

from 3.3.1. The present f belongs to $L^\infty(\Omega)$ and is such that all of its L^p-norms are comparable. In particular, $\|f\|_{L^1(\Omega)}\sim\|f\|_{L^\infty(\Omega)}\sim 1$ for all ℓ. Also, $\|f\|_{\mathcal{H}^1(\Omega)}\sim\|f\|_{\mathrm{BMO}(\Omega)}\sim 1$ and so there exist many good choices of ξ.

Take, for example, $\xi = f$. Then

$$\int_\Omega \xi f \mathrm{d}\boldsymbol{x} = \int_\Omega f^2 \mathrm{d}\boldsymbol{x} = \int_\Omega \left|\frac{1}{2}\cos\left(\frac{2y}{\ell}\right) - \frac{1}{2}\cos\left(\frac{2x}{\ell}\right)\right|^2 \mathrm{d}\boldsymbol{x} \sim 1$$

while

$$\|f\|_{\mathrm{BMO}(\Omega)} \le 2\|f\|_{L^\infty(\Omega)} \le 2.$$

Also,

$$\int_\Omega |\nabla\xi|^2 = \int_\Omega |\nabla f|^2 = \int_\Omega \left|-\frac{1}{\ell}\sin\left(\frac{2y}{\ell}\right)\hat{\boldsymbol{e}}_y - \frac{1}{\ell}\sin\left(\frac{2x}{\ell}\right)\hat{\boldsymbol{e}}_x\right|^2 \mathrm{d}\boldsymbol{x} \sim \frac{1}{\ell^2}.$$

Combining these estimates into III.27 yields the lower bound

$$\left\langle|\nabla T|^2\right\rangle \gtrsim \frac{1}{\ell^{-2}+Pe^2} \gtrsim \min\left\{\ell^2, \frac{1}{Pe^2}\right\}.$$

Proof of the upper bound We seek a steady velocity $\boldsymbol{u}(\boldsymbol{x})$ whose thermal dissipation is similar to the lower bound. To guide the search, consider the upper bound

$$\left\langle |\nabla T|^2 \right\rangle \leq \fint_\Omega |\nabla \eta|^2 \, \mathrm{d}\boldsymbol{x} + \fint_\Omega |\nabla \Delta^{-1}(\boldsymbol{u} \cdot \nabla \eta - f)|^2 \mathrm{d}\boldsymbol{x}$$

from 3.2.4, which holds in the present two-dimensional case for all $\eta \in H^1(\Omega)$. Making the change of variables

$$\boldsymbol{u} = \frac{\mathit{Pe}}{\sqrt{\fint_\Omega |\tilde{\boldsymbol{u}}|^2 \mathrm{d}\boldsymbol{x}}} \, \tilde{\boldsymbol{u}} \quad \text{and} \quad \eta = \frac{\sqrt{\fint_\Omega |\tilde{\boldsymbol{u}}|^2 \mathrm{d}\boldsymbol{x}}}{\mathit{Pe}} \, \tilde{\eta}$$

and dropping the tildes yields the estimate

$$\left\langle |\nabla T|^2 \right\rangle \leq \frac{1}{\mathit{Pe}^2} \fint_\Omega |\boldsymbol{u}|^2 \mathrm{d}\boldsymbol{x} \fint_\Omega |\nabla \eta|^2 \mathrm{d}\boldsymbol{x} + \fint_\Omega \left| \nabla \Delta^{-1}(\boldsymbol{u} \cdot \nabla \eta - f) \right|^2 \mathrm{d}\boldsymbol{x} \tag{III.28}$$

for all $\boldsymbol{u}$ and η. This reformulation simplifies the algebra, as it allows us to neglect the kinetic energy constraint. Of course, it is actually the unscaled velocity with kinetic energy equal to *Pe* whose thermal dissipation we are estimating.

There are two alternatives to consider, depending on whether we should take $\boldsymbol{u} = \boldsymbol{0}$ or not. In the case with no flow, the choice of η is immaterial and

$$\langle |\nabla T|^2 \rangle \leq \fint_\Omega \left| \nabla \Delta^{-1} f \right|^2 \mathrm{d}\boldsymbol{x} = \fint_\Omega \left| -\frac{\ell}{4} \sin\left(\frac{2x}{\ell}\right) \hat{\boldsymbol{e}}_x + \frac{\ell}{4} \sin\left(\frac{2y}{\ell}\right) \hat{\boldsymbol{e}}_y \right|^2 \mathrm{d}\boldsymbol{x} \sim \ell^2$$

with $\hat{\boldsymbol{e}}_x$ and $\hat{\boldsymbol{e}}_y$ being the unit vectors along the x- and y-coordinates. On the other hand, for the particular f in the example we can easily construct an admissible pair $(\boldsymbol{u}, \eta)$ satisfying the pure advection equation

$$\boldsymbol{u} \cdot \nabla \eta = f.$$

Simply take $\boldsymbol{u} = \nabla^{\perp}\psi = (\partial_y\psi, -\partial_x\psi)$ with the stream function

$$\psi(\boldsymbol{x}) = l \sin\left(\frac{x}{l}\right) \sin\left(\frac{y}{l}\right)$$

and use the test function

$$\eta(\boldsymbol{x}) = -l \cos\left(\frac{x}{l}\right) \cos\left(\frac{y}{l}\right).$$

In fact, the definition of f in III.26 was made precisely with these choices in mind. The second term in III.28 now vanishes, so that

$$\left\langle |\nabla T|^2 \right\rangle \leq \frac{1}{Pe^2} \fint_{\Omega} |\boldsymbol{u}|^2 \mathrm{d}\boldsymbol{x} \fint_{\Omega} |\nabla \eta|^2 \mathrm{d}\boldsymbol{x} \lesssim \frac{1}{Pe^2}.$$

Since we are always free to use either velocity field, the minimum thermal dissipation is bounded according as

$$\min \left\langle |\nabla T|^2 \right\rangle \lesssim \min\left\{ \ell^2, \frac{1}{Pe^2} \right\}.$$

The proof is complete. □

3.3.3.2 Concentrated heating and pinching flows

Next we consider source–sink profiles of the general form

$$f(\boldsymbol{x}) = f_+(\boldsymbol{x}) - f_-(\boldsymbol{x})$$

where $f_{\pm}$ are non-negative and supported in disjoint balls $B_{\epsilon}(\boldsymbol{x}_{\pm})$ centered at $\boldsymbol{x}_{\pm}$ with radii $\epsilon > 0$. Fixing units, we take

$$\int_{B_{\epsilon}(\boldsymbol{x}_{\pm})} f_{\pm}(\boldsymbol{x}) \mathrm{d}\boldsymbol{x} = 1$$

and $\boldsymbol{x}_{\pm} = (0, \pm 1/2)$. We also suppose that

$$\|f_{\pm}\|_{L^{\infty}(B_{\epsilon}(\boldsymbol{x}_{\pm}))} \lesssim \frac{1}{\epsilon^2} \qquad \text{and} \qquad \|\nabla f_{\pm}\|_{L^{\infty}(B_{\epsilon}(\boldsymbol{x}_{\pm}))} \lesssim \frac{1}{\epsilon^3}$$

and impose the 'up-down' symmetric condition

$$f_+(x,y) = f_-(x,-y) \tag{III.29}$$

saying that the heat added by f_+ at (x,y) matches the heat taken away by f_- at $(x,-y)$. A source–sink distribution satisfying these conditions can be constructed by smoothing a point source and point sink across a scale $\sim \epsilon$; there are of course many other possibilities. Regarding the domain, we assume for simplicity that it is the square $\Omega = (-1,1)^2$.

Proposition 3.3.4. *Under the above setup,*

$$\min_{\substack{\boldsymbol{u}(\boldsymbol{x},t) \\ \langle|\boldsymbol{u}|^2\rangle \le Pe^2 \\ \partial_t T + \boldsymbol{u}\cdot\nabla T = \Delta T + f}} \langle|\nabla T|^2\rangle \sim \min\left\{\log\frac{1}{\epsilon},\ \left(\log\frac{1}{\epsilon}\right)^2 \frac{1}{Pe^2}\right\}$$

for all $\epsilon \in (0, 1/20)$ and Pe ≥ 0. The alternatives are achieved by no flow ($\log(\epsilon^{-1})$) or by the pinching flow ($\log^2(\epsilon^{-1})\, Pe^{-2}$) depicted in Figure III.1b of the introduction.

Remark 3.3.5. Our setup is already quite general, but one can relax it further without altering the scaling of the result. This includes allowing the symmetry condition III.29 to hold only after integration in x, or considering general domains Ω that include the pinching flows we use to prove the upper bound.

Proof of the lower bound. Again we begin with the lower bound

$$\left\langle|\nabla T|^2\right\rangle \ge \frac{\left(⨍_\Omega \xi f \mathrm{d}\boldsymbol{x}\right)^2}{⨍_\Omega |\nabla\xi|^2 \mathrm{d}\boldsymbol{x} + C(\Omega)\|\xi\|^2_{\mathrm{BMO}(\Omega)}\, Pe^2} \tag{III.30}$$

from 3.3.1. Recall the example of the smoothed Dirac mass discussed in Section 3.3.1, which had logarithmically diverging $\mathcal{H}^1$-norm as $\epsilon \to 0$. This prompts us to look for a test function $\xi(\boldsymbol{x})$ with the properties that

$$\int_\Omega \xi f \mathrm{d}\boldsymbol{x} \gtrsim \log\frac{1}{\epsilon} \quad \text{and} \quad \|\xi\|_{\mathrm{BMO}(\Omega)} \lesssim 1,$$

which would prove in the present setting that $\|f\|_{\mathcal{H}^1} \gtrsim \log \epsilon^{-1}$. A suitable choice is given by

$$\xi(\boldsymbol{x}) = \begin{cases} \xi_0(|\boldsymbol{x}-\boldsymbol{x}_+|) & \text{if } |\boldsymbol{x}-\boldsymbol{x}_+| \leq \frac{1}{4} \\ -\xi_0(|\boldsymbol{x}-\boldsymbol{x}_-|) & \text{if } |\boldsymbol{x}-\boldsymbol{x}_-| \leq \frac{1}{4} \\ 0 & \text{otherwise} \end{cases} \qquad \text{where} \qquad \xi_0(r) = \begin{cases} \log(\frac{1}{4\epsilon}) & \text{if } r \leq \epsilon \\ \log(\frac{1}{4r}) & \text{if } \epsilon < r \leq 1/4 \cdot \\ 0 & \text{otherwise} \end{cases}$$

For one,

$$\int_\Omega \xi f \mathrm{d}\boldsymbol{x} = \int_{B_\epsilon(\boldsymbol{x}_+)} \xi_0(|\boldsymbol{x}-\boldsymbol{x}_+|) f_+(\boldsymbol{x}) \mathrm{d}\boldsymbol{x} + \int_{B_\epsilon(\boldsymbol{x}_-)} \xi_0(|\boldsymbol{x}-\boldsymbol{x}_-|) f_-(\boldsymbol{x}) \mathrm{d}\boldsymbol{x} = 2\log\left(\frac{1}{4\epsilon}\right) \gtrsim \log\frac{1}{\epsilon}.$$

Also, $\|\xi\|_{\mathrm{BMO}(\Omega)} \lesssim 1$ as $\log(|\boldsymbol{x}|) \in \mathrm{BMO}(\mathbb{R}^d)$, and since the minimum and maximum of two functions $g, h \in \mathrm{BMO}(\mathbb{R}^d)$ have BMO-norms bounded by a multiple of $\|g\|_{\mathrm{BMO}(\mathbb{R}^d)} + \|h\|_{\mathrm{BMO}(\mathbb{R}^d)}$ (see [Ste93, Ch. IV]).

Continuing, we compute the H^1-norm in the dominator of III.30. Evidently,

$$\int_\Omega |\nabla\xi|^2 \mathrm{d}\boldsymbol{x} = \int_{\Omega\setminus B_\epsilon(\boldsymbol{x}_+)} |\nabla\xi_0(|\boldsymbol{x}-\boldsymbol{x}_+|)|^2 \mathrm{d}\boldsymbol{x} + \int_{\Omega\setminus B_\epsilon(\boldsymbol{x}_-)} |\nabla\xi_0(|\boldsymbol{x}-\boldsymbol{x}_-|)|^2 \mathrm{d}\boldsymbol{x} \lesssim \int_{r=\epsilon}^{r=1/4} \frac{1}{r}\, dr \lesssim \log\frac{1}{\epsilon}.$$

Assembling the estimates shows that

$$\langle |\nabla T|^2 \rangle \gtrsim \frac{\left(\log\frac{1}{\epsilon}\right)^2}{\log\frac{1}{\epsilon} + \mathit{Pe}^2} \sim \min\left\{ \log\frac{1}{\epsilon},\ \left(\log\frac{1}{\epsilon}\right)^2 \frac{1}{\mathit{Pe}^2} \right\}.$$

Proof of the upper bound We turn to construct steady velocity fields $\boldsymbol{u}(\boldsymbol{x})$ saturating the lower bound. Arguing just as in proof of 3.3.3 (see the derivation leading up to III.28) we apply 3.2.4 to show that

$$\left\langle |\nabla T|^2 \right\rangle \leq \frac{1}{\mathit{Pe}^2} \fint_\Omega |\boldsymbol{u}|^2 \mathrm{d}\boldsymbol{x} \fint_\Omega |\nabla\eta|^2 \mathrm{d}\boldsymbol{x} + \fint_\Omega \left|\nabla\Delta^{-1}(\boldsymbol{u}\cdot\nabla\eta - f)\right|^2 \mathrm{d}\boldsymbol{x} \tag{III.31}$$

where T is the temperature field associated to the scaled version of $\boldsymbol{u}$ with mean kinetic energy *Pe*. Again, this upper bound applies for any choice of $\boldsymbol{u}$ and η, regardless of the L^2-norm of the

velocity. We shall consider two different choices for $(\boldsymbol{u}, \eta)$, the first of which involves no flow, and the second of which is the anticipated pinching flow.

No flow The first possibility is to take $\boldsymbol{u} = \mathbf{0}$. Then η drops out in III.31, and we see that

$$\langle |\nabla T|^2 \rangle \leq \fint_\Omega \left| \nabla \Delta^{-1} f \right|^2 \mathrm{d}\boldsymbol{x} = \max_{\substack{\varphi(\boldsymbol{x}) \\ \fint_\Omega \varphi \mathrm{d}\boldsymbol{x} = 0}} \frac{\left| \int_\Omega (\varphi_+ - \varphi_-)(f_+ - f_-) \right|^2}{\fint_\Omega |\nabla \varphi|^2}.$$

To prove that $\langle |\nabla T|^2 \rangle \lesssim \log(\epsilon^{-1})$, which is the desired upper bound in this case, it suffices to show that

$$\left| \int_\Omega (\varphi_+ - \varphi_-)(f_+ - f_-) \mathrm{d}\boldsymbol{x} \right|^2 \lesssim \log\left(\frac{1}{\epsilon}\right) \int_\Omega |\nabla \varphi|^2 \mathrm{d}\boldsymbol{x}. \tag{III.32}$$

Here, $\varphi_\pm$ are the positive and negative parts of φ, and we allow for any combination of pluses and minuses on the left (e.g., $\varphi_+ f_-$). Since the argument is the same for all combinations, we use $\varphi_+ f_+$. By our assumptions on f,

$$\int_\Omega \varphi_+ f_+ \mathrm{d}\boldsymbol{x} = \int_{B_\epsilon(\boldsymbol{x}_+)} \varphi_+ f_+ \mathrm{d}\boldsymbol{x} \lesssim \fint_{Q_\epsilon(\boldsymbol{x}_+)} \varphi_+ \mathrm{d}\boldsymbol{x}$$

where $Q_\epsilon(\boldsymbol{x}_+)$ is the open square of side length ϵ centered at $\boldsymbol{x}_+$. The desired bound now follows from a BMO-type argument, involving controlling consecutive jumps in the average of φ_+ along a sequence of squares starting with $Q_\epsilon(\boldsymbol{x}_+)$ and ending at Ω.

Since $\Omega = (-1, 1)^2$, there is a sequence of squares $Q_1, \ldots, Q_N \subset \Omega$ of ever increasing diameters and with the following properties: (i) the first square is $Q_1 = Q_\epsilon(\boldsymbol{x}_+)$ and the last square is Ω; (ii) consecutive squares intersect, with an area $|Q_i \cap Q_{i+1}|$ that is within a factor of 5 of the areas $|Q_i|$ and $|Q_{i+1}|$; (iii) no more than 10 squares include any given $\boldsymbol{x} \in \Omega$; (iv) there are $N \sim \log(1/\epsilon)$ squares in total. To use the squares, observe first that

$$\begin{aligned} \left| \fint_{Q_i} \varphi_+ \mathrm{d}\boldsymbol{x} - \fint_{Q_{i+1}} \varphi_+ \mathrm{d}\boldsymbol{x} \right|^2 &\lesssim \fint_{Q_i} \left| \varphi_+ - \fint_{Q_i} \varphi_+ \right|^2 \mathrm{d}\boldsymbol{x} + \fint_{Q_{i+1}} \left| \varphi_+ - \fint_{Q_{i+1}} \varphi_+ \right|^2 \mathrm{d}\boldsymbol{x} \\ &\lesssim \int_{Q_i \cup Q_{i+1}} |\nabla \varphi_+|^2 \mathrm{d}\boldsymbol{x} \end{aligned}$$

by condition (ii) and Poincaré's inequality for $d = 2$. Summing up over consecutive pairs of squares,

$$\left| \fint_{Q_\epsilon(\boldsymbol{x}_+)} \varphi_+ \mathrm{d}\boldsymbol{x} - \fint_\Omega \varphi_+ \mathrm{d}\boldsymbol{x} \right|^2 = \left| \sum_{i=1}^{N-1} \fint_{Q_i} \varphi_+ \mathrm{d}\boldsymbol{x} - \fint_{Q_{i+1}} \varphi_+ \mathrm{d}\boldsymbol{x} \right|^2 \lesssim N \sum_{i=1}^{N-1} \left| \fint_{Q_i} \varphi_+ \mathrm{d}\boldsymbol{x} - \fint_{Q_{i+1}} \varphi_+ \mathrm{d}\boldsymbol{x} \right|^2$$
$$\lesssim N \sum_{i=1}^{N-1} \int_{Q_i \cup Q_{i+1}} |\nabla \varphi_+|^2 \lesssim N \int_\Omega |\nabla \varphi_+|^2$$

where in the first step we used condition (i), in the second step we applied the Cauchy–Schwarz inequality and in the last step we used condition (iii). Since

$$\left| \fint_\Omega \varphi_+ \mathrm{d}\boldsymbol{x} \right|^2 \lesssim \int_\Omega |\varphi|^2 \mathrm{d}\boldsymbol{x} \lesssim \int_\Omega |\nabla \varphi|^2 \mathrm{d}\boldsymbol{x}$$

we can conclude the result. In particular,

$$\left| \int_\Omega \varphi_+ f_+ \right|^2 \lesssim \left| \fint_{Q_\epsilon(\boldsymbol{x}_+)} \varphi_+ \right|^2 \lesssim \left| \fint_\Omega \varphi_+ \right|^2 + \left| \fint_{Q_\epsilon(\boldsymbol{x}_+)} \varphi_+ - \fint_\Omega \varphi_+ \right|^2$$
$$\lesssim (1+N) \int_\Omega |\nabla \varphi|^2 \lesssim \log\left(\frac{1}{\epsilon}\right) \int_\Omega |\nabla \varphi|^2$$

by condition (iv). This shows III.32 and hence

$$\langle |\nabla T|^2 \rangle \lesssim \log \frac{1}{\epsilon}$$

for the choice $\boldsymbol{u} = \boldsymbol{0}$.

Pinching flows Next we show how to achieve $\langle |\nabla T|^2 \rangle \lesssim \log^2(\epsilon^{-1})\, Pe^{-2}$ using a 'pinching' flow. The flow we have in mind squeezes a large portion of the domain Ω into the balls $B_\epsilon(\boldsymbol{x}_\pm)$ where the heat is being added and taken away. This requires the velocity to grow as $1/|\boldsymbol{x} - \boldsymbol{x}_\pm|$, which results in a logarithmically diverging kinetic energy. At the same time we will enforce the pure advection equation $\boldsymbol{u} \cdot \nabla \eta = f$ leading to a similar divergence in the homogeneous H^1-norm of η. Using all

of this in the bound

$$\left\langle |\nabla T|^2 \right\rangle \leq \frac{1}{Pe^2} \fint_\Omega |\boldsymbol{u}|^2 \mathrm{d}\boldsymbol{x} \fint_\Omega |\nabla \eta|^2 \mathrm{d}\boldsymbol{x} \tag{III.33}$$

which follows from III.31 will lead to the desired result.

The key task is to find a way to solve the pure advection equation with the given source–sink functions $f = f_+ - f_-$. Our solution will be symmetric under the reflection $(x, y) \mapsto (x, -y)$, so we define it explicitly on the upper-half plane. Introduce polar coordinates (r, θ) centered at $(0, 1/2 + 2\epsilon)$, and let R_ϵ be the rectangle centered at $\boldsymbol{x}_+ = (0, 1/2)$ with vertical side length 2ϵ and horizontal side length $2\sqrt{3}\epsilon$. The rectangle is defined such that it contains the ball $B_\epsilon(\boldsymbol{x}_+)$ where the source f_+ is supported, and is such that its top and bottom sides are tangent to this ball. Outside of R_ϵ and for $y > 0$, we define $\boldsymbol{u} = \nabla^\perp \psi_1$ with

$$\psi_1(\theta) = \begin{cases} \frac{11\pi}{6} - \theta & \theta \in (\frac{5\pi}{3}, \frac{11\pi}{6}] \\ \frac{\pi}{6} & \theta \in (\frac{4\pi}{3}, \frac{5\pi}{3}] \\ \theta - \frac{7\pi}{6} & \theta \in (\frac{7\pi}{6}, \frac{4\pi}{3}] \\ 0 & \text{otherwise} \end{cases}.$$

The streamlines are left-right symmetric and are arranged in two trapezoidal channels, and the flow enters the rectangle R_ϵ from the right and exits it on the left. Inside R_ϵ, we use a horizontal flow that matches the inflow and outflow conditions of the prior construction on the vertical sides of R_ϵ. Specifically, we take $\boldsymbol{u} = \nabla^\perp \psi_2$ with

$$\psi_2(y) = \psi_1\left(2\pi - \arctan\left(\frac{2y - 1 - 4\epsilon}{2\sqrt{3}\epsilon}\right)\right) = -\frac{\pi}{6} - \arctan\left(\frac{2y - 1 - 4\epsilon}{2\sqrt{3}\epsilon}\right).$$

The rest of the flow is defined by odd reflection across the line $y = 0$.

Having chosen $\boldsymbol{u}$, we now show how to solve $\boldsymbol{u} \cdot \nabla \eta = f$ to produce the required test function

η. Inside R_ϵ the equation simplifies to $\partial_y \psi_2 \partial_x \eta = f$, which we integrate to get $\eta = \eta_2$ with

$$\eta_2(\boldsymbol{x}) = \int_0^x \frac{f(s,y)}{\partial_y \psi_2(y)}\,\mathrm{d}s = -\int_0^x \frac{12\epsilon^2 + (2y-1-4\epsilon)^2}{4\sqrt{3}\epsilon}\, f(s,y)\,\mathrm{d}s.$$

Outside of R_ϵ and for $y > 0$, we take $\eta = \eta_1 = 0$ in regions of no flow, and choose η_1 to be otherwise constant along the streamlines. Matching conditions are imposed to ensure continuity across the boundary of R_ϵ. In formulas,

$$\eta_1(\theta) = \begin{cases} \eta_2(\sqrt{3}\epsilon, \frac{1}{2} + 2\epsilon + \sqrt{3}\epsilon\tan\theta) & \text{if } \theta \in (\frac{5\pi}{3}, \frac{11\pi}{6}] \\ \eta_2(-\sqrt{3}\epsilon, \frac{1}{2} + 2\epsilon - \sqrt{3}\epsilon\tan\theta) & \text{if } \theta \in (\frac{7\pi}{6}, \frac{4\pi}{3}] \\ 0 & \text{otherwise} \end{cases}.$$

This gives $\boldsymbol{u}\cdot\nabla\eta_1 = 0$ outside of R_ϵ, and then we define η for $y < 0$ by reflection about $y = 0$. Altogether, we have produced a pair $(\boldsymbol{u}, \eta)$ solving the pure advection equation $\boldsymbol{u}\cdot\nabla\eta = f$ on Ω.

To complete the proof we must estimate the L^2-norms of $\boldsymbol{u}$ and $\nabla\eta$. By the up-down symmetry,

$$\begin{aligned}\int_\Omega |\boldsymbol{u}|^2\,\mathrm{d}\boldsymbol{x} &\lesssim \int_{(\Omega\setminus R_\epsilon)\cap\{y>0\}} |\nabla\psi_1|^2\,\mathrm{d}\boldsymbol{x} + \int_{R_\epsilon} |\nabla\psi_2|^2\,\mathrm{d}\boldsymbol{x} \\ &\lesssim \int_0^{2\pi}\int_{2\sqrt{3}}^{\frac{1}{2}} |\partial_r\psi_1|^2 + \left|\frac{1}{r}\partial_\theta\psi_1\right|^2 r\mathrm{d}r\mathrm{d}\theta + \int_{R_\epsilon}\left|\frac{4\sqrt{3}\epsilon}{12\epsilon^2 + (2y-1-4\epsilon)^2}\right|^2 \mathrm{d}\boldsymbol{x} \\ &\lesssim \log\left(\frac{1}{\epsilon}\right) + 1\end{aligned}$$

A similar calculation using the bounds $|f| \lesssim \epsilon^{-2}$ and $|\nabla f| \lesssim \epsilon^{-3}$ assumed at the start of the example give that

$$\int_\Omega |\nabla\eta|^2\,\mathrm{d}\boldsymbol{x} \lesssim \log\left(\frac{1}{\epsilon}\right) + 1.$$

Plugging these estimates into III.33 shows that

$$\left\langle |\nabla T|^2 \right\rangle \lesssim \frac{\log^2(1/\epsilon)}{\boldsymbol{Pe}^2}$$

for our pinching flow.

Using the better of the two flows — no flow or the pinching flow — bounds the minimum thermal dissipation by

$$\min \langle |\nabla T|^2 \rangle \lesssim \min \left\{ \log \frac{1}{\epsilon}, \left(\log \frac{1}{\epsilon} \right)^2 \frac{1}{Pe^2} \right\}.$$

The proof is complete. □

3.4 Asymptotic analysis of steady optimal flows

Each of the lower bounds from the previous section rearranges to give an asymptotic result: given a sequence $\{(\boldsymbol{u}_n, T_n)\}$ solving the advection-diffusion equation with source–sink $f(\boldsymbol{x})$ and with $\langle |\boldsymbol{u}_n|^2 \rangle \to \infty$,

$$\liminf_{n\to\infty} \langle |\boldsymbol{u}_n|^2 \rangle \cdot \langle |\nabla T_n|^2 \rangle \gtrsim_{\Omega,d} \|f\|^2_{\mathcal{H}^1(\Omega)} > 0.$$

The cellular and pinching flow examples from Section 3.3.3 give scenarios in which this bound is sharp in its scaling with respect to the mean kinetic energy $\langle |\boldsymbol{u}_n|^2 \rangle$, as well as features of f. Motivated by this, we now ask what it takes for a sequence of velocity fields to be 'almost optimal' in the sense that their thermal dissipation is minimized at leading order. Focusing on the fully steady case where $\boldsymbol{u} = \boldsymbol{u}(\boldsymbol{x})$, $f = f(\boldsymbol{x})$ and $T = T(\boldsymbol{x})$, we obtain a limiting variational problem whose minimizers encode key asymptotic properties of almost minimizers (including minimizers as a special case). The minimum value of this problem gives the sharpest possible asymptotic lower bound.

A word about setup is required, especially regarding the regularity of our velocity fields. Depending on the application, one may wish to constrain a different norm of the velocity other than the kinetic energy-based L^2-one we have used so far (e.g., the convection problem treated in Section 3.5 lends itself to the H^1-norm). In this section, we consider divergence-free and no-penetration velocities $\boldsymbol{u}$ belonging to a general Banach space $(X, \|\cdot\|_X)$, which for a technical reason we must assume is continuously embedded into $L^d(\Omega)$ via the inequality $\|\cdot\|_{L^d(\Omega)} \lesssim \|\cdot\|_X$. We further

assume X is a dual space, so that its unit ball $\|\cdot\|_X \leq 1$ is weak-$*$ compact [Bre11]; this ensures the existence of optimizers for the problems we consider below. Following remark 3.2.6, we let $f \in H^{-1}(\Omega)$ and be mean-free.

Given this setup, we ask to take the parameter $Pe \to \infty$ in the sequence of minimization problems

$$\min_{\substack{\boldsymbol{u}(\boldsymbol{x}) \\ \|\boldsymbol{u}\|_X \leq Pe \\ \boldsymbol{u}\cdot\nabla T = \Delta T + f}} \fint_\Omega |\nabla T|^2 \mathrm{d}\boldsymbol{x}. \tag{III.34}$$

Applying the sharp variational upper bound from 3.2.4, we learn that

$$\min_{\substack{\boldsymbol{u}(\boldsymbol{x}) \\ \|\boldsymbol{u}\|_X \leq Pe \\ \boldsymbol{u}\cdot\nabla T = \Delta T + f}} \fint_\Omega |\nabla T|^2 \mathrm{d}\boldsymbol{x} = \min_{\substack{\boldsymbol{u}(\boldsymbol{x}), \eta(\boldsymbol{x}) \\ \|\boldsymbol{u}\|_X \leq Pe}} \fint_\Omega |\nabla \eta|^2 + |\nabla \Delta^{-1}(\boldsymbol{u}\cdot\nabla\eta - f)|^2 \mathrm{d}\boldsymbol{x} \tag{III.35}$$

where the admissible η belong to $H^1(\Omega)$. The differential equation on the left-hand side is embedded in the optimization on the right. It follows from the right-hand formulation that optimal velocities achieve $\|\boldsymbol{u}\|_X = Pe$ if f is not identically zero, since otherwise one could decrease the minimum by replacing $(\boldsymbol{u}, \eta)$ with $(\lambda\boldsymbol{u}, \lambda^{-1}\eta)$ for some $\lambda > 1$.

First, we identify a sufficient and necessary condition for the minimum to scale as Pe^{-2}.

Lemma 3.4.1. *There holds*

$$\limsup_{Pe\to\infty} \min_{\substack{\boldsymbol{u}(\boldsymbol{x}) \\ \|\boldsymbol{u}\|_X \leq Pe \\ \boldsymbol{u}\cdot\nabla T = \Delta T + f}} Pe^2 \fint_\Omega |\nabla T|^2 \mathrm{d}\boldsymbol{x} < \infty$$

if and only if there exists $(\boldsymbol{u}_0, T_0) \in X \times H^1(\Omega)$ *satisfying*

$$\begin{cases} \boldsymbol{u}_0 \cdot \nabla T_0 = f & \text{in } \Omega \\ \nabla \cdot \boldsymbol{u}_0 = 0 & \text{in } \Omega \\ \boldsymbol{u}_0 \cdot \hat{\boldsymbol{n}} = 0 & \text{at } \partial\Omega \end{cases} . \tag{III.36}$$

Proof. That the existence of $(\boldsymbol{u}_0, T_0)$ implies the asserted Pe^{-2} bound follows from the right-hand formulation of the optimization in III.35. Indeed, we can always assume that $\|\boldsymbol{u}_0\|_X = 1$, and then setting $(\boldsymbol{u}, \eta) = (Pe\,\boldsymbol{u}_0, Pe^{-1}\,T_0)$ into III.35 shows that $\min \fint_\Omega |\nabla T|^2 \leq Pe^{-2} \fint_\Omega |\nabla T_0|^2$ for all Pe.

For the reverse implication, let $\{\boldsymbol{u}_{Pe}\}$ be an admissible sequence for the finite-Pe problems, with $\|\boldsymbol{u}_{Pe}\|_X \leq Pe$ and whose temperatures $\{T_{Pe}\}$ obey $\fint_\Omega |\nabla T_{Pe}|^2 \lesssim Pe^{-2}$. Rescale to the variables $(\tilde{\boldsymbol{u}}_{Pe}, \tilde{T}_{Pe}) := (Pe^{-1}\boldsymbol{u}_{Pe}, Pe\,T_{Pe})$ to find that

$$\|\boldsymbol{u}_{Pe}\|_X = 1, \quad \|\nabla T_{Pe}\|_{L^2(\Omega)} \leq 1 \quad \text{and} \quad \boldsymbol{u}_{Pe} \cdot \nabla T_{Pe} = \frac{1}{Pe}\Delta T_{Pe} + f$$

after dropping the tildes. Applying the Banach-Alaoglu theorem [Lax02] to the dual Banach space X and using our assumption that it is continuously embedded into $L^d(\Omega)$, hence also in $L^2(\Omega)$ since $d \geq 2$, we can extract a subsequence $\{\boldsymbol{u}_{Pe}, T_{Pe}\}$ (not relabeled) converging weakly-$*$ to $(\boldsymbol{u}_0, T_0)$ both in $X \times H^1(\Omega)$ and in $L^2(\Omega) \times H^1(\Omega)$. Note

$$\|\boldsymbol{u}_{Pe} \cdot \nabla T_{Pe} - f\|_{H^{-1}(\Omega)} = \left\| \frac{1}{Pe}\Delta T_{Pe} \right\|_{H^{-1}(\Omega)} = \frac{1}{Pe}\|\nabla T_{Pe}\|_{L^2(\Omega)} \leq \frac{1}{Pe} \to 0$$

by the definition of the H^{-1}-norm in II.7. An application of the div-curl lemma [Eva90, Theorem 4 in §5.B] then verifies that the dot product $\boldsymbol{u}_{Pe} \cdot \nabla T_{Pe}$ converges to $\boldsymbol{u}_0 \cdot \nabla T_0$, and hence $\boldsymbol{u}_0 \cdot \nabla T_0 = f$. The incompressibility and no-penetration conditions for $\boldsymbol{u}_{Pe}$ are also preserved in the weak-$*$ limit, so that they hold for $\boldsymbol{u}_0$. □

We come now to the main result of this section, in which we rescale the minimization problem III.34 by Pe^{-2} and take $Pe \to \infty$. A sequence of admissible velocities $\{\boldsymbol{u}_{Pe}\}$ with $\|\boldsymbol{u}_{Pe}\|_X \leq Pe$ is said to be *almost minimizing* if their corresponding (steady) temperature fields $\{T_{Pe}\}$ satisfy

$$\fint_\Omega |\nabla T_{Pe}|^2 \mathrm{d}\boldsymbol{x} = \min_{\substack{\boldsymbol{u}(\boldsymbol{x}) \\ \|\boldsymbol{u}\|_X \leq Pe \\ \boldsymbol{u}\cdot\nabla T = \Delta T + f}} \fint_\Omega |\nabla T|^2 \mathrm{d}\boldsymbol{x} + o(Pe^{-2}) \quad \text{as } Pe \to \infty. \tag{III.37}$$

Included in this definition are sequences of optimizers.

Theorem 3.4.2. *Assume the pure advection system III.36 has a solution in $X \times H^1(\Omega)$. Then,*

$$\lim_{Pe\to\infty} \min_{\substack{\boldsymbol{u}(\boldsymbol{x}) \\ \|\boldsymbol{u}\|_X \le Pe \\ \boldsymbol{u}\cdot\nabla T = \Delta T + f}} Pe^2 \fint_\Omega |\nabla T|^2 \mathrm{d}\boldsymbol{x} = \min_{\substack{\boldsymbol{u}_0(\boldsymbol{x}), T_0(\boldsymbol{x}) \\ \|\boldsymbol{u}_0\|_X \le 1 \\ \boldsymbol{u}_0\cdot\nabla T_0 = f}} \fint_\Omega |\nabla T_0|^2 \mathrm{d}\boldsymbol{x} \tag{III.38}$$

where the minimization on the right is over all solutions of III.36 in $X \times H^1(\Omega)$. Also, $\boldsymbol{u}_0$ solves this limiting problem if and only if it is the weak-$*$ limit point in X of a sequence $\{Pe^{-1}\,\boldsymbol{u}_{Pe}\}$ where $\{\boldsymbol{u}_{Pe}\}$ is almost minimizing on the left.

Remark 3.4.3. So long as f is not identically zero, any optimal velocity $\boldsymbol{u}_0$ in the limiting problem must have unit norm, i.e., $\|\boldsymbol{u}_0\|_X = 1$. Indeed, increasing the norm of $\boldsymbol{u}_0$ decreases the value of $\fint_\Omega |\nabla T_0|^2$ via the coupling $\boldsymbol{u}_0 \cdot \nabla T_0 = f$. This is the limiting version of the similar observation made directly after III.35 regarding finite *Pe*.

Remark 3.4.4. Both the dependence of T on $\boldsymbol{u}$ in the finite-*Pe* problems, and of optimal T_0 on $\boldsymbol{u}_0$ at $Pe = \infty$ are one-to-one. The former is simply the uniqueness-property of steady advection-diffusion; the latter comes from the fact that the limiting minimization problem is strictly convex, hence its minimizers are unique. A partial converse holds: if the closed unit ball $\|\cdot\|_X \le 1$ of X is strictly convex, then the correspondence between optimal $\boldsymbol{u}_0$ and optimal T_0 is one-to-one. To see this, note that any two optimizers $\boldsymbol{u}_0$ and $\boldsymbol{u}_0'$ must lie on the boundary of the closed unit ball (by the previous remark). But then their average $(\boldsymbol{u}_0 + \boldsymbol{u}_0')/2$ would also be optimal, which is a contradiction unless $\boldsymbol{u}_0 = \boldsymbol{u}_0'$.

Remark 3.4.5. It is natural to ask whether the limit points of the rescaled temperatures $\{Pe\,T_{Pe}\}$ generated by almost minimizers $\{\boldsymbol{u}_{Pe}\}$ are also captured by the limiting problem. In one direction, it follows from the proof below that the weak-H^1 limit points of $\{Pe\,T_{Pe}\}$ are always optimal for the limiting problem. The converse holds if the space X has an additional 'Radon–Riesz like' property, which requires that every sequence $\{\boldsymbol{u}_n\}$ converging weakly-$*$ to a vector $\boldsymbol{u}$ with $\|\boldsymbol{u}_n\|_X \to \|\boldsymbol{u}\|_X$ also converges strongly to $\boldsymbol{u}$. If X is a Hilbert space then it has this property; uniformly convex spaces such as $L^p(\Omega)$ for $p \in (1, \infty)$ do as well [Bre11]. Under this additional assumption, one can

prove that the sequence of almost minimizing rescaled velocities $\{Pe^{-1}\,\boldsymbol{u}_{Pe}\}$ recovering $\boldsymbol{u}_0$ as in the statement actually converge strongly in X to $\boldsymbol{u}_0$ (they consistently lie on the boundary of the unit ball). This and the first part of the previous remark imply that $\{Pe\,T_{Pe}\}$ converge strongly in H^1, to the unique optimizer T_0 corresponding to $\boldsymbol{u}_0$.

Proof. The proof is a tightening of the argument behind 3.4.1. The upper bound

$$\limsup_{Pe\to\infty} \min_{\substack{\boldsymbol{u}(\boldsymbol{x}) \\ \|\boldsymbol{u}\|_X \le Pe \\ \boldsymbol{u}\cdot\nabla T = \Delta T + f}} Pe^2 \fint_\Omega |\nabla T|^2 \mathrm{d}\boldsymbol{x} \le \min_{\substack{\boldsymbol{u}_0(\boldsymbol{x}), T_0(\boldsymbol{x}) \\ \|\boldsymbol{u}_0\|_X \le 1 \\ \boldsymbol{u}_0\cdot\nabla T_0 = f}} \fint_\Omega |\nabla T_0|^2 \mathrm{d}\boldsymbol{x} \tag{III.39}$$

follows just as in the 'if' part of the lemma. In particular, any admissible $(\boldsymbol{u}_0, T_0)$ with $\|\boldsymbol{u}_0\|_X = 1$ on the right satisfies

$$Pe^2 \fint_\Omega |\nabla T_{Pe}|^2 \le \fint_\Omega |\nabla T_0|^2 \tag{III.40}$$

where T_{Pe} solves the advection-diffusion equation with $\boldsymbol{u}_{Pe} = Pe\,\boldsymbol{u}_0$ (use $\eta = Pe^{-1}\,T_0$ in 3.2.4). The desired inequality III.39 follows from minimizing over $(\boldsymbol{u}_0, T_0)$. In particular, when f is not identically zero we can discard the case $\|\boldsymbol{u}_0\|_X < 1$ as being sub-optimal per remark 3.4.3; if f is identically zero, there is nothing to show.

Next, we show the lower bound

$$\min_{\substack{\boldsymbol{u}_0(\boldsymbol{x}), T_0(\boldsymbol{x}) \\ \|\boldsymbol{u}_0\|_X \le 1 \\ \boldsymbol{u}_0\cdot\nabla T_0 = f}} \fint_\Omega |\nabla T_0|^2 \mathrm{d}\boldsymbol{x} \le \liminf_{Pe\to\infty} \min_{\substack{\boldsymbol{u}(\boldsymbol{x}) \\ \|\boldsymbol{u}\|_X \le Pe \\ \boldsymbol{u}\cdot\nabla T = \Delta T + f}} Pe^2 \fint_\Omega |\nabla T|^2 \mathrm{d}\boldsymbol{x}. \tag{III.41}$$

Start by considering a general admissible sequence $\{\boldsymbol{u}_{Pe}\}$ on the right, with $\|\boldsymbol{u}_{Pe}\|_X \le Pe$ and whose temperatures $\{T_{Pe}\}$ can be taken to obey $\fint_\Omega |\nabla T_{Pe}|^2 \lesssim Pe^{-2}$ as otherwise there is nothing to show. Again following the proof of 3.4.1, we rescale to $\{(Pe^{-1}\boldsymbol{u}_{Pe}, Pe\,T_{Pe})\}$ and extract a weak-$*$

limit point $(\boldsymbol{u}_0, T_0) \in X \times H^1(\Omega)$ solving the pure advection system III.36. Moreover,

$$\|\boldsymbol{u}_0\|_X \leq \liminf_{Pe\to\infty} \|\, Pe^{-1}\, \boldsymbol{u}_{Pe}\|_X \leq 1, \tag{III.42a}$$

$$⨍_\Omega |\nabla T_0|^2 \,\mathrm{d}\boldsymbol{x} \leq \liminf_{Pe\to\infty} Pe^2 ⨍_\Omega |\nabla T_{Pe}|^2 \,\mathrm{d}\boldsymbol{x} \tag{III.42b}$$

by the weak-$*$ lower semi-continuity of (dual) norms. Minimizing over all sequences $\{\boldsymbol{u}_{Pe}\}$ with the above properties yields III.41. At this stage, it is clear that both inequalities in III.39 and III.41 are actually equalities, so III.38 is proved.

We end with the claim regarding the pairing between weak-$*$ limit points of almost minimizers $\{\boldsymbol{u}_{Pe}\}$, which by definition obey III.37, and the solutions $(\boldsymbol{u}_0, T_0)$ of the limiting problem. On the one hand, suppose $\boldsymbol{u}_0$ is optimal in the limit. Going back to the proof of the upper bound III.39, we see that the rescaled velocities $\{Pe\,\boldsymbol{u}_0\}$ must be almost minimizers. In particular, the left-hand sides of III.39 and the optimized version of III.40 are equal up to $o(1)$ terms. Conversely, if the sequence $\{\boldsymbol{u}_{Pe}\}$ used in the proof of III.41 is almost minimizing, then the weak-$*$ limit points $(\boldsymbol{u}_0, T_0)$ found by rescaling must be optimal in the limit. This is because the left-hand sides of III.41 and III.42b become equal when the latter is applied to an almost minimizing sequence. □

3.5 Internally heated buoyancy-driven flows

We finally come to the problem of bounding the heat transport of an internally heated buoyancy-driven flow. As usual, we assume the source–sink function $f(\boldsymbol{x})$ is mean-free so that its heating and cooling is balanced, and suppose it is not identically zero. The velocity $\boldsymbol{u}(\boldsymbol{x}, t)$ and temperature $T(\boldsymbol{x}, t)$ are required to satisfy the equations

$$Pr^{-1}\,(\partial_t \boldsymbol{u} + \boldsymbol{u}\cdot\nabla\boldsymbol{u}) = \Delta\boldsymbol{u} + Ra\,T\boldsymbol{g} - \nabla p \tag{III.43a}$$

$$\partial_t T + \boldsymbol{u}\cdot\nabla T = \Delta T + f \tag{III.43b}$$

in addition to the usual divergence-free and no-penetration boundary conditions. Here, $\boldsymbol{g}(\boldsymbol{x}) = \nabla\varphi(\boldsymbol{x})$ is a conservative gravitational acceleration field with a non-constant potential $\varphi \in H^1(\Omega)$. For example, setting $\varphi = z$ gives $\boldsymbol{g} = \hat{\boldsymbol{k}}$ which is a common choice in studies of convection.

Momentum conservation implies balance laws relating the flow's mean enstrophy $\langle|\nabla\boldsymbol{u}|^2\rangle$ to the Rayleigh-like number *R* measuring the strength of buoyancy relative to viscosity. These balances laws are insensitive to the Prandtl number *Pr*, so it drops out of the analysis. (See the introduction for formulas giving *R* and *Pr* in terms of dimensional parameters). Requiring $\boldsymbol{u}$ to satisfy such balance laws should in principle significantly restrict heat transport. We obtain a trio of lower bounds confirming this intuition for sources and sinks that are not aligned with gravity.

3.5.1 Bounds on enstrophy-constrained flows

We start by deriving bounds on the heat transport achieved by general incompressible flows in terms of their mean enstrophy $\langle|\nabla\boldsymbol{u}|^2\rangle$. These follow from 3.3.1 and the fact that Poincaré's inequality allows us to relate the mean enstrophy to the mean energy $\langle|\boldsymbol{u}|^2\rangle$. Namely,

$$\langle|\boldsymbol{u}|^2\rangle \leq \mu^2\langle|\nabla\boldsymbol{u}|^2\rangle \tag{III.44}$$

for all divergence-free $\boldsymbol{u}$ with $\boldsymbol{u}\cdot\hat{\boldsymbol{n}} = 0$ at $\partial\Omega$. This can be checked for an arbitrary bounded Lipschitz domain Ω using an argument-by-contradiction, with the crucial point being that the only constant flow satisfying no-penetration conditions is no flow (see, e.g., [Bis88]). The optimal constant is

$$\mu^2 = \min_{\boldsymbol{u}(\boldsymbol{x})} \frac{\int_\Omega |\nabla\boldsymbol{u}|^2 \,\mathrm{d}\boldsymbol{x}}{\int_\Omega |\boldsymbol{u}|^2 \,\mathrm{d}\boldsymbol{x}}$$

with divergence-free and no-penetration conditions. Applying III.44 to the lower bound from 3.3.1 and eliminating the test function ξ proves the following result:

Corollary 3.5.1. *Suppose the hypotheses of 3.3.1 hold and let $\langle|\nabla\boldsymbol{u}|^2\rangle < \infty$. There are positive constants C_1, C_2 and C_3 depending on the domain Ω, the dimension d and the source–sink*

distribution f such that

$$\langle |\nabla T|^2 \rangle \geq \frac{C_1}{C_2 + C_3 \langle |\nabla \boldsymbol{u}|^2 \rangle}. \tag{III.45}$$

Remark 3.5.2. For flows in dimensions $d = 2, 3$ this result does not require the second assumption on f in III.7. This follows from remark 3.2.2 because flows with bounded mean enstrophy belong to $L^p(\Omega)$ at a.e. time for $p < 2d/(d-2)$, by the Sobolev embedding theorem.

3.5.2 Balance laws

The next ingredient for deriving Rayleigh-dependent bounds on $\langle |\nabla T|^2 \rangle$ is a pair of balance laws relating the mean enstrophy $\langle |\nabla \boldsymbol{u}|^2 \rangle$ to the flux-based Rayleigh number R in the momentum equation. The first law states that the rate of energy loss to viscous dissipation must balance the total power supplied to drive the flow:

$$\left\langle |\nabla \boldsymbol{u}|^2 \right\rangle = \langle R\, T \boldsymbol{g} \cdot \boldsymbol{u} \rangle . \tag{III.46}$$

To prove it, dot III.43a by $\boldsymbol{u}$ and integrate by parts in space and time, using the no-penetration conditions to drop the boundary terms.

A second balance law is obtained by testing the advection-diffusion equation III.43b against the gravitational potential φ. Recalling that $\boldsymbol{g} = \nabla \varphi$, this yields

$$-\langle f \varphi \rangle = \langle \boldsymbol{g} \cdot (\boldsymbol{u} T - \nabla T) \rangle . \tag{III.47}$$

In the Boussinesq approximation, temperature and density variations are negatively proportional to one another (see, e.g., [SV60]). Thus, we can interpret this balance law as expressing a conservation of total gravitational potential energy: the change in potential energy due to the heating and cooling must balance a similar change from the total heat flux.

Combining III.46 with III.47 and applying the Cauchy–Schwarz inequality, we deduce that

$$\begin{aligned}\langle|\nabla \boldsymbol{u}|^2\rangle &= R\,\langle \boldsymbol{g}\cdot\nabla T - f\varphi\rangle \\ &\leq R\,\langle|\boldsymbol{g}|^2\rangle^{\frac{1}{2}}\langle|\nabla T|^2\rangle^{\frac{1}{2}} - R\,\langle f\varphi\rangle\,. \end{aligned} \tag{III.48}$$

This sets a Rayleigh-dependent limit on the advective intensity of buoyancy-driven internally heated flows.

3.5.3 Bounds on buoyancy-driven flows

It is now an algebraic exercise to obtain lower bounds on the heat transport of internally heated buoyancy-driven flows. Here is the result:

Theorem 3.5.3. *Let $\boldsymbol{u}(\boldsymbol{x},t)$ and $T(\boldsymbol{x},t)$ solve the Boussinesq equations III.43 with insulating and no-penetration boundary conditions. Let $f(\boldsymbol{x})$ be a balanced and steady source–sink distribution satisfying the assumptions of 3.3.1, and take C_1, C_2 and C_3 to be as in 3.5.1. We have the following bounds:*

1. *If $\langle f\varphi\rangle > 0$,*
$$\langle|\nabla T|^2\rangle \geq \frac{\langle f\varphi\rangle^2}{\langle|\boldsymbol{g}|^2\rangle} \quad \textit{for all } R;$$
2. *If $\langle f\varphi\rangle = 0$, there exists $R_0 > 0$ such that*
$$\langle|\nabla T|^2\rangle \geq \left(\frac{C_1}{2C_3\langle|\boldsymbol{g}|^2\rangle^{\frac{1}{2}}R}\right)^{\frac{2}{3}} \quad \textit{for all } R > R_0;$$
3. *If $\langle f\varphi\rangle < 0$, there exists $R_1 > 0$ such that*
$$\langle|\nabla T|^2\rangle \geq \frac{C_1}{2C_2 + 2C_3\,|\langle f\varphi\rangle|\,R} \quad \textit{for all } R > R_1\,.$$

Remark 3.5.4. 3.5.3 actually applies to all divergence-free and no-penetration velocities $\boldsymbol{u}$ and temperatures T that need not solve the Boussinesq equations, but only satisfy the balance laws

III.47 and the (time-averaged) energy inequality $\langle|\nabla \boldsymbol{u}|^2\rangle \leq \langle R T \boldsymbol{g}\cdot \boldsymbol{u}\rangle$, which is a weakening of III.46. These conditions, and hence our bounds, hold for Leray–Hopf solutions of III.43 (see [CNO16, Nob23] for similar comments in the context of Rayleigh–Bénard convection).

Proof. Statement 1 is a direct consequence of estimate III.48, the nonnegativity of $\langle|\nabla \boldsymbol{u}|^2\rangle$ and the positivity of $\langle f\varphi\rangle$.

For the other two statements, start by combining III.48 with the general lower bound in III.45 to deduce that

$$\langle|\nabla T|^2\rangle \geq \frac{C_1}{C_2 + C_3 R \langle|\boldsymbol{g}|^2\rangle^{\frac{1}{2}}\langle|\nabla T|^2\rangle^{\frac{1}{2}} + C_3 R\,|\langle f\varphi\rangle|}. \tag{III.49}$$

To prove statement 2, set $\langle f\varphi\rangle = 0$ to obtain

$$\langle|\nabla T|^2\rangle \geq \frac{C_1}{C_2 + C_3 R \langle|\boldsymbol{g}|^2\rangle^{\frac{1}{2}}\langle|\nabla T|^2\rangle^{\frac{1}{2}}}. \tag{III.50}$$

This implies that $\langle|\nabla T|^2\rangle \geq C_1/(2C_2)$ if $\langle|\nabla T|^2\rangle \leq C_2^2/(C_3^2 R^2 \langle|\boldsymbol{g}|^2\rangle)$, a contradiction if R is sufficently large. Thus, we can find $R_0 > 0$ so that $\langle|\nabla T|^2\rangle \geq C_2^2/(C_3^2 R^2 \langle|\boldsymbol{g}|^2\rangle)$ if $R > R_0$. With this, III.50 follows from the stronger bound

$$\langle|\nabla T|^2\rangle \geq \left(\frac{C_1}{2C_3\langle|\boldsymbol{g}|^2\rangle^{\frac{1}{2}} R}\right)^{\frac{2}{3}}.$$

Statement 3 follows analogously. If

$$C_3 R \langle|\boldsymbol{g}|^2\rangle^{\frac{1}{2}}\langle|\nabla T|^2\rangle^{\frac{1}{2}} \leq C_2 + C_3 R\,|\langle f\varphi\rangle|\,, \tag{III.51}$$

then III.49 implies

$$\langle|\nabla T|^2\rangle \geq \frac{C_1}{2C_2 + 2C_3\,|\langle f\varphi\rangle|\,R}. \tag{III.52}$$

This is consistent with the assumed upper bound III.51 only when

$$C_2 + C_3|\langle f\varphi\rangle|\,R \geq (C_1 C_3^2/2)^{1/3}\langle|\boldsymbol{g}|^2\rangle^{1/3} R^{2/3},$$

which is true when R is sufficiently small or large, and in particular for $R \geq (C_1\langle|\boldsymbol{g}|^2\rangle)/(2C_3\,|\langle f\varphi\rangle|^3)$. For all other values of R we must instead have the opposite of III.51, in which case III.49 gives $\langle|\nabla T|^2\rangle \geq [C_1/(2C_3\langle|\boldsymbol{g}|^2\rangle^{\frac{1}{2}}\,R)]^{2/3}$. In this case,

$$\langle|\nabla T|^2\rangle \geq \max\left\{\frac{1}{\langle|\boldsymbol{g}|^2\rangle}\left(\frac{C_2}{C_3\,R}+|\langle f\varphi\rangle|\right)^2,\ \left(\frac{C_1}{2C_3\langle|\boldsymbol{g}|^2\rangle^{\frac{1}{2}}\,R}\right)^{\frac{2}{3}}\right\}. \tag{III.53}$$

If R is large enough that both lower bounds III.52,III.53 are possible, we must choose the weakest of the two. There clearly exists a large enough $R_1 > 0$ so that III.52 is the weakest bound for $R \geq R_1$. □

We close by discussing the physical meaning of $\langle f\varphi\rangle$ and the role it plays in 3.5.3. As was mentioned briefly after III.47, under the Boussinesq approximation temperature variations δT in the fluid are negatively proportional to density variations $\delta\rho$ via the coefficient of thermal expansion. So, f can be thought of not only as a distributed heat source/sink but also as a sink/source of density. In this light, the three cases in 3.5.3 have to do with whether there is a net negative, zero or positive supply of gravitational potential energy from f. With a positive supply, a strongly convecting and perhaps turbulent flow can result, leading to highly efficient heat transport consistent with our third bound ($\langle f\varphi\rangle < 0$). In contrast, a zero or negative potential energy supply inhibits convection and with it heat transport. This is reflected by the significant barriers to heat transport expressed in the first and second bounds ($\langle f\varphi\rangle > 0$ or $= 0$). We wonder whether, in these cases, turbulence could in some sense be ruled out.

3.6 Conclusion

This section discussed heat transport by incompressible flows in an insulated domain with a balanced distribution of heat sources and sinks. When the temperature $T(\boldsymbol{x},t)$ is a passive scalar that diffuses and is advected by a divergence-free and no-penetration velocity field $\boldsymbol{u}(\boldsymbol{x},t)$, we

showed in Section 3.3 that

$$\langle |\nabla T|^2 \rangle \geq \frac{\left(\fint_\Omega \xi f \mathrm{d}\boldsymbol{x} \right)^2}{\fint_\Omega |\nabla \xi|^2 \mathrm{d}\boldsymbol{x} + C(\Omega, d) \|\xi\|^2_{\mathrm{BMO}(\Omega)} \langle |\boldsymbol{u}|^2 \rangle}. \tag{III.54}$$

This bound holds for mean-free and steady source–sink functions $f(\boldsymbol{x})$, with a constant $C(\Omega, d)$ depending on the flow domain Ω and the dimension $d \geq 2$. It involves a choice of test function $\xi(\boldsymbol{x})$ which can be optimized to obtain a best-case lower bound (see 3.3.1, and also remark 3.3.2 which discusses unsteady f and ξ). Actually, III.54 derives from a more general bound on the heat transport of unsteady source–sink functions and flows, proved in Section 3.2 with a complementary upper bound. As shown by 3.2.4, these bounds are sharp if both $\boldsymbol{u}(\boldsymbol{x})$ and $f(\boldsymbol{x})$ are steady.

We then applied our bounding framework to construct optimal, or at least highly competitive, flows. One example in Section 3.3.3 was of a two-dimensional cellular flow adapted to sinusoidal heating and cooling. A second example involved a pinching flow between concentrated sources and sinks. The latter highlighted our use of Hardy and BMO norms, which came with the choice to apply the div-curl inequality of Coifman, Lions, Meyers and Semmes [CLMS90] to control the non-local term $\langle |\nabla \Delta^{-1} \boldsymbol{u} \cdot \nabla \xi|^2 \rangle$ in an intermediate step. This extended the estimates of [STD07, DT06, Thi12] from the setting of statistically homogeneous and isotropic flows in periodic domains to general flows and domains. The Hardy space norm was pivotal for identifying the optimal scaling of $\min \langle |\nabla T|^2 \rangle$ with respect to the size of the sources and sinks, and for showing the (near) optimality of our pinching flows. The status of pinching flows for other objectives such as $\langle T^2 \rangle$, or in higher dimensions with $d > 2$, remains to be seen.

More generally, for a fixed distribution of heating and cooling $f(\boldsymbol{x})$ such that the pure and steady advection equation $\boldsymbol{u} \cdot \nabla T = f$ is solvable, we showed the convergence

$$\min_{\substack{\boldsymbol{u}(\boldsymbol{x}) \\ \|\boldsymbol{u}\|_X \leq Pe \\ \boldsymbol{u} \cdot \nabla T = \Delta T + f}} Pe^2 \fint_\Omega |\nabla T|^2 \mathrm{d}\boldsymbol{x} \;\to\; \min_{\substack{\boldsymbol{u}_0(\boldsymbol{x}), T_0(\boldsymbol{x}) \\ \|\boldsymbol{u}_0\|_X \leq 1 \\ \boldsymbol{u}_0 \cdot \nabla T_0 = f}} \fint_\Omega |\nabla T_0|^2 \mathrm{d}\boldsymbol{x} \quad \text{as } Pe \to \infty \tag{III.55}$$

where the Péclet number *Pe* set the maximum flow intensity measured in a Banach space norm,

$||\cdot||_X$. The argument in Section 3.4 showed that the minimum values converge, and also that the minimizers (and almost minimizers) of the finite-*Pe* problems on the left-hand side of III.55 converge to those of the limiting problem on its right. Whether or not the pure advection equation is actually solvable is a fascinating and generally open question, even in two dimensions (see [Lin17] and the references therein). Solving it was a key part of the examples in Section 3.3.3.

Finally, we leveraged balance laws implied by momentum conservation to produce lower bounds on $\langle|\nabla T|^2\rangle$ for buoyancy-driven internally heated flows. Section 3.5 considered flows driven by steady heating and cooling $f(\boldsymbol{x})$ and a steady conservative gravitational acceleration $\boldsymbol{g}(\boldsymbol{x}) = \nabla\varphi(\boldsymbol{x})$, with the standard setting being $\varphi = z$. For asymptotically large values of the flux-based Rayleigh number R, we proved that

$$\langle|\nabla T|^2\rangle \gtrsim_{\Omega,d,f,\boldsymbol{g}} \begin{cases} 1 & \text{if } \langle f\varphi\rangle > 0 \\ R^{-2/3} & \text{if } \langle f\varphi\rangle = 0 \\ R^{-1} & \text{if } \langle f\varphi\rangle < 0 \end{cases} \tag{III.56}$$

with a prefactor depending on the domain Ω, the dimension d, the source–sink distribution f and the gravity $\boldsymbol{g}$. The three scaling regimes distinguish whether the spatial arrangement of the heat sources and sinks supplies the fluid with a net negative, zero or positive input of gravitational potential energy. Quite naturally, in the first two cases buoyancy-driven flows have severely limited heat transfer. This leaves open questions about the actual flow. We wonder if $\langle f\varphi\rangle > 0$ implies that 'turbulence' cannot occur, as one might expect it to produce well-mixed temperatures with $\langle|\nabla T|^2\rangle \ll 1$. It should be especially interesting to investigate the borderline case $\langle f\varphi\rangle = 0$, where the possibility of turbulence may be sensitive to the details of the setup (e.g., the shape of the flow domain, or the fine details of the heat sources and sinks versus the gravity).

Contrary to our lower bounds on passive advection-diffusion, we do not know if the estimates in III.56 are ever sharp, or even if they depend optimally on *R*. Turbulent flows observed in experiments and simulations with $\langle f\varphi\rangle < 0$ have $\langle|\nabla T|^2\rangle \sim R^{-1/2}$ [LAG18, BLAG19, KGOM22, MLBG19],

which is much larger than our lower bound. This gap is in line with the broader literature on convection. For instance, with uniformly heated convection between cool boundaries, the lower bound $\langle|\nabla T|^2\rangle \gtrsim R^{-1/3}$ by Lu and Doering [LDB04] is far from the $\langle|\nabla T|^2\rangle \sim R^{-1/5}$ scaling observed in simulations [GS12]. Similarly, upper-bound theory for boundary-driven Rayleigh–Bénard convection proves heat transport bounds that grow with a 'mixing length' scaling [DC96], while most turbulent data displays a slower boundary-limited scaling law [Doe19, Doe20]. This does not mean that the bounds are never sharp — the *a priori* scaling bounds just mentioned are sharp up to possible logarithmic corrections [TD] and without log-corrections in three dimensions [Kum22] for general enstrophy-constrained flows. Likewise, the known bounds on imbalanced internal heating are sharp up to log-corrections [Tob22], and this section has produced sharp bounds for balanced heating has well. In any case, power-law improvements of the known *a priori* bounds must use information from the momentum equation beyond the usual balance laws.

None of this rules out the possibility that there exist other, non-turbulent solutions of the Boussinesq equations for which $\langle|\nabla T|^2\rangle$ displays the same scaling as the lower bounds in III.56. In fact, an asymptotic construction and numerical simulations in [MLBG19] produce steady flows achieving $\langle|\nabla T|^2\rangle \sim R^{-1}$ in a two-dimensional box with insulating vertical boundaries, isothermal bottom boundaries and a sinusoidal heating and cooling profile. Our bounds extend to this configuration with the same scaling results, and different prefactors. Perhaps this suggests the bounds are sharp, or perhaps there are still obstructions to sharpness that have to do with the particular choice of heating and cooling. Enunciating the conditions under which asymptotically optimal heat transport is achievable by momentum-conserving flows remains an interesting open problem.

CHAPTER IV

Oscillatory and Concentrated Heating in General Dimensions and Domains

In Section 3.3.3, our examples are built on 2-d disks and squares. As our result in Section 3.3.2 only requires $d \geq 2$, some optimal flow designs should also be possible in higher dimensions and non-disk type domains. We will adapt the ideas for 2-d heat source–sink functions and corresponding flows and construct examples in general dimensions. Similar to the 2-d case, we will discuss optimal bounds for $\left\langle |\nabla T|^2 \right\rangle$. In Section 4.1, we show that the same scaling of the bounds proved in Section 3.3.3.1 holds for oscillatory heating in general dimensions $d > 2$. For concentrated heating though, we will show in Section 4.2 that the $\log \frac{1}{\epsilon}$ terms in our scalings proved in Section 3.3.3.2 is replaced with ϵ^{d-2} terms in the upper bound resulting in a gap between lower and upper bounds in the strong flow case. Finally in Section 4.3 we will also discuss 2-d concentrated heating on thin neck regions instead of disks and show an optimal bound with scaling $\max\left\{\min\left\{\log\frac{1}{\epsilon},\ \left(\log\frac{1}{\epsilon}\right)^2\frac{1}{Pe^2}\right\},\ \min\left\{\frac{l}{w},\ \left(\frac{l}{w}\right)^2\frac{1}{Pe^2}\right\}\right\}$ where w stands for neck width and l stands for neck length. We will discuss the meaning of these terms there.

4.1 Periodic Heating in General Dimensions

In Section 3.3.3.1, we built an example of high frequency rolls using trigonometric functions. As our result depends on the frequency l and is built upon the periodicity of trigonometric functions, we may adapt our ideas to a lager class of periodic functions and obtain similar results in general dimensions $d \geq 2$. In this section, we'll construct flows corresponding to more general periodic heating $f(\boldsymbol{x})$ on region $\Omega = (0, 2\pi)^d$ for $d \geq 2$ achieving optimal scaling.

Proposition 4.1.1. *Suppose over domain $\Omega = (0, 2\pi)^d$, we have spatially periodic functions $\boldsymbol{u}_0, f_0, \eta_0$ satisfying*

$$\boldsymbol{u}_0 \cdot \nabla \eta_0 = f_0, \quad \fint_\Omega f_0(\boldsymbol{x}, t) \mathrm{d}\boldsymbol{x} = 0$$

with $f_0, \eta_0, \boldsymbol{u}_0 \in L^\infty(\Omega) \cap H^1(\Omega)$ and $\boldsymbol{u}$ satisfying divergence-free and no-penetration boundary conditions. Let

$$f_\ell(\boldsymbol{x}) = f_0(\boldsymbol{x}/\ell)$$

be the periodic extension of f_0 with scaling ℓ^{-1} a positive integer. Then we have

$$\min_{\substack{\boldsymbol{u}(\boldsymbol{x},t) \\ \langle |\boldsymbol{u}|^2 \rangle \le Pe^2 \\ \partial_t T + \boldsymbol{u}\cdot\nabla T = \Delta T + f}} \langle |\nabla T|^2 \rangle \sim \min\left\{ \ell^2, \frac{1}{Pe^2} \right\}$$

for all $\ell^{-1} \in \mathbb{N}$ and $Pe \ge 0$. The alternatives are achieved by no flow (ℓ^2) or by the periodic flow (Pe^{-2}).

Proof. The following proof follows a similar procedures as we did in Section 3.3.3.1. As $f_0, \eta_0, \boldsymbol{u}_0 \in L^\infty(\Omega) \cap H^1(\Omega)$, we will just treat $\|f\|_{H^{-1}(\Omega)}, \|f\|_{L^\infty(\Omega)}, \|\boldsymbol{u}\|_{L^2(\Omega)}, \|\nabla\eta\|_{L^2(\Omega)}$ as bounded constants independent of ℓ^{-1} and *Pe*.

Proof of the lower bound The lower bound is similar to what we had in Proposition 3.3.3. With the general lower bound,

$$\left\langle |\nabla T|^2 \right\rangle \ge \frac{\left(\fint_\Omega \xi f \mathrm{d}\boldsymbol{x} \right)^2}{\fint_\Omega |\nabla \xi|^2 \mathrm{d}\boldsymbol{x} + C(\Omega) \|\xi\|^2_{\mathrm{BMO}(\Omega)} Pe^2}$$

from Corollary 3.3.1, by taking $\xi = f_\ell$, we get

$$\fint_\Omega \xi f_\ell \mathrm{d}\boldsymbol{x} = \fint_\Omega f_\ell^2 \mathrm{d}\boldsymbol{x} = \fint_\Omega f_0^2 \mathrm{d}\boldsymbol{x},$$
$$\fint_\Omega |\nabla \xi|^2 \,\mathrm{d}\boldsymbol{x} = \frac{1}{\ell^2} \fint_\Omega |\nabla f_0|^2 \,\mathrm{d}\boldsymbol{x},$$
$$\|\xi\|_{\mathrm{BMO}(\mathbb{R}^d)} \le 2\|\xi\|_\infty = 2\|f_0\|_\infty.$$

Combining these estimates yields the following lower bound,

$$\left\langle |\nabla T|^2 \right\rangle \ge \frac{\left(\fint_\Omega f_0^2 \mathrm{d}\boldsymbol{x}\right)^2}{\ell^{-2} \fint_\Omega |\nabla f_0|^2 \,\mathrm{d}\boldsymbol{x} + C(\Omega)\|f_0\|_\infty Pe^2} \gtrsim \frac{1}{\ell^{-2} + Pe^2} \gtrsim \min\left\{\ell^2, \frac{1}{Pe^2}\right\}.$$

Proof of the upper bound Using estimate III.28, we still consider the two cases whether $\boldsymbol{u} = \boldsymbol{0}$ or not. In the case with no flow,

$$\left\langle |\nabla T|^2 \right\rangle \le \fint_\Omega \left|\nabla \Delta^{-1} f_\ell\right|^2 \mathrm{d}\boldsymbol{x} = \ell^2 \fint_\Omega \left|\nabla \Delta^{-1} f_0\right|^2 \mathrm{d}\boldsymbol{x}.$$

On the other hand, simply take

$$\boldsymbol{u}(\boldsymbol{x}) = \boldsymbol{u}_0(\boldsymbol{x}/\ell), \quad \eta(\boldsymbol{x}) = \ell \eta_0(\boldsymbol{x}/\ell).$$

We have

$$\boldsymbol{u} \cdot \nabla \eta = f_\ell,$$
$$\fint_\Omega |\boldsymbol{u}|^2 \,\mathrm{d}\boldsymbol{x} = \fint_\Omega |\boldsymbol{u}_0|^2 \,\mathrm{d}\boldsymbol{x},$$
$$\fint_\Omega |\nabla \eta|^2 \,\mathrm{d}\boldsymbol{x} = \fint_\Omega |\nabla \eta_0|^2 \,\mathrm{d}\boldsymbol{x}.$$

so we get

$$\left\langle |\nabla T|^2 \right\rangle \le \frac{1}{Pe^2} \fint_\Omega |\boldsymbol{u}_0|^2 \mathrm{d}\boldsymbol{x} \fint_\Omega |\nabla \eta_0|^2 \mathrm{d}\boldsymbol{x} \lesssim \frac{1}{Pe^2}.$$

Combining the two cases, gives us

$$\min \left\langle |\nabla T|^2 \right\rangle \lesssim \min \left\{ \ell^2, \frac{1}{Pe^2} \right\}.$$

The proof is complete. □

4.2 Concentrated Heating in General Dimensions

Now let's consider point source and sink heat profile in general dimensions. Recall in the 2-d case, the flow is designed to depends on distance from the source-sink only away from the source sink. In higher dimensions, we may adapt this idea. Suppose the domain $\Omega = B(0,1)$ is the unit ball in dimension $d \geq 3$, and the sink-source $f_\pm$ are located symmetrically across the 'equator' in the sense that they center on $\boldsymbol{x}_\pm = (\pm\frac{1}{2}, 0, \ldots, 0)$. Furthermore, we assume the symmetric condition on the value of sink and source as in the 2-d case. More specifically, our f satisfies the following conditions:

$$\begin{aligned} f(\boldsymbol{x}) &= f_+(\boldsymbol{x}) - f_-(\boldsymbol{x}), \\ \text{supp}(f_\pm) &\subset B_\epsilon(\boldsymbol{x}_\pm), \\ \int_{B_\epsilon(\boldsymbol{x}_\pm)} f_\pm(\boldsymbol{x}) \mathrm{d}\boldsymbol{x} &= 1, \\ f_+(x_1, \cdots, x_{d-1}, x_d) &= f_-(-x_1, \cdots, x_{d-1}, x_d). \end{aligned}$$

Proposition 4.2.1. *Let $f(\boldsymbol{x})$ be the intensity of the heat source satisfying above conditions. Suppose*

$$|f| \lesssim \epsilon^{-d}, \quad |\nabla f| \lesssim \epsilon^{-d-1}. \tag{IV.1}$$

Then under the above assumptions,

$$\min\left\{1/\epsilon^{d-2},\, \log^2(\frac{1}{\epsilon})\frac{1}{\mathit{Pe}^2}\right\} \lesssim \min_{\substack{\boldsymbol{u}(\boldsymbol{x},t)\\ \langle|\boldsymbol{u}|^2\rangle\le \mathit{Pe}^2\\ \partial_t T+\boldsymbol{u}\cdot\nabla T=\Delta T+f}} \langle|\nabla T|^2\rangle \lesssim \min\left\{1/\epsilon^{d-2},\, \frac{1}{\epsilon^{d-2}}\frac{1}{\mathit{Pe}^2}\right\}$$

for all $\epsilon \in (0, 1/20)$ *and* $\mathit{Pe} \geq 0$*. The alternatives in the upper bound are achieved by no flow* $(1/\epsilon^{d-2})$ *or by the pinching flow* $(\frac{1}{\epsilon^{d-2}}\,\mathit{Pe}^{-2})$*.*

Proof. To make the calculation simpler, we make use of the hyperspherical coordinates $(r, \varphi_1, \ldots, \varphi_{d-1})$, where $\varphi_1, \ldots, \varphi_{d-2} \in [0, \pi]$ and $\varphi_{d-1} \in [0, 2\pi)$ and

$$\begin{aligned} x_1 &= r\cos\varphi_1,\\ x_2 &= r\sin\varphi_1\cos\varphi_2,\\ &\vdots\\ x_d &= r\sin\varphi_1\cdots\sin(\varphi_{d-1}). \end{aligned}$$

Proof of the lower bound Now we begin with the lower bound, using

$$\left\langle|\nabla T|^2\right\rangle \geq \frac{\left(⨍_\Omega \xi f \mathrm{d}\boldsymbol{x}\right)^2}{⨍_\Omega |\nabla\xi|^2 \mathrm{d}\boldsymbol{x} + C(\Omega)\|\xi\|^2_{\mathrm{BMO}(\Omega)}\,\mathit{Pe}^2}$$

from Corollary 3.3.1. As with the 2-d case, we want to try a $\xi(\boldsymbol{x})$ approaching the Dirac mass, say

$$\xi = \frac{1}{r^{d-2}} \wedge \frac{1}{\epsilon^{d-2}}$$

which would give us

$$
\begin{aligned}
\fint_\Omega \xi f \mathrm{d}\boldsymbol{x} &\sim \frac{1}{\epsilon^{d-2}}, \\
\fint_\Omega |\nabla \xi|^2 \, \mathrm{d}\boldsymbol{x} &\sim \int_\epsilon^1 \frac{(d-2)^2}{r^{2d-2}} r^{d-1} \mathrm{d}r \sim \frac{d-2}{\epsilon^{d-2}}, \\
\|\xi\|_{\mathrm{BMO}(\mathbb{R}^d)} &\leq 2\|\xi\|_\infty = \frac{2}{\epsilon^{d-2}}.
\end{aligned}
$$

Assembling the estimates shows that

$$
\langle |\nabla T|^2 \rangle \gtrsim \frac{1/\epsilon^{2d-4}}{(d-2)/\epsilon^{d-2} + \mathit{Pe}^2 \, /\epsilon^{2d-4}} \sim \min\left\{ 1/\epsilon^{d-2}, \, \frac{1}{\mathit{Pe}^2} \right\}.
$$

Now using the test function $\log \frac{1}{r} \wedge \log \frac{1}{\epsilon}$ as in the 2-d case, we would get lower bound $\log^2(\frac{1}{\epsilon}) \frac{1}{\mathit{Pe}^2}$ for large Pe. Combining these two estimates gives us the lower bound:

$$
\langle |\nabla T|^2 \rangle \gtrsim \min\left\{ 1/\epsilon^{d-2}, \, \log^2(\frac{1}{\epsilon}) \frac{1}{\mathit{Pe}^2} \right\}.
$$

Proof of the upper bound For the upper bound, as before, we use III.28,

$$
\left\langle |\nabla T|^2 \right\rangle \leq \frac{1}{\mathit{Pe}^2} \fint_\Omega |\boldsymbol{u}|^2 \mathrm{d}\boldsymbol{x} \fint_\Omega |\nabla \eta|^2 \mathrm{d}\boldsymbol{x} + \fint_\Omega \left| \nabla \Delta^{-1} (\boldsymbol{u} \cdot \nabla \eta - f) \right|^2 \mathrm{d}\boldsymbol{x}
$$

and consider two different choices for $(\boldsymbol{u}, \eta)$, the first of which involves no flow, and the second of which is the pinching flow.

No flow The first possibility is to take $\boldsymbol{u} = \boldsymbol{0}$. Then η drops out and we get

$$
\langle |\nabla T|^2 \rangle \leq \fint_\Omega \left| \nabla \Delta^{-1} f \right|^2 \mathrm{d}\boldsymbol{x} = \max_{\substack{\varphi(\boldsymbol{x}) \\ \fint_\Omega \varphi \mathrm{d}\boldsymbol{x} = 0}} \frac{\left| \int_\Omega \varphi f \right|^2}{\fint_\Omega |\nabla \varphi|^2}
$$

and near the sink and source, we have

$$|\fint_\Omega f\varphi|^2 \lesssim |\epsilon^{-d}\int_{r<\epsilon}\varphi|^2 \lesssim \left(\epsilon^{-d}\left(\int_{r<\epsilon}1\right)^{\frac{d+2}{2d}}\|\varphi\|_{L^{\frac{2d}{d-2}}(\Omega)}\right)^2 \lesssim \epsilon^{2-d}\|\nabla\varphi\|^2_{L^2(\Omega)}$$

via Sobolev embedding on Ω. Thus we have for no flow case,

$$\left\langle|\nabla T|^2\right\rangle \lesssim 1/\epsilon^{d-2}$$

as wanted.

Pinching flows By the symmetric nature of the location of sink source, we may construct the flow around the sink only and the source will simply be the negative symmetry of the sink as in the 2-d case in Section 3.3.3.2.

First let's fix $O = (\frac{1}{2} + \frac{3+\sqrt{3}}{2}\epsilon, 0, \dots, 0)$ as the center for hyperspherical coordinates. Suppose the sink lies in a small box R_ϵ which is the subset of the ball $B(O, 2\sqrt{3})$ bounded by $x_1 = \frac{1}{2} + \frac{3-\sqrt{3}}{2}\epsilon$ and $x_1 = \frac{1}{2} - \frac{3-\sqrt{3}}{2}\epsilon$. As in the 2-$d$ case, we assume near the sink, the flow goes into the box and flows along the last coordinate x_d. To ensure divergence free conditions, away from the box R_ϵ, the velocity should be given by $\frac{1}{r^{d-1}}$ and in the box, the velocity is determined by the location it enters the box from the sides and remains constant along x_d throughout the box. More precisely, outside box R_ϵ we let

$$u_r(r, \varphi_1, \cdots, \varphi_{d-1}) = \begin{cases} -\frac{1}{r^{d-1}} & \varphi_{d-1} \in (\frac{-\pi}{4}, \frac{\pi}{4}) \\ & \varphi_1, \cdots, \varphi_{d-2} \in (\frac{3\pi}{4}, \frac{5\pi}{6}) \\ \frac{1}{r^{d-1}} & \varphi_{d-1} \in (\frac{3\pi}{4}, \frac{5\pi}{4}) \\ & \varphi_1, \cdots, \varphi_{d-2} \in (\frac{3\pi}{4}, \frac{5\pi}{6}) \\ 0 & \text{otherwise} \end{cases}.$$

The flow defined above enters the box from the right and exits from the left with matching flow speed determined by the speed of the boundary given above. Note that by the construction of the

box R_ϵ, the speed $|\boldsymbol{u}|$ inside the box stays constant and $|\boldsymbol{u}| = \frac{1}{(2\sqrt{3}\epsilon)^{d-1}}$ as the flow enters the box from the same radius $2\sqrt{3}\epsilon$. With the above construction, the main contribution of the L^2 norm of the velocity comes from the boundary of the box R_ϵ. That is we have the estimate

$$\begin{aligned}
⨍_\Omega |\boldsymbol{u}|^2 \mathrm{d}\boldsymbol{x} &\sim \int_{\Omega - R_\epsilon} |\boldsymbol{u}|^2 \mathrm{d}\boldsymbol{x} + \int_{R_\epsilon} |\boldsymbol{u}|^2 \mathrm{d}\boldsymbol{x} \\
&\sim \int_\epsilon^1 \frac{1}{r^{2d-2}} r^{d-1} \mathrm{d}r + \frac{1}{\epsilon^{2d-2}} \epsilon^d \\
&\lesssim \frac{1}{\epsilon^{d-2}}.
\end{aligned}$$

Then we need to define η so that $\boldsymbol{u} \cdot \nabla \eta = f$. So inside the box R_ϵ, we want η_1 to satisfy $u_d \partial_{x_d} \eta_1 = f$, i.e.,

$$\eta_1(\boldsymbol{x}) = \int_0^{x_d} \frac{f(x_1, \cdots, x_{d-1}, s)}{u_1} \mathrm{d}s = -(2\sqrt{3}\epsilon)^{d-1} \int_0^{x_d} f(x_1, \cdots, x_{d-1}, s) \mathrm{d}s \tag{IV.2}$$

in the box and outside the box, the values are constant along streamlines with matching values on the boundary of the box. That is we can define η_2 as follows:

$$\eta_2(\varphi_1, \cdots, \varphi_{d-1}) = \begin{cases} \eta_1(2\sqrt{3}\epsilon, \varphi_1, \cdots, \varphi_{d-1}) & \varphi_{d-1} \in (\frac{-\pi}{4}, \frac{\pi}{4}) \cup (\frac{3\pi}{4}, \frac{5\pi}{4}) \\ & \varphi_1, \cdots, \varphi_{d-2} \in (\frac{3\pi}{4}, \frac{5\pi}{6}) \\ 0 & \text{otherwise} \end{cases}. \tag{IV.3}$$

With this construction, we have

$$\boldsymbol{u} \cdot \nabla \eta = f$$

and thus

$$\left\langle |\nabla T|^2 \right\rangle \leq \frac{1}{Pe^2} ⨍_\Omega |\boldsymbol{u}|^2 \mathrm{d}\boldsymbol{x} ⨍_\Omega |\nabla \eta|^2 \mathrm{d}\boldsymbol{x}.$$

Also, using IV.2 and the bound on $f, \nabla f$ (IV.1), we have inside the box R_ϵ,

$$\int_{R_\epsilon} |\nabla \eta_1|^2 \mathrm{d}\boldsymbol{x} \sim |R_\epsilon| \, \epsilon^{2d-2} \left(\int_0^\epsilon \epsilon^{-d-1} \right)^2 \sim \epsilon^{d-2}.$$

Outside the box, as $\varphi_1, \cdots, \varphi_{d-2} \in (\frac{3\pi}{4}, \frac{5\pi}{6})$, we have $\sin(\varphi_i)$ can be treated as constants for $i = 1, \cdots, d-2$. So we have

$$\int_{\Omega - R_\epsilon} |\nabla \eta_1|^2 \mathrm{d}\boldsymbol{x} \sim \int_\epsilon^1 \frac{1}{r^2} r^{d-1} dr \sim 1.$$

Adding the previous two estimations, we have the following estimate on Ω:

$$⨍_\Omega |\nabla \eta|^2 \mathrm{d}\boldsymbol{x} \sim 1.$$

Together with the estimate on velocity $\boldsymbol{u}$, this gives us

$$\langle |\nabla T|^2 \rangle \lesssim \frac{1}{\epsilon^{d-2}} \frac{1}{Pe^2}.$$

Using the better of the two flows — no flow or the pinching flow — bounds the minimum thermal dissipation by

$$\min \langle |\nabla T|^2 \rangle \lesssim \min \left\{ 1/\epsilon^{d-2}, \, \frac{1}{\epsilon^{d-2}} \frac{1}{\boldsymbol{Pe}^2} \right\}.$$

The proof is complete. □

4.3 Thin Neck Flow

Now that we considered extensions of Section 3.3.3.1 to higher dimensions, another topic we could look at is how would a different domain in 2-d affect the flows and optimizers. Would pinching flow still be an optimal choice for concentrated heating and how would the shape of the domain change the optimization? In this section, we analyze the case where the concentrated sink and source are connected by a thin neck. Taking into account the thickness and length of the

neck, we try to find the scaling with respect to all these parameters. More specifically, consider the following heating and domain: let $f_\pm$ locate symmetrically in the sense that their support center on $\boldsymbol{x}_\pm = (\pm\frac{l+2}{2}, 0)$ with radius ϵ. The domain Ω is given by a dumbbell shaped region: two disks $B(\boldsymbol{x}_-, 1)$ and $B(\boldsymbol{x}_+, 1)$ are connected by a thin neck $L = [-l/2, l/2] \times [-w/2, w/2]$ along the x-axis with thickness w and length l.

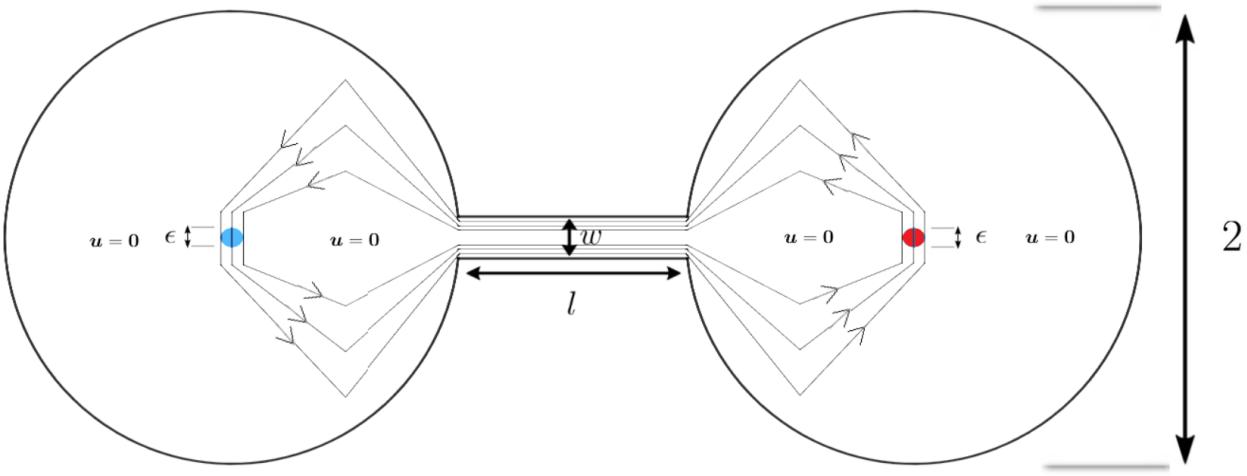

Figure IV.1: Example of thin neck flow. Heat source (red) and sink (blue) are concentrated in regions of size $\sim \epsilon$. Black lines with arrows show streamlines of the 'pinching' flow achieving optimal scaling proved in the following proposition.

Proposition 4.3.1. *Let Ω be the domain given by*

$$\Omega = B(\boldsymbol{x}_-, 1) \cup B(\boldsymbol{x}_+, 1) \cup L$$

and let f satisfy the usual conditions:

$$\begin{aligned} f(\boldsymbol{x}) &= f_+(\boldsymbol{x}) - f_-(\boldsymbol{x}), \\ \mathit{supp}(f_\pm) &\subset B_\epsilon(\boldsymbol{x}_\pm), \\ \int_{B_\epsilon(\boldsymbol{x}_\pm)} f_\pm(\boldsymbol{x}) \mathrm{d}\boldsymbol{x} &= 1, \\ f_+(x, y) &= f_-(-x, y), \\ |f| \lesssim \epsilon^{-2}, &\quad |\nabla f| \lesssim \epsilon^{-3}. \end{aligned}$$

We have

$$\min_{\substack{\boldsymbol{u}(\boldsymbol{x},t)\\ \langle|\boldsymbol{u}|^2\rangle\le Pe^2\\ \partial_t T+\boldsymbol{u}\cdot\nabla T=\Delta T+f}} \langle|\nabla T|^2\rangle \sim \max\left\{\min\left\{\log\frac{1}{\epsilon},\left(\log\frac{1}{\epsilon}\right)^2\frac{1}{Pe^2}\right\},\min\left\{\frac{l}{w},\left(\frac{l}{w}\right)^2\frac{1}{Pe^2}\right\}\right\} \tag{IV.4}$$

for $\epsilon\in(0,1/20)$, $l>w>0$ and $Pe\ge 0$. The alternatives are achieved by no flow ($\max\{\frac{l}{w},\log\frac{1}{\epsilon}\}$) or pinching flow($\max\{\log\frac{1}{\epsilon}\frac{1}{Pe^2},\frac{l}{w}\frac{1}{Pe^2}\}$) as demonstrated in Figure IV.1 where the maximum in each case can be determined by width w and sink source size ϵ.

Remark 4.3.2. Even though we are mainly interested in the case when w is small and l is a constant comparable to the size of the disks, our result also applies to the case when w gets large and approaches l. Intuitively, when w gets large, our dumbbell is becoming closer and closer to our original 2-d case as the neck is disappearing and the two disks are merging. In which case, the $\frac{l}{w}$ term will vanish and our result just turns into the normal 2-d disk result we showed in 3.3.4.

Proof. In the following lower bound proof, we'll be using two different test functions ξ instead of one as in the previous cases. And these two different ξ will lead to V.3 in our main result.

Proof of lower bound For the lower bound part, using the general lower bound III.27 as before, we can choose the following two test functions:

The first one resembles what we had in the 2-d case, i.e. using $\log(1/\epsilon)$. In this case, $\xi=0$ along the neck and not contributing anything to our calculations. We would end up with the same lower bound:

$$\langle|\nabla T|^2\rangle \gtrsim \frac{\log(1/\epsilon)^2}{\log(1/\epsilon)+Pe^2}.$$

For the second one, we can use the following ξ:

$$\xi(\boldsymbol{x})=\begin{cases}-a & \boldsymbol{x}\in B(-l/2-1,1)\\ a & \boldsymbol{x}\in B(l/2+1,1)\end{cases}$$

where a is any fixed non-zero constant and ξ is linear along the neck. In this case:

$$\begin{aligned}
\fint_{\Omega} \xi f \mathrm{d}\boldsymbol{x} &\sim a, \\
\fint_{\Omega} |\nabla \xi|^2 \mathrm{d}\boldsymbol{x} &\sim wa^2/l, \\
\|\xi\|_{\mathrm{BMO}(\Omega)} &\lesssim \frac{aw}{l}.
\end{aligned}$$

Plugging into 3.3.1 gives us

$$\begin{aligned}
\left\langle |\nabla T|^2 \right\rangle &\gtrsim \frac{a^2}{wa^2/l + C(\Omega)\left(wa/l\right)^2 Pe^2}, \\
&= \frac{l^2}{lw + C(\Omega) w^2 Pe^2}, \\
&= \frac{(l/w)^2}{l/w + C(\Omega) Pe^2}.
\end{aligned}$$

Combining the two cases, we get

$$\min \left\langle |\nabla T|^2 \right\rangle \gtrsim \max \left\{ \min \left\{ \log \frac{1}{\epsilon}, \left(\log \frac{1}{\epsilon} \right)^2 \frac{1}{Pe^2} \right\}, \min \left\{ \frac{l}{w}, \left(\frac{l}{w} \right)^2 \frac{1}{Pe^2} \right\} \right\}. \tag{IV.5}$$

Proof of the upper bound With III.28, the no flow case is similar to what we did in the usual 2-d disk case. Here to prove V.3 stated in the proposition, it suffices to show that

$$\left| \int_{\Omega} (\varphi_+ - \varphi_-)(f_+ - f_-) \mathrm{d}\boldsymbol{x} \right|^2 \lesssim \left(\frac{l}{w} + \log \left(\frac{1}{\epsilon} \right) \right) \int_{\Omega} |\nabla \varphi|^2 \mathrm{d}\boldsymbol{x}. \tag{IV.6}$$

Though this bound seems different from the one we want to prove, we'll see that when we combine the no-flow and flow case together, the lower and upper bounds match. Again, as argument is the same for all combinations, we will start with the combination $\varphi_+ f_+$. The proof is adopted

from the 2-d case. By our assumptions on f,

$$\int_{\Omega} \varphi_+ f_+ \mathrm{d}\boldsymbol{x} = \int_{B_\epsilon(\boldsymbol{x}_+)} \varphi_+ f_+ \mathrm{d}\boldsymbol{x} \lesssim \fint_{Q_\epsilon(\boldsymbol{x}_+)} \varphi_+ \mathrm{d}\boldsymbol{x}$$

where $Q_\epsilon(\boldsymbol{x}_+)$ is the open square of side length ϵ centered at $\boldsymbol{x}_+$. Now we want to find a sequence of squares starting from $Q_\epsilon(\boldsymbol{x}_+)$, ending at $B(\boldsymbol{x}_-, 1)$ with all the squares together covering the whole neck Ω. Let N be the largest integer such that the cube of side length $2^{N-1}\epsilon$ centered at x_+ is contained in Ω, i.e., the largest square contained in right disk. Then similar to our assumptions in the 2-d case, there is a sequence of squares $Q_1, \ldots, Q_{N-1} \subset \Omega$ of ever increasing diameters and with the following properties: (i) the first square is $Q_1 = Q_\epsilon(\boldsymbol{x}_+)$ and the last square is the above mentioned largest square; (ii) consecutive squares intersect, with an area $|Q_i \cap Q_{i+1}|$ that is within a factor of 5 of the areas $|Q_i|$ and $|Q_{i+1}|$; (iii) no more than 10 squares include any given $\boldsymbol{x} \in \Omega$; (iv) there are $N \sim \log(1/\epsilon)$ squares in total.

Then we let $Q_N = B(\boldsymbol{x}_+, 1)$ and with this added region, the above four conditions are not violated. For convenience, we'll still call Q_N a square though technically it's a disk. Similarly, we can find another decreasing sequence of squares $Q_N, \ldots, Q_{N+M}$ starting at Ω with decreasing diameters ending at $Q_{N+M} = [l/2 - w/2, l/2 + w/2] \times [-w/2, w/2]$. This last square is half in the neck, and half in the disk. We still require the sequence of squares to satisfy conditions (ii) and (iii) above, and we want $M \sim \log(1/w)$ in this case as the smallest square has side length w.

For the next step, we want another sequence of squares $Q_{N+M}, \ldots, Q_{N+M+O}$ starting at $Q_{N+M} = [l/2 - w/2, l/2 + w/2] \times [-w/2, w/2]$, marching through the neck and ending at $Q_{N+M} = [-l/2 - w/2, -l/2 + w/2] \times [-w/2, w/2]$. We still assume condition (ii) and (iii) on these squares. Though different from the previous cases, these squares are assumed to have the same side length w which are the largest possible squares that can fit in the neck L. Then as the squares all have the same size, we would have $O \sim \frac{l}{w}$.

By symmetry, we can find squares $Q_{N+M+O}, \ldots, Q_{N+M+O+M}$ with increasing diameters ending at $Q_{N+M+O+M} = B(\boldsymbol{x}_-, 1)$.

With the above construction, we have the squares $Q_0, \ldots, Q_{N+M+O+M}$ covers Ω and we still have

$$\begin{aligned}\left|\fint_{Q_i} \varphi_+ \mathrm{d}\boldsymbol{x} - \fint_{Q_{i+1}} \varphi_+ \mathrm{d}\boldsymbol{x}\right|^2 &\lesssim \fint_{Q_i} \left|\varphi_+ - \fint_{Q_i} \varphi_+\right|^2 \mathrm{d}\boldsymbol{x} + \fint_{Q_{i+1}} \left|\varphi_+ - \fint_{Q_{i+1}} \varphi_+\right|^2 \mathrm{d}\boldsymbol{x} \\ &\lesssim \int_{Q_i \cup Q_{i+1}} |\nabla \varphi_+|^2 \mathrm{d}\boldsymbol{x}.\end{aligned}$$

Summing up over consecutive pairs of squares,

$$\begin{aligned}\left|\fint_{Q_\epsilon(\boldsymbol{x}_+)} \varphi_+ \mathrm{d}\boldsymbol{x} - \fint_{Q_{N+2M+O}} \varphi_+ \mathrm{d}\boldsymbol{x}\right|^2 &= \left|\sum_{i=1}^{N+M+O+M-1} \fint_{Q_i} \varphi_+ \mathrm{d}\boldsymbol{x} - \fint_{Q_{i+1}} \varphi_+ \mathrm{d}\boldsymbol{x}\right|^2 \\ &\lesssim (N+M+O) \sum_{i=1}^{N+2M+O-1} \left|\fint_{Q_i} \varphi_+ \mathrm{d}\boldsymbol{x} - \fint_{Q_{i+1}} \varphi_+ \mathrm{d}\boldsymbol{x}\right|^2 \\ &\lesssim (N+M+O) \sum_{i=1}^{N+2M+O-1} \int_{Q_i \cup Q_{i+1}} |\nabla \varphi_+|^2 \mathrm{d}\boldsymbol{x} \\ &\lesssim (N+M+O) \int_\Omega |\nabla \varphi_+|^2 \mathrm{d}\boldsymbol{x}.\end{aligned}$$

Then, as φ has mean zero on Ω, we can apply Poincaré's inequality to get

$$\begin{aligned}\left|\fint_{Q_{N+2M+O}} \varphi_+ \mathrm{d}\boldsymbol{x}\right|^2 = \left|\fint_{B(\boldsymbol{x}_-,1)} \varphi_+ \mathrm{d}\boldsymbol{x}\right|^2 &\lesssim \left|\int_\Omega \varphi_+ \mathrm{d}\boldsymbol{x}\right|^2 \\ &\lesssim \int_\Omega |\varphi|^2 \mathrm{d}\boldsymbol{x} \lesssim \int_\Omega |\nabla \varphi|^2 \mathrm{d}\boldsymbol{x}\end{aligned}$$

where the third step follows from Cauchy-Schwartz inequality. Together with our assumptions on

the sizes of N, M, O, we can conclude that

$$\begin{aligned}\left|\int_\Omega \varphi_+ f_+ \mathrm{d}\boldsymbol{x}\right|^2 &\lesssim \left|⨍_{Q_\epsilon(\boldsymbol{x}_+)} \varphi_+ \mathrm{d}\boldsymbol{x} - ⨍_{Q_{N+2M+O}} \varphi_+ \mathrm{d}\boldsymbol{x}\right|^2 + \left|⨍_{Q_{N+2M+O}} \varphi_+ \mathrm{d}\boldsymbol{x}\right|^2 \\ &\lesssim (N+M+O)\int_\Omega |\nabla\varphi|^2 \\ &\lesssim \left(\log\left(\frac{1}{\epsilon}\right) + \log\left(\frac{l}{w}\right) + \frac{l}{w}\right)\int_\Omega |\nabla\varphi_+|^2 \\ &\lesssim \left(\log\left(\frac{1}{\epsilon}\right) + \frac{l}{w}\right)\int_\Omega |\nabla\varphi|^2\end{aligned}$$

by condition (iv). This shows IV.6 and hence

$$\langle |\nabla T|^2 \rangle \lesssim \max\left\{\log\frac{1}{\epsilon},\ \frac{l}{w}\right\} \tag{IV.7}$$

for the choice $\boldsymbol{u} = \mathbf{0}$.

Pinching flow for thin neck For the upper bound, let's try pinching flow in the following way: Near the source and sink, the flow unpinches as in the 2-d disk case. Then the flow pinches through the thin neck with flow of width scale w and length scale l. In this case, the estimates for $\boldsymbol{u}, \eta$ remains the same near source and sink. And along the neck, by divergence free condition, the contribution of velocity along the neck is given by

$$\int_L |\boldsymbol{u}|^2 \mathrm{d}\boldsymbol{x} \sim l/w$$

and near the exit and entrance of the neck, a similar estimate near the sink and source gives estimate $\log(1/w)$. So we have the total velocity contribution given by

$$⨍_\Omega |\boldsymbol{u}|^2 \mathrm{d}\boldsymbol{x} \sim \log(\frac{1}{\epsilon}) + \log(\frac{1}{w}) + \frac{l}{w}.$$

To satisfy $\boldsymbol{u}\cdot\nabla\eta = f$, we construct the η in a similar way as in the 2-d case, and η would have the same disk estimate near the sink and source. Near the entrance and exit, the contribution of $\nabla\eta$

scales as $\log(1/w)$ and along the neck, we have

$$\int_L |\nabla \eta|^2 \mathrm{d}\boldsymbol{x} \sim \frac{l}{w}.$$

Following are the detailed construction:

Using polar coordinate centered at $(-l/2 - 1 - 2\epsilon, 0)$, and let R_ϵ be the rectangle that contains the support of the sink with vertical side length $2\sqrt{3}\epsilon$ and horizontal side length 2ϵ. And we can define the stream function as follows:

$$\psi_1(\theta) = \begin{cases} \frac{\pi}{3} - \theta & (\frac{\pi}{6}, \frac{\pi}{3}] \\ \frac{\pi}{6} & (-\frac{\pi}{6}, \frac{\pi}{6}] \\ \theta + \frac{\pi}{3} & (-\frac{\pi}{3}, -\frac{\pi}{6}] \\ 0 & \text{otherwise} \end{cases}.$$

With this construction, the flow enters from the top and exits from the bottom. Inside R_ϵ, the flow matches the sides and flows vertically. So we can define the flow as follows:

$$\psi_2(x) = \psi_1(\arctan(\frac{2x + l + 1 + 4\epsilon}{2\sqrt{3}\epsilon})) = \frac{\pi}{3} - \arctan(\frac{2x + l + 1 + 4\epsilon}{2\sqrt{3}\epsilon})$$

using $-\partial_x \psi_2 \partial_y \eta = f$, we can define η inside R_ϵ as

$$\eta_2(x, y) = -\int_0^y \frac{f(x, s)}{\partial_x \psi_2(x, s)} \mathrm{d}s = \int_0^y \frac{12\epsilon^2 + (2x + l + 1 + 4\epsilon)^2}{4\sqrt{3}\epsilon} f(x, s) \mathrm{d}s.$$

Outside R_ϵ, we match the value along boundaries of R_ϵ to get

$$\eta_1(\theta) = \begin{cases} \eta_2(-l/2 - 1 - 2\epsilon + \sqrt{3}\epsilon \cot(\theta), \sqrt{3}\epsilon) & (\frac{\pi}{6}, \frac{\pi}{3}] \\ \eta_2(-l/2 - 1 - 2\epsilon - \sqrt{3}\epsilon \cot(\theta), -\sqrt{3}\epsilon) & (-\frac{\pi}{3}, -\frac{\pi}{6}] \end{cases}.$$

Then near the entrance of thin neck, we can use $(-l/2+\frac{\sqrt{3}}{4}w,0)$ as the center in polar coordinates to define the following stream function

$$\psi_3(\theta)=\begin{cases}\frac{4}{3}\pi-\theta & (\frac{7\pi}{6},\frac{4\pi}{3}]\\ \frac{\pi}{6} & (\frac{5\pi}{6},\frac{7\pi}{6}]\\ \theta-\frac{2\pi}{3} & (\frac{2\pi}{3},\frac{5\pi}{6}]\end{cases}.$$

After entering the neck, the stream function matches the entrance by

$$\psi_4(y)=\psi_3(\pi-\arctan(\frac{y}{\sqrt{3}w/6})).$$

Now for the test function η, as we want it to stay constant along streamlines, it can be defined using η_2 at the boundary of R_ϵ, i.e.,

$$\eta_4(y)=\begin{cases}\eta_2(-l/2-1+3\epsilon+\frac{8\epsilon}{w}y,-\sqrt{3}\epsilon) & y<0\\ \eta_2(-l/2-1+3\epsilon-\frac{8\epsilon}{w}y,\sqrt{3}\epsilon) & y>0\end{cases}$$

and near the entrance we have

$$\eta_3(\theta)=\begin{cases}\eta_4(-\sqrt{3}w\tan(\theta)/6) & (\frac{7\pi}{6},\frac{4\pi}{3}]\\ \eta_4(-\sqrt{3}w\tan(\theta)/6) & (\frac{2\pi}{3},\frac{5\pi}{6}]\\ 0 & \text{otherwise}\end{cases}.$$

With these constructions, we get the following upper bound with pinching flows:

$$\begin{aligned}\left\langle|\nabla T|^2\right\rangle &\lesssim \frac{1}{Pe^2}\left(\log(\frac{1}{\epsilon})+\log(\frac{1}{w})+\frac{l}{w}\right)^2\\ &\lesssim \max\left\{\frac{1}{Pe^2}\log^2(\frac{1}{\epsilon}),\ \frac{1}{Pe^2}\left(\frac{l}{w}\right)^2\right\}.\end{aligned}$$

Matching Bounds Combining the above upper bound and no-flow upper bound IV.7, we have

$$\langle|\nabla T|^2\rangle \lesssim \min\left\{\max\left\{\log\frac{1}{\epsilon},\ \frac{l}{w}\right\},\ \max\left\{\frac{1}{Pe^2}\log^2(\frac{1}{\epsilon}),\ \frac{1}{Pe^2}\left(\frac{l}{w}\right)^2\right\}\right\}. \tag{IV.8}$$

Comparing with the lower bound IV.5,

$$\langle|\nabla T|^2\rangle \gtrsim \max\left\{\min\left\{\log\frac{1}{\epsilon},\ \left(\log\frac{1}{\epsilon}\right)^2\frac{1}{Pe^2}\right\},\ \min\left\{\frac{l}{w},\ \left(\frac{l}{w}\right)^2\frac{1}{Pe^2}\right\}\right\}$$

at first glance, they might seem to be different. However, we can show that these two bounds match by a simple case analysis. Note that there is a symmetry between $\frac{l}{w}$ and $\log\frac{1}{\epsilon}$, we'll focus the cases when $\frac{l}{w} > \log\frac{1}{\epsilon}$ and demonstrate how $\frac{l}{w} > \log\frac{1}{\epsilon}$ works only for the first case.

Case I: $Pe^2 > \frac{l}{w} > \log\frac{1}{\epsilon}$. In this case, we have

$$\frac{l}{w} > \frac{1}{Pe^2}\left(\frac{l}{w}\right)^2,\ \log\frac{1}{\epsilon} > \left(\log\frac{1}{\epsilon}\right)^2\frac{1}{Pe^2}.$$

So we have upper bound $\frac{1}{Pe^2}\left(\frac{l}{w}\right)^2$ and lower bound $\frac{1}{Pe^2}\left(\frac{l}{w}\right)^2$, they match as we wanted.

Case I': $Pe^2 > \log\frac{1}{\epsilon} > \frac{l}{w}$. In this case, we have

$$\frac{l}{w} > \frac{1}{Pe^2}\left(\frac{l}{w}\right)^2,\ \log\frac{1}{\epsilon} > \left(\log\frac{1}{\epsilon}\right)^2\frac{1}{Pe^2}.$$

So we have upper bound $\frac{1}{Pe^2}\left(\log\frac{1}{\epsilon}\right)^2$ and lower bound $\frac{1}{Pe^2}\left(\log\frac{1}{\epsilon}\right)^2$, they match as we wanted. Comparing the above two cases, it's easy to see the symmetric relationship between $\frac{l}{w}$ and $\log\frac{1}{\epsilon}$ as we mentioned earlier. So we'll only work on the cases when $\frac{l}{w} > \log\frac{1}{\epsilon}$.

Case II: $\frac{l}{w} > Pe^2 > \log\frac{1}{\epsilon}$. In this case, we have

$$\frac{1}{Pe^2}\left(\frac{l}{w}\right)^2 > \frac{l}{w} > \log\frac{1}{\epsilon} > \left(\log\frac{1}{\epsilon}\right)^2\frac{1}{Pe^2}.$$

So we have upper bound $\frac{l}{w}$ and lower bound $\frac{l}{w}$, they match as well.

Case III: $\frac{l}{w} > \log\frac{1}{\epsilon} > Pe^2$. In this case, we have

$$\frac{1}{Pe^2}\left(\frac{l}{w}\right)^2 > \frac{l}{w},\ \left(\log\frac{1}{\epsilon}\right)^2\frac{1}{Pe^2} > \log\frac{1}{\epsilon}.$$

So we have upper bound $\frac{l}{w}$ and lower bound $\frac{l}{w}$, they still match.

Combining the above three cases, we see that the upper and lower bounds match in all possible cases. Thus the result is proved.

□

Note that when constructing the pinching flows in Section 4.2 and Section 4.3, we do have some freedom in designing the flows and some numbers are just chosen for convenience. For example, in the thin neck case, on the left side of the neck, we chose to enter the neck with angles $(\frac{7\pi}{6}, \frac{4\pi}{3}]$ and exit with angles $(\frac{2\pi}{3}, \frac{5\pi}{6}]$. These numbers can be changed to any angle as long as the closure of entering and exiting angle do not intersect. This leads us to thinking that in the 2-d case, the pinching structure gives us the optimal scaling and the structure's behaviors near the sink and source would give us some clues of the prefactor for concentrated heatings. In the next chapter we'll discuss what the best prefactor could be along with how the best prefactor would guide us choose the structure's behaviors near the sink and source.

CHAPTER V

Optimal Prefactor Analysis for 2D Concentrated Flows

In the previous sections, we focused on achieving the optimal scaling for various setups of the optimal heat transfer problem with internal heating and cooling. The 2-d examples in Section 3.3.3 and Chapter IV do give us some candidates for prefactors but none of them closes the gap between prefactors for upper and lower bounds. Since we have some freedom in designing the flows as demonstrated at the end of Section 4.3, we'll try to take advantage of the freedom in the flow structure to reach an optimal prefactor in 2-d.

Recall for the no-flow or small kinetic energy case, we showed that the best prefactor was $\|f\|^2_{H^{-1}(\Omega)}$ in III.24 for a given heat profile f. Thus, in this chapter, we'll focus on finding the prefactor for $\langle|\nabla T|^2\rangle$ assuming large mean kinetic energy Pe^2. Also, as our method relies on manipulating the pinching flow structure designed for concentrated heat profiles, we would assume all the heat functions f are concentrated in the sense that it's supported on two relatively small interior regions in Ω with f being always non-negative in one region and non-positive in the other.

In Section 5.1, we'll try to analyze what the best prefactor would be. In Section 5.2, we'll show the prefactor deduced is obtainable with a specific example. Then in Section 5.3, we prove that the best possible optimal prefactor is always obtainable for radially symmetric heat functions satisfying certain constraints. We leave the question of obtaining the optimal prefactor for general heat sources and sinks open.

5.1 Bounds on the Optimal Prefactor

Recall in Chapter III where we started with the weak formulation of our advection diffusion equation and proved the variational bound III.9:

$$\left\langle 2f\xi - |\nabla\xi|^2 - |\nabla\Delta^{-1}(\partial_t\xi + \boldsymbol{u}\cdot\nabla\xi)|^2\right\rangle \le \left\langle |\nabla T|^2\right\rangle \le \left\langle |\nabla\eta|^2 + |\nabla\Delta^{-1}(\partial_t\eta + \boldsymbol{u}\cdot\nabla\eta - f)|^2\right\rangle.$$

Using the lower bound above, we proved in Corollary 3.3.1 that

$$\left\langle |\nabla T|^2\right\rangle \ge \frac{\left(\fint_\Omega \xi f \mathrm{d}\boldsymbol{x}\right)^2}{\fint_\Omega |\nabla\xi|^2\mathrm{d}\boldsymbol{x} + C\|\xi\|^2_{\mathrm{BMO}(\Omega)}\left\langle|\boldsymbol{u}|^2\right\rangle}$$

which we used as our main tool to show the lower bound scalings of the examples in Section 3.3.3. So to obtain a possibly best prefactor, we could keep track of all the inequalities we used from the above lower bound to our final scaling results in Section 3.3.3. Then, combining all the best prefactors for those known inequalities would give us a guess for the best possible prefactor. However, some of the constants in the above analysis are hard to determine. For example, the constant C in the above lower bound comes from the duality between $\mathcal{H}^1$ and BMO and the div-curl inequality III.21 for which we do not have a clear estimate. Instead we shall return to our original advection-diffusion equation

$$\partial_t T + \boldsymbol{u}\cdot\nabla T = \Delta T + f \tag{V.1}$$

and try to find an easier method with trackable inequalities to prove the same lower bound.

As we only want to have a best possible prefactor to guide our later analysis, we may assume a simple disk domain with symmetric heat profile f. And we have the following result:

Proposition 5.1.1. *Suppose our domain $\Omega = B(0,4) \in \mathbf{R}^2$ has concentrated sink-source function f_ϵ, centered at $\boldsymbol{x}_\pm = (0, \pm\frac{1}{2})$ and supported in ball of radius $\epsilon < 1/20$ with mass ± 1. The best possible prefactor for the pinching flow is at least $\frac{4}{|\Omega|^2}$, i.e.,*

$$\left\langle |\nabla T|^2\right\rangle \ge \frac{4}{|\Omega|^2}\log^2(\frac{1}{\epsilon})\,\boldsymbol{Pe}^{-2}$$

for $\epsilon \in (0, 1/20)$ *and* $Pe > 0$.

Proof. As f has mass ± 1 in the sink and source respectively, if we integrate equation (V.1) on the ball B_ρ of radius $\epsilon \leq \rho < |x_+ - x_-| - \epsilon$ centered around source $\boldsymbol{x}_+$ and take long time average, we get

$$\begin{aligned} 1 &= \limsup_{\tau\to\infty} \frac{1}{\tau} \int_{B_\rho} T(\boldsymbol{x}, \tau) - T(\boldsymbol{x}, 0) \mathrm{d}\boldsymbol{x} + \overline{\int_{\partial B_\rho} (\boldsymbol{u}T - \nabla T) \cdot \boldsymbol{n} \mathrm{dS}} \\ &= \limsup_{\tau\to\infty} \frac{1}{\tau} \int_{B_\rho} T(\boldsymbol{x}, \tau) - T(\boldsymbol{x}, 0) \mathrm{d}\boldsymbol{x} + \overline{\int_0^{2\pi} (\boldsymbol{u}T - \nabla T) \cdot \boldsymbol{n} \rho \mathrm{d}\theta}. \end{aligned}$$

As shown in (II.17), the L^∞ norm of T is bounded and as $\tau \to \infty$, $\frac{\|T\|_{L^\infty(\Omega)}}{\tau} \to 0$, we have

$$1 + \overline{\int_0^{2\pi} \nabla T \cdot \boldsymbol{n} \rho \mathrm{d}\theta} = \overline{\int_0^{2\pi} \boldsymbol{u}T \cdot \boldsymbol{n} \rho \mathrm{d}\theta}. \tag{V.2}$$

Let $\boldsymbol{e_r}$ denote the unit outward radial vector. Now for each time slice $t > 0$, we have

$$\begin{aligned} \fint_\Omega |\boldsymbol{u}|^2 \mathrm{d}\boldsymbol{x} \fint_\Omega |\nabla T|^2 \mathrm{d}\boldsymbol{x} &\geq \frac{1}{|\Omega|^2} \int_0^{2\pi} \int_0^1 |(\boldsymbol{u} \cdot \boldsymbol{e_r})|^2 r dr d\theta \int_0^1 \int_0^{2\pi} |\partial_\theta T|^2 d\theta \frac{1}{r} dr \\ &\geq \frac{1}{|\Omega|^2} \int_0^{2\pi} \int_0^1 |(\boldsymbol{u} \cdot \boldsymbol{e_r})|^2 r dr d\theta \int_0^1 C_0 \int_0^{2\pi} |T - \frac{1}{2\pi} \int_0^{2\pi} T(r, \theta') d\theta'|^2 d\theta \frac{1}{r} dr \\ &\geq \left(\frac{1}{|\Omega|} C \int_0^1 \int_0^{2\pi} \boldsymbol{u} \left(T - \frac{1}{2\pi} \int_0^{2\pi} T(r, \theta') d\theta' \right) \cdot \boldsymbol{n} dr d\theta \right)^2 \\ &= \left(\frac{1}{|\Omega|} C \int_0^1 \int_0^{2\pi} \boldsymbol{u}T \cdot \boldsymbol{n} dr d\theta \right)^2 \end{aligned}$$

where we used Poincaré's inequality on circles in the second step and Cauchy-Schwartz in the third step. The last equality follows from $\boldsymbol{u}$ being divergence-free. Note that starting from the first inequality, we're only integrating on Ω_+, the positive half of the domain. By symmetry, the negative half of the domain will give us a same lower bound. Adding them up, taking time average and then plugging in V.2, we get, after taking square root,

$$\begin{aligned}
\sqrt{\langle |u|^2 \rangle \, \langle |\nabla T|^2 \rangle} &\geq \frac{2}{|\Omega|} C \overline{\int_\epsilon^1 \frac{1}{r} \left(1 + \int_0^{2\pi} \nabla T \cdot \boldsymbol{n} \mathrm{d}\theta \right) dr} \\
&\geq \frac{2}{|\Omega|} C \int_\epsilon^1 \frac{1}{r} dr - \frac{2}{|\Omega|} C \sqrt{\overline{\int_0^1 \int_0^{2\pi} |\nabla T|^2 r dr d\theta} \int_\epsilon^1 \int_0^{2\pi} \frac{1}{r} dr d\theta} \\
&= \frac{2}{|\Omega|} C \log(\frac{1}{\epsilon}) - \frac{2}{|\Omega|} C \sqrt{\overline{\int_0^1 \int_0^{2\pi} |\nabla T|^2 r dr d\theta} \cdot 2\pi \log(\frac{1}{\epsilon})}
\end{aligned}$$

which implies

$$\begin{aligned}
\frac{1}{C} \sqrt{\langle |u|^2 \rangle \, \langle |\nabla T|^2 \rangle} + \sqrt{\langle |\nabla T|^2 \rangle \frac{2}{|\Omega|} 2\pi \log(\frac{1}{\epsilon})} &\geq \frac{2}{|\Omega|} \log(\frac{1}{\epsilon}) \\
\left(\frac{1}{C} Pe + \sqrt{\frac{2}{|\Omega|} 2\pi \log(\frac{1}{\epsilon})} \right) \sqrt{\langle |\nabla T|^2 \rangle} &\geq \frac{2}{|\Omega|} \log(\frac{1}{\epsilon}) \\
\left\langle |\nabla T|^2 \right\rangle &\geq \left(\frac{\frac{2}{|\Omega|} \log(\frac{1}{\epsilon})}{\frac{1}{C} Pe + \sqrt{\frac{2}{|\Omega|} 2\pi \log(\frac{1}{\epsilon})}} \right)^2
\end{aligned}$$

multiplying both sides by $\frac{Pe^2}{\log^2 \frac{1}{\epsilon}}$ we get

$$\frac{Pe^2}{\log^2 \frac{1}{\epsilon}} \langle |\nabla T|^2 \rangle \geq \left(\frac{\frac{2}{|\Omega|}}{\frac{1}{C} + \frac{\sqrt{2\pi \log(\frac{1}{\epsilon})}}{Pe}} \right)^2 \to \frac{4}{|\Omega|^2} C^2$$

when $\frac{\sqrt{\log(\frac{1}{\epsilon})}}{Pe} \to 0$. The C is a prefactor coming from Cauchy-Schwarz inequality and Poincaré's inequality on circles, which is 1 in the best case (we'll show this result in Lemma 5.2.1 below as the proof would guide us to an example obtaining our wanted prefactor). Thus the best possible prefactor is $\frac{4}{|\Omega|^2}$. □

5.2 An Example Obtaining the Prefactor $\frac{4}{|\Omega|^2}$

Following the line of the above proof, we see that to achieve the best possible prefactor, we need to saturate the Cauchy-Schwartz inequality and Poincaré's inequality on circles. This observation gives us some guide on how to construct flows obtaining best prefactor which we'll work through now in the following proof:

Lemma 5.2.1. *Let $\varphi \in H^1(\mathbb{T})$ have mean zero on $\mathbb{T}$ where $\mathbb{T}$ stands for the circle in 2-d parametrized by angle $\theta \in [0, 2\pi]$. Then we have*

$$\int_0^{2\pi} \varphi d\theta \leq \int_0^{2\pi} \varphi' d\theta.$$

Proof. Let C be a constant such that

$$C \int_0^{2\pi} \varphi^2 d\theta \leq \int_0^{2\pi} (\varphi')^2 \, d\theta.$$

Then we have the constant satisfies

$$C \leq \frac{\int_0^{2\pi} (\varphi')^2 \, d\theta}{\int_0^{2\pi} \varphi^2 d\theta}.$$

If we write out φ using fourier series, as φ has mean zero, we get

$$\varphi = \sum_{k=1}^{\infty} c_k e^{ik\theta},$$
$$\varphi' = \sum_{k=1}^{\infty} ikc_k e^{ik\theta}.$$

so we get

$$C \leq \frac{\sum_{k=1}^{\infty} 2\pi |c_k|^2 k^2}{\sum_{k=1}^{\infty} 2\pi |c_k|^2}$$

which implies $C \leq 1$ and equality is obtained when φ only has frequency 1. □

In the above proof, we see that to obtained the best prefactor for Poinceré's inequality on circles, we want a heat profile with frequency 1. Together with the saturation of Cauchy-Schwartz inequality, these calculations gives us a direction to construct a temperature and flow field obtaining the prefactor $\frac{4}{|\Omega|^2}$ which leads to the following result:

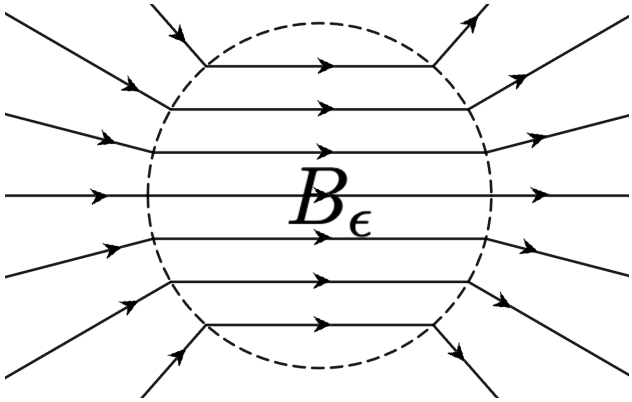

Figure V.1: Example flow obtaining the optimal prefactor $\frac{4}{|\Omega|^2}$. Black lines with arrows show streamlines of the 'pinching' flow achieving optimal scaling proved in the following proposition.

Proposition 5.2.2. *Let $\Omega = B(0,4)$ as before, and consider the heat profile f given by*

$$f(\boldsymbol{x}) = \begin{cases} \frac{1}{\pi\epsilon^2} & \boldsymbol{x} \in B_\epsilon \\ 0 & \boldsymbol{x} \notin B_\epsilon \end{cases}$$

near the source $\boldsymbol{x}_+ = (0, \frac{1}{2})$ where $B_\epsilon = B(\boldsymbol{x}_+, \epsilon)$ for fixed $\epsilon \in (0, 1/20)$. Near the sink, f is defined symmetrically with negative strength. For the above f, we can find 'pinching' flow obtaining the optimal scaling and prefactor as $Pe \to \infty$, i.e.,

$$\min_{\substack{\boldsymbol{u}(\boldsymbol{x},t) \\ \langle|\boldsymbol{u}|^2\rangle \le Pe^2 \\ \partial_t T + \boldsymbol{u}\cdot\nabla T = \Delta T + f}} \langle|\nabla T|^2\rangle = \frac{4}{|\Omega|^2}\frac{1}{Pe^2}\log^2(\frac{1}{\epsilon}) + \frac{1}{Pe^2}o(\log^2(\frac{1}{\epsilon})). \tag{V.3}$$

Proof. As our heat profile f has symmetrical behavior on Ω, we will focus on the stream function

ψ near the source $\boldsymbol{x}_+$. The structure of ψ near the sink follows symmetrically. Let

$$\psi(\boldsymbol{x}) = \frac{\sin\theta}{\sqrt{\pi}} = \frac{y}{\epsilon\sqrt{\pi}}$$

outside B_ϵ and near ∂B_ϵ. As we've seen in the previous examples in Section 3.3.3.2 and Section 4.2, the leading term contribution comes from this area, it suffices to do the calculations near B_ϵ. Inside B_ϵ, we let the stream lines be horizontal lines and let $\boldsymbol{u}$ remain constant along the stream lines. Let $\boldsymbol{e_x}, \boldsymbol{e_r}$ be the unit vectors in the cartesian $x-$direction and polar r-direction. This construction gives us the following flow structure:

$$\boldsymbol{u}(\boldsymbol{x}) = \begin{cases} u_r \boldsymbol{e_r} = \frac{\cos\theta}{\sqrt{\pi} r} \boldsymbol{e_r} & \boldsymbol{x} \notin B_\epsilon \\ u_x \boldsymbol{e_x} = \frac{1}{\sqrt{\pi}\epsilon} \boldsymbol{e_x} & \boldsymbol{x} \in B_\epsilon \end{cases}$$

and as in our previous pinching flow examples, we can define η using $\boldsymbol{u} \cdot \nabla\eta = \nabla^\perp\psi \cdot \nabla\eta = f$ inside B_ϵ which gives us

$$\eta_1(x, y) = \int_0^x \frac{f(s, y)}{u_x} ds = \sqrt{\pi}\epsilon \int_0^x f(s, y) ds = \frac{x}{\sqrt{\pi}\epsilon}.$$

Outside the ball B_ϵ, we again match η_2 with η_1 along the boundary and let η_2 remain constant along the streamlines to get

$$\eta_2(\theta) = \eta_1\left(\epsilon\cos(\theta), \epsilon\sin(\theta)\right) = \frac{\cos\theta}{\sqrt{\pi}}.$$

With the above constructions, together with the symmetric flow structure, we can easily calculate the mean kinetic energy and spatial-temporal average of η to get

$$\fint_\Omega |\boldsymbol{u}|^2 \mathrm{d}\boldsymbol{x} = \frac{2}{|\Omega|} \log\frac{1}{\epsilon} + o(\log\frac{1}{\epsilon}),$$
$$\fint_\Omega |\nabla\eta|^2 \mathrm{d}\boldsymbol{x} = \frac{2}{|\Omega|} \log\frac{1}{\epsilon} + o(\log\frac{1}{\epsilon})$$

which implies

$$\left\langle |\nabla T|^2 \right\rangle \leq \frac{4}{|\Omega|^2} \frac{1}{Pe^2} \log^2(\frac{1}{\epsilon}) + \frac{1}{Pe^2} o(\log^2(\frac{1}{\epsilon}))$$

by III.28.

□

5.3 Optimal Prefactor for Radial Heating and Cooling

In the previous sections, we've seen that the best possible prefactor is at least $\frac{4}{|\Omega|^2}$ and this bound is sharp when the sink–source function f is constant inside its support. What is the largest possible set of balanced heat profiles f such that the optimal prefactor for the lower bound in 5.1.1 is $\frac{4}{|\Omega|^2}$? One interesting feature we notice from the previous section is that

$$\Phi(x, y) = (\eta(x, y), \psi(x, y)) = (\frac{x}{\epsilon\sqrt{\pi}}, \frac{y}{\epsilon\sqrt{\pi}}),$$

on ∂B_ϵ the boundary of the ball where the source or sink is supported on. The reason we define Φ as above is if we calculate the Jacobian determinant of Φ, we get f, i.e.,

$$\det \mathrm{D}\Phi = \boldsymbol{u} \cdot \nabla\eta = f.$$

To make the calculation cleaner, we may do a change of coordinate so that Φ becomes the identity on the boundary of unit ball ∂B_1 where the source is now supported on after the transformation. That is, if we let

$$\begin{aligned} g(\boldsymbol{x}) &= \epsilon^2 \pi f(\epsilon \boldsymbol{x}), \\ \Psi(\boldsymbol{x}) &= \sqrt{\pi}\Phi(\epsilon \boldsymbol{x}) \end{aligned} \tag{V.4}$$

we would have

$$\begin{cases} \det \mathrm{D}\Psi(\boldsymbol{x}) & = \pi\epsilon^2 \det \mathrm{D}\Phi(\epsilon\boldsymbol{x}) = \pi\epsilon^2 f(\epsilon\boldsymbol{x}) = g(\boldsymbol{x}) \quad \text{in} \quad B_1, \\ \Psi(\boldsymbol{x}) & = (x, y) \quad \text{on} \quad \partial B_1 \end{cases} \tag{V.5}$$

as wanted. As we've seen in all our pinching flow calculations, the main contribution to $\left\langle |\nabla T|^2 \right\rangle$ comes from the pinching near ∂B_ϵ, so if we can ensure such behavior near ∂B_1 in the rescaled case, we would be able to get our best possible prefactor. So now our goal is to show that for given g, whether we can find Ψ such that equations (V.5) is satisfied. Note that solving equations (V.5) is just solving the prescribed Jacobian with identity boundary conditions. As we need $\boldsymbol{u} \in L^2(B_1)$ and $\eta \in H^1(B_1)$, we would want $\Psi \in H^1(B_1)$ to satisfy our regularity requirements. However, in [GKL21a], one result obtained is that we can find

$$g \in L\log L(\Omega) := \{h \in L^1(\Omega) | \int_\Omega |h| \max(\log|h|, 0) \mathrm{d}x < \infty\},$$

satisfying

$$\inf_{B_1} g > 0$$

such that (V.5) has no solutions in $H^1(B_1)$. So in the next proposition, we'll show that with further assumptions on g, we may find solutions to (V.5).

Proposition 5.3.1. *If $g \in L^2(B_1)$ is radially symmetric and for all $0 < r \leq 1$ satisfying*

$$\begin{aligned} g(r) &\lesssim \fint_{B_r(0)} g(\boldsymbol{x}) \mathrm{d}\boldsymbol{x}, \\ \frac{1}{\pi}\int_{B_1} g(\boldsymbol{x}) \mathrm{d}\boldsymbol{x} &= 1, \\ g(\boldsymbol{x}) &\geq 0 \quad \textit{on} \quad B_1 \end{aligned} \tag{V.6}$$

then there exists unique $\Psi \in H^1(B_1)$ solving (V.5).

Remark 5.3.2. The following proof uses the construction of 'radial stretching' from [GKL21a] which gives us a candidate for radial symmetric solution. Furthermore, with our given constraint(V.6) on g, we can show that our Ψ lies in $H_1(B_1)$ as wanted and uniqueness also follows.

Proof. Note that if g is radially symmetric, we can define function $\rho(r)$ as follows:

$$\rho(r) = \sqrt{2\int_0^r g(s)s\mathrm{d}s} \tag{V.7}$$

where $g(s)$ in the integrand is written in polar coordinates. In this case, it's easy to see that

$$\rho(1) = \sqrt{2\int_0^1 g(r)r\mathrm{d}r} = \sqrt{\frac{1}{\pi}\int_0^{2\pi}\int_0^1 g(r)r\mathrm{d}r\mathrm{d}\theta} = 1$$

So if we let

$$\Psi(\boldsymbol{x}) = \rho(|x|)\frac{\boldsymbol{x}}{|\boldsymbol{x}|}$$

we would have

$$\begin{aligned}\det \mathrm{D}\Psi(\boldsymbol{x}) = \begin{vmatrix} \frac{\rho(r)}{r} + \frac{\dot{\rho}(r)x^2}{r^2} - \frac{\rho(r)x^2}{r^3} & \frac{\dot{\rho}(r)xy}{r^2} - \frac{\rho(r)xy}{r^3} \\ \frac{\dot{\rho}(r)xy}{r^2} - \frac{\rho(r)xy}{r^3} & \frac{\rho(r)}{r} + \frac{\dot{\rho}(r)y^2}{r^2} - \frac{\rho(r)y^2}{r^3} \end{vmatrix} = \frac{1}{r}\rho(r)\dot{\rho(r)} = \frac{1}{2r}(\dot{\rho^2(r)}) = g(r), \\ \Psi(\boldsymbol{x}) = (x, y) \quad \text{on} \quad \partial B_1\end{aligned} \tag{V.8}$$

which solves (V.5) as we wanted.

Then, using Lemma 3.1 from [GKL21a], we have

$$\|\mathrm{D}\Psi\|^2_{L^2(B_1)} \lesssim \int_0^1 \left(\left|\dot{\rho(r)}\right|^2 + \left|\frac{\rho(r)}{r}\right|^2\right) r\mathrm{d}r. \tag{V.9}$$

For the second term, we can use Jensen's inequality and get

$$\left|\frac{\rho(r)}{r}\right|^2 = \frac{1}{r^2}\int_0^r 2g(s)s\mathrm{d}s \lesssim \frac{1}{r}\sqrt{\int_0^r g^2(s)s\mathrm{d}s} \lesssim \frac{1}{r}\|g\|_{L^2(B_1)}.$$

For the first term, using V.8 we have

$$\dot{\rho}(r) = \frac{rg(r)}{\rho(r)}$$

which implies

$$\int_0^1 |\dot{\rho}(r)|^2 \, r\mathrm{d}r = \int_0^1 \frac{r^2 g^2(r)}{\rho^2(r)} r\mathrm{d}r.$$

Under our assumption V.6, we have

$$r^2 g(r) \lesssim \int_0^r g(s) s\mathrm{d}s \lesssim \rho^2(r)$$

so we have

$$\int_0^1 |\dot{\rho}(r)|^2 \, r\mathrm{d}r \lesssim \int_0^1 gr\mathrm{d}r \sim \|g\|_{L^1(B_1)}.$$

Combining the two terms gives us the result we want:

$$\|\mathrm{D}\Psi\|_{L^2(B_1)} \lesssim \|g\|_{L^1(B_1)}^{1/2} + \|g\|_{L^2(B_1)}^{1/2} < \infty. \tag{V.10}$$

We have $\Psi(\boldsymbol{x}) \in H^1(B_1)$ as wanted. □

As we've shown $\Psi(\boldsymbol{x}) \in H^1(B_1)$ exists, it remains to show that the L^2 bounds of the original $\boldsymbol{u}$ and $\nabla\eta$ are of size $o(\log(\frac{1}{\epsilon}))$ so that they will not affect the leading order heat transfer.

Lemma 5.3.3. *Under the transformation given in V.4, if our heat profile f satisfies*

$$|f| \lesssim \frac{1}{\epsilon^2} \tag{V.11}$$

we would have

$$\int_{B_\epsilon} |\boldsymbol{u}|^2 \, \mathrm{d}\boldsymbol{x} + \int_{B_\epsilon} |\nabla\eta|^2 \, \mathrm{d}\boldsymbol{x} = O(1)$$

Proof. Under our change of coordinate (V.4) and assumption (V.11) on f, we have

$$\begin{aligned}
\|g\|_{L^1(B_1)} &= \int_{B_1} g(\boldsymbol{x})\mathrm{d}\boldsymbol{x} = \pi \int_{B_1} \epsilon^2 f(\epsilon\boldsymbol{x})\mathrm{d}\boldsymbol{x} = \pi \int_{B_\epsilon} f(\boldsymbol{x})\mathrm{d}\boldsymbol{x} = \pi, \\
\|g\|^2_{L^2(B_1)} &= \pi^2\epsilon^2 \int_{B_1} \epsilon^2 f^2(\epsilon\boldsymbol{x})\mathrm{d}\boldsymbol{x} = \pi^2\epsilon^2 \int_{B_\epsilon} f^2(\boldsymbol{x})\mathrm{d}\boldsymbol{x} \sim 1, \\
\|\mathrm{D}\Psi\|^2_{L^2(B_1)} &= \pi \int_{B_1} \epsilon^2 |\mathrm{D}\Phi|^2(\epsilon\boldsymbol{x})\mathrm{d}\boldsymbol{x} = \pi \int_{B_\epsilon} |\mathrm{D}\Phi|^2(\boldsymbol{x})\mathrm{d}\boldsymbol{x} \\
&= \pi \int_{B_\epsilon} |\boldsymbol{u}|^2 \,\mathrm{d}\boldsymbol{x} + \pi \int_{B_\epsilon} |\nabla\eta|^2 \,\mathrm{d}\boldsymbol{x}.
\end{aligned}$$

So (V.10) gives us

$$\int_{B_\epsilon} |\boldsymbol{u}|^2 \,\mathrm{d}\boldsymbol{x} + \int_{B_\epsilon} |\nabla\eta|^2 \,\mathrm{d}\boldsymbol{x} = O(1)$$

as wanted. □

Combining our result from Lemma 5.3.3 and Proposition 5.3.1, we have the following result regarding the set of heat profiles for which we can achieve optimal prefactor $\frac{4}{|\Omega|^2}$ and scaling $\log^2(\frac{1}{\epsilon})\frac{1}{Pe^2}$ using 'pinching' flows.

Theorem 5.3.4. *Let f be the heat profile satisfying*

$$\begin{aligned}
f(\boldsymbol{x}) &= f_+(\boldsymbol{x}) - f_-(\boldsymbol{x}), \\
\textit{supp}(f_\pm) &\subset B_\epsilon(\boldsymbol{x}_\pm), \\
\int_{B_\epsilon(\boldsymbol{x}_\pm)} f_\pm(\boldsymbol{x})\mathrm{d}\boldsymbol{x} &= 1, \\
f_+(x,y) &= f_-(-x,y), \\
|f| \lesssim \epsilon^{-2}, &\quad |\nabla f| \lesssim \epsilon^{-3}
\end{aligned}$$

for $\epsilon \in (0, 1/20)$. Suppose after the change of coordinate

$$g_\pm(\boldsymbol{x}) = \epsilon^2\pi f(\epsilon(\boldsymbol{x} - \boldsymbol{x}_\pm)),$$

$g_\pm$ is radially symmetric and for all $0 < r \leq 1$ satisfying

$$g_\pm(r) \lesssim \fint_{B_r(0)} g_\pm(\boldsymbol{x})\mathrm{d}\boldsymbol{x} \tag{V.12}$$

then there exits 'pinching' flow construction such that the optimal heat transfer up to the leading term is satisfied, i.e.,

$$\min_{\substack{\boldsymbol{u}(\boldsymbol{x},t)\\ \langle|\boldsymbol{u}|^2\rangle\leq Pe^2\\ \partial_t T+\boldsymbol{u}\cdot\nabla T=\Delta T+f}} \langle|\nabla T|^2\rangle = \frac{4}{|\Omega|^2}\frac{1}{Pe^2}\log^2(\frac{1}{\epsilon}) + \frac{1}{Pe^2}o(\log^2(\frac{1}{\epsilon})). \tag{V.13}$$

as $Pe \to \infty$.

Proof. As g satisfies (V.12), Proposition 5.3.1 implies we can find solution to the system (V.5). That being said, we can find function $\Phi \in H^1(\Omega)$ such that on $\partial B_\epsilon(\boldsymbol{x}_\pm)$, we have

$$\Phi(x,y) = (\frac{x}{\epsilon\sqrt{\pi}}, \frac{x}{\epsilon\sqrt{\pi}})$$

if we use the center of $B_\epsilon(\boldsymbol{x}_\pm)$ as the origin respectively.

Then according to our calculations in Proposition 5.2.2, outside $B_\epsilon(\boldsymbol{x}_\pm)$, we can find velocity field $\boldsymbol{u} \in L^2(\Omega)$ and $\eta \in H^1(\Omega)$ such that

$$\begin{aligned}
\boldsymbol{u}\cdot\nabla\eta &= f,\\
\frac{1}{|\Omega|}\int_{\Omega-B_\epsilon(\boldsymbol{x}_\pm)} |\boldsymbol{u}|^2\mathrm{d}\boldsymbol{x} &= \frac{2}{|\Omega|}\log\frac{1}{\epsilon} + o(\log\frac{1}{\epsilon}),\\
\frac{1}{\Omega}\int_{\Omega-B_\epsilon(\boldsymbol{x}_\pm)} |\nabla\eta|^2\mathrm{d}\boldsymbol{x} &= \frac{2}{|\Omega|}\log\frac{1}{\epsilon} + o(\log\frac{1}{\epsilon}).
\end{aligned}$$

Inside the balls $B_\epsilon(\boldsymbol{x}_\pm)$, using Lemma 5.3.3, we get

$$\int_{B_\epsilon} |\boldsymbol{u}|^2 \,\mathrm{d}\boldsymbol{x} + \int_{B_\epsilon} |\nabla\eta|^2 \,\mathrm{d}\boldsymbol{x} = O(1).$$

So now the upper bound III.28 tells us

$$\langle |\nabla T|^2 \rangle \leq \frac{4}{|\Omega|^2} \frac{1}{Pe^2} \log^2(\frac{1}{\epsilon}) + \frac{1}{Pe^2} o(\log^2(\frac{1}{\epsilon})).$$

Together with the lower bound proved in Proposition 5.1.1, we have

$$\min_{\substack{\boldsymbol{u}(\boldsymbol{x},t) \\ \langle |\boldsymbol{u}|^2 \rangle \leq Pe^2 \\ \partial_t T + \boldsymbol{u}\cdot\nabla T = \Delta T + f}} \langle |\nabla T|^2 \rangle = \frac{4}{|\Omega|^2} \frac{1}{Pe^2} \log^2(\frac{1}{\epsilon}) + \frac{1}{Pe^2} o(\log^2(\frac{1}{\epsilon})). \tag{V.14}$$

as $Pe \to \infty$.

□

Our result 5.3.1 relies on the assumptions (V.6). These conditions control g to be radially symmetric and roughly decreasing. These facts seem to hold for some heat sink–sources but definitely not all the heat functions we discussed in Chapter III. We close this chapter by noting that in [CDK12], it was shown that for $g \in C^r$, solutions to the system (V.5) exist in C^r. Their idea shed some light on possible ways to relax our constraints in (V.6). However, in our case, we need solutions in $H^1(\Omega)$ while assuming no continuity and differentiability on f. Also, their proof relies on choosing diffeomorphisms so that the function g satisfies

$$\int_0^r sg(s\frac{\boldsymbol{x}}{|\boldsymbol{x}|})\mathrm{d}s > 0$$

for all $\boldsymbol{x} \neq \boldsymbol{0}$ and $0 < r \leq 1$ after transformation. As we do care about the L^p norm of g after transformations, we need to be careful about the norm of those chosen diffeomorphisms.

CHAPTER VI

Conclusion and Further Objectives

In this dissertation, we obtained optimal bounds for heat transfer in internally heated domains with balanced heat sinks and sources motivated by the problem of understanding turbulent heat transfer in internally heated convections. After introducing the governing equations and well-posedness of our problems, we then summarized our results from [SFT23] in Chaper III where we produced the *a priori* bound

$$\langle |\nabla T|^2 \rangle \geq \frac{\left(\fint_\Omega \xi f \, \mathrm{d}\boldsymbol{x} \right)^2}{\fint_\Omega |\nabla \xi|^2 \, \mathrm{d}\boldsymbol{x} + C(\Omega, d) \|\xi\|^2_{\mathrm{BMO}(\Omega)} \langle |\boldsymbol{u}|^2 \rangle}.$$

By choosing test function ξ and solving a pure advection equation

$$\boldsymbol{u} \cdot \nabla \eta = f,$$

we showed the optimal heat transfer scaling

$$\min_{\substack{\boldsymbol{u}(\boldsymbol{x},t) \\ \langle |\boldsymbol{u}|^2 \rangle \leq Pe^2 \\ \partial_t T + \boldsymbol{u} \cdot \nabla T = \Delta T + f}} \langle |\nabla T|^2 \rangle \sim \min \left\{ \log \frac{1}{\epsilon}, \left(\log \frac{1}{\epsilon} \right)^2 \frac{1}{Pe^2} \right\}$$

using 'pinching' flow design for 2-d concentrated heat profiles.

In Chapter IV we extended our results to higher dimensional concentrated heat profiles, giving

us a heat transfer scaling

$$\min\left\{1/\epsilon^{d-2},\ \left(\log\frac{1}{\epsilon}\right)^2\frac{1}{Pe^2}\right\}\lesssim \min_{\substack{\boldsymbol{u}(\boldsymbol{x},t)\\ \langle|\boldsymbol{u}|^2\rangle\le Pe^2\\ \partial_t T+\boldsymbol{u}\cdot\nabla T=\Delta T+f}} \langle|\nabla T|^2\rangle \lesssim \min\left\{1/\epsilon^{d-2},\ \frac{1}{\epsilon^{d-2}}\frac{1}{Pe^2}\right\}$$

for $d>2$. Again 'pinching' flows achieved the optimal scaling in the upper bound as $Pe\to\infty$.

We also studied a bell-shaped domain with a thin neck of width w and length l and showed

$$\min_{\substack{\boldsymbol{u}(\boldsymbol{x},t)\\ \langle|\boldsymbol{u}|^2\rangle\le Pe^2\\ \partial_t T+\boldsymbol{u}\cdot\nabla T=\Delta T+f}} \langle|\nabla T|^2\rangle \sim \max\left\{\min\left\{\log\frac{1}{\epsilon},\ \left(\log\frac{1}{\epsilon}\right)^2\frac{1}{Pe^2}\right\},\ \min\left\{\frac{l}{w},\ \left(\frac{l}{w}\right)^2\frac{1}{Pe^2}\right\}\right\}.$$

This showed how the domain shape could affect the heat transfer significantly.

Note that for the above three scaling laws, there is a competition between 'pinching' flow (terms involving Pe) and no flow (terms without Pe). Depending on relative size of the parameters (Pe,ϵ,w,l), we can choose whether it's better to use no flow or 'pinching' flow. As the kinetic energy gets larger (i.e., as Pe get larger), we starts to prefer the 'pinching' flow over the no flow.

Another question one may raise is the mismatching of the ϵ in the prefactor of $\frac{1}{Pe^2}$ for 'pinching' flow bound when we go beyond $d=2$. A intuitive explanation is to look at the equation

$$\boldsymbol{u}\cdot\nabla\eta = f.$$

In dimension d, our concentrated heat profile f have scale $\frac{1}{\epsilon^d}$. As $\boldsymbol{u}$ is divergence-free, when the 'pinching' happens near the sink or source, we need

$$\boldsymbol{u}\sim\frac{1}{r^{d-1}}.$$

To compensate that factor of ϵ^{-d}, our η should have scale

$$\nabla\eta\sim\frac{1}{r}.$$

Now taking product of the L^2 norm of these two estimations, we would end up with $\log^2(\frac{1}{\epsilon})$ when $d = 2$ and $1/\epsilon^{d-2}$ when $d > 2$.

Finally in Chapter V, we focused on the advection-dominated limit where we proved a best possible prefactor $\frac{4}{|\Omega|^2}$ and updated our result in Chapter III to get the bound

$$\left\langle |\nabla T|^2 \right\rangle \geq \frac{4}{|\Omega|^2} \frac{1}{Pe^2} \log^2(\frac{1}{\epsilon}).$$

We found the bound to be sharp for a class of 2-d radially symmetric heat profiles using pinching flows and obtain

$$\min_{\substack{\boldsymbol{u}(\boldsymbol{x},t) \\ \langle |\boldsymbol{u}|^2 \rangle \leq Pe^2 \\ \partial_t T + \boldsymbol{u}\cdot\nabla T = \Delta T + f}} \langle |\nabla T|^2 \rangle = \frac{4}{|\Omega|^2} \frac{1}{Pe^2} \log^2(\frac{1}{\epsilon}) + \frac{1}{Pe^2} o(\log^2(\frac{1}{\epsilon})).$$

as $Pe \to \infty$.

Several questions remain open and interesting:

1. As shown by our examples in Sections 3.3.3.2, 4.2, 4.3, 5.2, the scaling and prefactor of our bounds is determined by the behavior of the flow locally near the sink and source for the concentrated heat cases. In the remaining part of the domain, the flow structure does not affect the leading order result. If we look at the second leading term instead, i.e., if we try to find the scaling and prefactor of the bounds for

$$\left\langle |\nabla T|^2 \right\rangle - \frac{4}{|\Omega|^2} \frac{\log^2(\frac{1}{\epsilon})}{Pe^2}$$

the design of flow away from the sink and source may come into the picture.

2. Another part of the story of the concentrated heat functions we did not really step into is the case when there are more than two sink and source structures. It seems reasonable to say the leading term in our bound would still come from the flow design near the sinks and sources. However, as we've seen in our thin neck example presented in Section 4.3, the contribution to the leading term of our bounds may be overtaken by pinching happening away from the sink and source. For example, if the neck is thin enough such that $\frac{l}{w} > \log(\frac{1}{\epsilon})$, then the leading term would have $\frac{l}{w}$

instead of $\log(\frac{1}{\epsilon})$ as a component. So how the sink and sources should be connected to optimize the heat transfer also seems important to the bound. A straightforward guess would be that we connect pairwise sink and sources with flows optimizing the heat transfer between each pair. This method would require more thoughts in 2-d where intersection of the flows seems inevitable if we just connect all pairs of sink and sources. And when we have unequal number of sink and sources, how would the flow structures look seems like a interesting question as branching and merging events may need to occur in this case.

3. One constraint on the concentrated heat profile we studied in our examples is that the location and strength of the heat sink and source are not affected by the fluid flow. However, in real world situations, one is likely to encounter heat transfer problems where we need to consider not only the effect of heat profile on the flow structure, but also the momentum exerted on the heat sinks and sources given by the fluid flow. One example of such problem is the heat releasing particles, [DY22].

4. Other than the ones mentioned above, there are a whole class of new questions we could ask for the multiple sink–source structure setups. If we drive two sinks (or sources) closer and closer, how should we design the flows near them? If we drive a sink close to a source, will they annihilate? If we have a sink or source with strength going to zero or infinity, how would the flow structure change accordingly? Each of these questions may give us some idea of the relationship between flows and heat functions behind the scenes.

BIBLIOGRAPHY

[AFCW21] A. Arslan, G. Fantuzzi, J. Craske, and A. Wynn. Bounds for internally heated convection with fixed boundary heat flux. *Journal of Fluid Mechanics*, 992:R1, 2021.

[AFCW22] Ali Arslan, Giovanni Fantuzzi, John Craske, and Andrew Wynn. Rigorous scaling laws for internally heated convection at infinite Prandtl number. arXiv:2205.03175 [physics.flu-dyn], 2022.

[Alb17] S. Alben. Optimal convection cooling flows in general 2D geometries. *Journal of Fluid Mechanics*, 814:484–509, 2017.

[Bis88] N. T. Bishop. The Poincaré inequality for a vector field with zero tangential or normal component on the boundary. *Quaestiones Mathematicae*, 11(2):195–199, 1988.

[BLAG19] V. Bouillaut, S. Lepot, S. Aumaître, and B. Gallet. Transition to the ultimate regime in a radiatively driven convection experiment. *Journal of Fluid Mechanics*, 861:R5, 2019.

[Bre11] Haim Brezis. *Functional analysis, Sobolev spaces and partial differential equations*. Universitext. Springer, New York, 2011.

[Bus69] Friedrich H. Busse. On Howard's upper bound for heat transport by turbulent convection. *Journal of Fluid Mechanics*, 37(3):457–477, 1969.

[Bus79] Friedrich H. Busse. The optimum theory of turbulence. *Advances in Applied Mechanics*, 18:77–121, 1979.

[Bé00] Henri Bénard. Les tourbillons cellulaires dans une nappe liquide. *Revue Générale des Sciences Pures et Appliquées*, 11:1261–1271, 1309–1328, 1900.

[CCC+01] X. Chavanne, F. Chillà, B. Chabaud, B. Castaing, and B. Hébral. Turbulent Rayleigh–Bénard convection in gaseous and liquid He. *Physics of Fluids*, 13(5):1300–1320, 05 2001.

[CD95] Peter Constantin and Charles R. Doering. Variational bounds on energy dissipation in incompressible flows. II. Channel flow. *Physical Review E*, 51(4):3192–3198, 1995.

[CD12] Guillaume Carlier and Bernard Dacorogna. Résolution du problème de Dirichlet pour l'équation du jacobien prescrit via l'équation de Monge-Ampère. *C. R. Math. Acad. Sci. Paris*, 350(7-8):371–374, 2012.

[CDK12] G. Csató, B. Dacorogna, and O. Kneuss. *The pullback equation for differential forms.*, volume 83. Birkhäuser/Springer, New York, 2012.

[CDS05] Der-Chen Chang, Galia Dafni, and Cora Sadosky. A div-curl lemma in BMO on a domain. In I. Sabadini, D. C. Struppa, and D. F. Walnut, editors, *Harmonic Analysis, Signal Processing, and Complexity. Progress in Mathematics*, volume 238, pages 55–65, 2005.

[Cha94] Der-Chen Chang. The dual of Hardy spaces on a bounded domain in $\mathbb{R}^n$. *Forum Mathematicum*, 6:65–81, 1994.

[CLMS90] R Coifman, P.-L. Lions, Y Meyer, and S Semmes. Compacité par compensation et espaces de Hardy. *Séminaire Équations aux Dérivées Partielles*, 1990.

[CNO16] Antoine Choffrut, Camilla Nobili, and Felix Otto. Upper bounds on Nusselt number at finite Prandtl number. *J. Differential Equations*, 260(4):3860–3880, 2016.

[DC94] Charles R. Doering and Peter Constantin. Variational bounds on energy dissipation in incompressible flows: Shear flow. *Physical Review E*, 49(5):4087–4099, 1994.

[DC96] Charles R. Doering and Peter Constantin. Variational bounds on energy dissipation in incompressible flows. III. Convection. *Physical Review E*, 53(6):5957–5981, 1996.

[DM90] Bernard Dacorogna and Jürgen Moser. On a partial differential equation involving the jacobian determinant. *Annales de l'Institut Henri Poincaré C, Analyse non linéaire*, 7(1):1–26, 1990.

[Doe19] Charles R. Doering. Thermal forcing and 'classical' and 'ultimate' regimes of Rayleigh–Bénard convection. *Journal of Fluid Mechanics*, 868(1958):1–4, 2019.

[Doe20] Charles R. Doering. Turning up the heat in turbulent thermal convection. *Proceedings of the National Academy of Sciences*, 117(18):9671–9673, 2020.

[DT06] Charles R. Doering and Jean-Luc Thiffeault. Multiscale mixing efficiencies for steady sources. *Phys. Rev. E*, 74:025301, Aug 2006.

[DT19] C. R. Doering and I. Tobasco. On the optimal design of wall-to-wall heat transport. *Communications on Pure and Applied Mathematics*, 72(11):2385–2448, 2019.

[DY22] Yuhang Du and Yantao Yang. Wall-bounded thermal turbulent convection driven by heat-releasing point particles. *J. Fluid Mech.*, 953:Paper No. A41, 27, 2022.

[Eva90] L. C. Evans. *Weak convergence methods for nonlinear partial differential equations*. CBMS Regional Conference Series in Mathematics. AMS, 1990.

[Eva10] Lawrence C. Evans. *Partial differential equations*, volume 19 of *Graduate Studies in Mathematics*. American Mathematical Society, Providence, RI, second edition, 2010.

[FADJ21] F. Feppon, G. Allaire, C. Dapogny, and P. Jolivet. Body-fitted topology optimization of 2D and 3D fluid-to-fluid heat exchangers. *Comput. Methods Appl. Mech. Engrg.*, 376:113638, 2021.

[GKL21a] André Guerra, Lukas Koch, and Sauli Lindberg. The Dirichlet problem for the Jacobian equation in critical and supercritical Sobolev spaces. *Calc. Var. Partial Differential Equations*, 60(1):Paper No. 55, 14, 2021.

[GKL21b] André Guerra, Lukas Koch, and Sauli Lindberg. Energy minimisers with prescribed Jacobian. *Arch. Ration. Mech. Anal.*, 242(2):1059–1090, 2021.

[GKL23] André Guerra, Lukas Koch, and Sauli Lindberg. Nonlinear open mapping principles, with applications to the Jacobian equation and other scale-invariant PDEs. *Adv. Math.*, 415:Paper No. 108869, 39, 2023.

[Gol15] David Goluskin. Internally heated convection beneath a poor conductor. *Journal of Fluid Mechanics*, 771:36–56, 2015.

[Gol16] David Goluskin. *Internally heated convection and Rayleigh-Bénard convection*. Springer Briefs in Applied Sciences and Technologies. Springer, Cham, 2016.

[GR86] Vivette Girault and Pierre-Arnaud Raviart. *Finite element methods for Navier-Stokes equations*, volume 5 of *Springer Series in Computational Mathematics*. Springer-Verlag, Berlin, 1986.

[GS12] David Goluskin and Edward A. Spiegel. Convection driven by internal heating. *Physics Letters A*, 377(1-2):83–92, 2012.

[HCD14] Pedram Hassanzadeh, Gregory P. Chini, and Charles R. Doering. Wall to wall optimal transport. *Journal of Fluid Mechanics*, 751:627–662, 2014.

[HFN+12] Xiaozhou He, Denis Funfschilling, Holger Nobach, Eberhard Bodenschatz, and Guenter Ahlers. Transition to the ultimate state of turbulent rayleigh-bénard convection. *Phys. Rev. Lett.*, 108:024502, Jan 2012.

[How63] Louis N. Howard. Heat transport by turbulent convection. *Journal of Fluid Mechanics*, 17(3):405–432, 1963.

[How72] Louis N. Howard. Bounds on Flow Quantities. *Annual Review of Fluid Mechanics*, 4(1):473–494, 1972.

[IKJK20] Scheel JD Iyer KP, Schumacher J, and Sreenivasan KR. Classical 1/3 scaling of convection holds up to ra = 10¡sup¿15¡/sup¿. *Proceedings of the National Academy of Sciences*, 117(14):7594–7598, 2020.

[INRZ10] Gautam Iyer, Alexei Novikov, Lenya Ryzhik, and Andrej Zlatoš. Exit times of diffusions with incompressible drift. *SIAM J. Math. Anal.*, 42(6):2484–2498, 2010.

[IV22] Gautam Iyer and Truong-Son Van. Bounds on the heat transfer rate via passive advection. *SIAM J. Math. Anal.*, 54(2):1927–1965, 2022.

[JN61] F. John and L. Nirenberg. On functions of bounded mean oscillation. *Comm. Pure Appl. Math.*, 14:415–426, 1961.

[KAF+22] Anuj Kumar, Ali Arslan, Giovanni Fantuzzi, John Craske, and Andrew Wynn. Analytical bounds on the heat transport in internally heated convection. *Journal of Fluid Mechanics*, 938:A26, 2022.

[KGOM22] S. Kazemi, D. Goluskin, and R. Ostilla-Mónico. Transition between boundary-limited and mixing-length scalings of turbulent transport in internally heated convection. Physical Review Letters (to appear), 2022.

[KRR12] A. Kiselev, Jean-Michel Roquejoffre, and L. Ryzhik. PDEs for a Metro Ride, 2012.

[Kum22] Anuj Kumar. Three dimensional branching pipe flows for optimal scalar transport between walls. arXiv:2205.03367 [math.AP], 2022.

[LAG18] S. Lepot, S. Aumaître, and B. Gallet. Radiative heating achieves the ultimate regime of thermal convection. *Proceedings of the National Academy of Sciences of the United States of America*, 115(36):8937–8941, 2018.

[Lax02] Peter D. Lax. *Functional analysis*. Pure and Applied Mathematics (New York). Wiley-Interscience [John Wiley & Sons], New York, 2002.

[LDB04] Lu Lu, Charles R. Doering, and Friedrich H. Busse. Bounds on convection driven by internal heating. *Journal of Mathematical Physics*, 45(7):2967–2986, 2004.

[Lie96] Gary M. Lieberman. *Second order parabolic differential equations*. World Scientific Publishing Co., Inc., River Edge, NJ, 1996.

[Lin17] Sauli Lindberg. On the Hardy space theory of compensated compactness quantities. *Arch. Ration. Mech. Anal.*, 224(2):709–742, 2017.

[Mal54] Willem V. R. Malkus. The heat transport and spectrum of thermal turbulence. *Proceedings of the Royal Society A*, 225(1161):196, 1954.

[MB20] E. Mulyukova and D. Bercovici. Mantle convection in terrestrial planets. *Oxford Research Encyclopedia of Planetary Science*, 03 2020.

[MDTY17] Florence Marcotte, Charles R. Doering, Jean-Luc Thiffeault, and William R. Young. Optimal heat transfer and optimal exit times. *SIAM Journal on Applied Mathematics*, 78(1):591–608, 2017.

[Miy90] A. Miyachi. H^p spaces over open subsets of $\mathbb{R}^n$. *Studia Mathematica*, 95:205–228, 1990.

[MLBG19] Benjamin Miquel, Simon Lepot, Vincent Bouillaut, and Basile Gallet. Convection driven by internal heat sources and sinks: Heat transport beyond the mixing-length or "ultimate" scaling regime. *Physical Review Fluids*, 4(12):121501, 2019.

[Mos65] Jürgen Moser. On the volume elements on a manifold. *Trans. Amer. Math. Soc.*, 120:286–294, 1965.

[Nob23] Camilla Nobili. The role of boundary conditions in scaling laws for turbulent heat transport. *Math. Eng.*, 5(1):Paper No. 013, 41, 2023.

[NSD00] J. J. Niemela, K. R. Skrbek, L. Sreenivasan, and R. J. Donnelly. Turbulent convection at very high rayleigh numbers. *Nature*, 404(6780):837–840, 2000.

[Pri54] CHB Priestley. Convection from a large horizontal surface. *Australian Journal of Physics*, 7(1):176–201, 1954.

[PW84] Murray H. Protter and Hans F. Weinberger. *Maximum principles in differential equations*. Springer-Verlag, New York, 1984.

[Ray16] Lord Rayleigh. On the convective currents in a horizontal layer of fluid when the higher temperature is on the under side. *Philosophical Magazine. 6th series.*, 32(192):529–546, 1916.

[RBLY19] C. B. Rocha, T. Bossy, S. G. Llewellyn Smith, and W. R. Young. Improved bounds on horizontal convection. *Journal of Fluid Mechanics*, 883:A41, 2019.

[SFT23] Binglin Song, Giovanni Fantuzzi, and Ian Tobasco. Bounds on heat transfer by incompressible flows between balanced sources and sinks . *Physica D: Nonlinear Phenomena*, 444:133591, 2023.

[SKB04] J. H. Siggers, R. R. Kerswell, and N. J. Balmforth. Bounds on horizontal convection. *Journal of Fluid Mechanics*, 517:55–70, 2004.

[Spi63] Edward A Spiegel. A generalization of the mixing-length theory of turbulent convection. *Astrophysical Journal, vol. 138, p. 216*, 138:216, 1963.

[STD07] Tiffany A. Shaw, Jean-Luc Thiffeault, and Charles R. Doering. Stirring up trouble: multi-scale mixing measures for steady scalar sources. *Phys. D*, 231(2):143–164, 2007.

[STD20] Andre N. Souza, Ian Tobasco, and Charles R. Doering. Wall-to-wall optimal transport in two dimensions. *Journal of Fluid Mechanics*, 889:A34, 2020.

[Ste93] Elias M. Stein. *Harmonic analysis : real-variable methods, orthogonality, and oscillatory integrals*. Princeton mathematical series ; 43. Princeton University Press, 1993.

[STO01] G. Schubert, D. L. Turcotte, and P. Olson. *Mantle convection in the Earth and planets*. Cambridge University Press, 2001.

[SV60] E. A. Spiegel and G. Veronis. On the Boussinesq approximation for a compressible fluid. *Astrophys. J.*, 131:442–447, 1960.

[SZ16] Yuxin Shen and Oleg Zikanov. Thermal convection in a liquid metal battery. *Theoretical and Computational Fluid Dynamics*, 30(4):275–294, 2016.

[TD] Ian Tobasco and Charles R. Doering.

[TDG04] Jean-Luc Thiffeault, Charles R. Doering, and John D. Gibbon. A bound on mixing efficiency for the advection-diffusion equation. *J. Fluid Mech.*, 521:105–114, 2004.

[Thi12] Jean-Luc Thiffeault. Using multiscale norms to quantify mixing and transport. *Nonlinearity*, 25(2):R1–R44, 2012.

[Tob22] Ian Tobasco. Optimal cooling of an internally heated disc. *Philosophical Transactions of the Royal Society A*, 310(1):20210040, 2022.

[TP08] Jean-Luc Thiffeault and Grigorios A. Pavliotis. Optimizing the source distribution in fluid mixing. *Phys. D*, 237(7):918–929, 2008.

[UMS11] P. Urban, V. Musilová, and L. Skrbek. Efficiency of heat transfer in turbulent rayleigh-bénard convection. *Phys. Rev. Lett.*, 107:014302, Jul 2011.

[WD11] Jared P. Whitehead and Charles R. Doering. Internal heating driven convection at infinite Prandtl number. *Journal of Mathematical Physics*, 52(9):093101, 2011.

[WD12] Jared P. Whitehead and Charles R. Doering. Rigid bounds on heat transport by a fluid between slippery boundaries. *Journal of Fluid Mechanics*, 707:241–259, 2012.

[WY09] K. B. Winters and W. R. Young. Available potential energy and buoyancy variance in horizontal convection. *Journal of Fluid Mechanics*, 629:221–230, 2009.